Evaluation of High Power Density Annular Fuel Application in the Korean OPR-1000 Reactor

by

Liang Zhang

B.S., Nuclear Engineering and Technology (2007)
Shanghai Jiao Tong University

Submitted to the Department of Nuclear Science and Engineering
in partial fulfillment of the requirements for the degree of

Master of Science in Nuclear Science & Engineering

at the

MASSACHUSETTS INSTITUTE OF TECHNOLOGY

June 2009

Signature of Author: ______________________________
Department of Nuclear Science and Engineering
May 9, 2009

Certified By: ______________________________
Mujid S. Kazimi, Ph.D.
TEPCO Professor of Nuclear Science and Engineering
Professor of Mechanical Engineering
Thesis Supervisor

Read By: ______________________________
Pavel Hejzlar, Sc.D.
Principal Research Scientist
Thesis Reader

Accepted By: ______________________________
Jacquelyn C. Yanch, Ph.D.
Chair, Deparment Committee on Graduate Students

Evaluation of High Power Density Annular Fuel Application in the Korean OPR-1000 Reactor

By

Liang Zhang

Submitted to the Department of Nuclear Science and Engineering on May 9, 2009,
in partial fulfillment of the requirements for the Degrees of
Master of Science in Nuclear Science and Engineering

Abstract

Compared to the traditional solid fuel geometry for PWRs, the internally and externally cooled annular fuel offers the potential to increase the core power density while maintaining or increasing safety margins. It is demonstrated that for the Korean OPR-1000 reactor, power density can be increased by 20% when the 16x16 solid fuel assemblies are replaced by 12x12 annular fuel assemblies. In this annular fuel design, the assembly dimensions, coolant flow rate, and core outlet coolant temperature are kept fixed at the reference values for the OPR-1000 with solid fuel. The core inlet temperature is decreased to accommodate the additional 20% energy.

Thermal hydraulic steady state analyses are carried out to determine the Minimum Departure Nucleate Boiling Ratio (MDNBR) margin and evaluate improvement in the design to maximize this margin. Whole core VIPRE-01 model results show that a proposed 14x14 annular fuel design cannot achieve high power uprate because of sub-limit MDNBR in the inner channel. To better optimize the 12x12 annular fuel design, the rod dimensions are fine-tuned by slightly increasing the inner channel diameter and outer channel diameter, while keeping the fuel to moderator ratio fixed. The modified design can achieve 20% power uprate. In addition, MDNBR sensitivity to manufacturing tolerances is investigated, showing that the new proposed design can accommodate typical manufacturing tolerances. Partial blockage at the inlet of the inner channel and the impact of corrosion and crud growth are also analyzed by conservertive models. The inner channel can accommodate a blockage of up to 43% of its flow area before MNDBR falls below the 1.3 limit.The crud and ZrO_2 buildup does not reduce MDNBR margin below the 1.3 limit, as long as the combined thickness is less than 74μm~94μm.

Neutronic analyses are performed for OPR-1000 with both the solid fuel and the annular fuel. The results from an MCNP model of the reference solid fuel assembly and a CASMO-4 model show excellent agreement. The benchmark of annular fuel array shows that CASMO-4 overpredicts the eigenvalues and the slope of the reactivity burnup curve. Fictitiously increasing U-238 number densities in CASMO-4 inputs by 10% produces good match with the MCNP-based burnup code, MCODE2.2. The whole core model of Ulchin Nuclear Unit 5 is established as a benchmark using SIMULATE-3 to calculate the steady state reactor core performance. Last but not least, an equilibrium annular fuel core is proposed, and its steady state core performance is analyzed. The proposed annular fuel assemblies composed of 7.5% and 6.5% U-235 enriched fuel rods, and burnable poisons with various Gd_2O_3 weight percentages (4%, 6%, 8%, 10%, and 16%) can satisfy the design targets, such as peak boron concentration, cycle length, and peaking factors in a certain equilibrium loading pattern.

Thesis Supervisor: Mujid S. Kazimi
Title: TEPCO Professor of Nuclear Science and Engineering
Professor of Mechanical Engineering

Acknowledgements

I would like to express my gratefulness to Prof. Mujid S. Kazimi, my research supervisor, for providing me this precious opportunity to work with him. It was an invaluable experience to be one of his students, not only because he is a very knowledgable and competent advisor, but for his kind-heartness and patience.

I would like to thank Dr. Pavel Hejzlar, who has guided me through numerous problems that I faced. His thoughtful advice, technical support, and availability made my life so much easier. It was really a pleasure to work with him, and he will always be a wonderful example for me. I would also like to thank Dr. Ed Pillat for his insightful comments and Prof. Ben Forget for his help on the neutronic benchmark calculations.

I acknowledge the Korea Atomic Energy Research Institute (KAERI) for funding this research, and providing the necessary data about OPR-1000.

I wish to give my thanks to my dear friend, Bo Feng, who gave me strong support both in research and in life. Same thanks to my colleagues and friends, Paul Romano, Rui Hu, and Yu-chih Ko.

Lastly, I would like to thank my beloved wife, Lili, for her constant encouragement through the challenges and difficulties in my life. It is you who make my life so much brighter.

Table of Contents

List of Figures

List of Tables

1. Introduction and Background

Extracting more power from existing power plants has been identified as one of the least costly options for increasing nuclear energy production. It has been noted that even though only three nuclear power plants have been built in the U.S. in the last twenty years, there has been a substantial increase in the amount of power generated by the nuclear fleet as a result of significant improvements in capacity factors and power uprates. Power uprates of operating plants are attractive to utilities as they allow an increase of revenue without the need for large capital investment.

A promising approach to reducing cost in new plants is to make use of economy of scale and increase plant power output. Large power ratings are attractive in countries with limited site options, like Korea. However, there are limits on how much power can be generated in LWR cores under existing design conditions, particularly those of the fuel. For example, there are limits on power increase by simply increasing the number of assemblies, in particular on reactor vessel size. Hence, it is desirable to increase power density so that large power uprates can be accomplished without the need to significantly increase the size of the reactor vessel for new construction or by backfitting new cores into existing reactor vessels.

One of the key components affecting the allowable power density in the nuclear island is nuclear fuel. This has been recognized from the early days of nuclear technology and significant improvements in fuel design and cladding quality were made, which allowed a remarkable reduction of failure rate, and better performance at steady state and during accidents. Although some incremental benefits have been realized in terms of power density, significantly larger power uprates are desirable to impact economy. Recognizing this need, MIT and several industrial collaborators have recently developed internally and externally cooled annular fuel

[Hejzlar et al., 2001, Kazimi et al., 2005], which can achieve 50% power density increase at the same safety margin and which received significant attention in the industry.

1.1. Annular Fuel Description

The internally and externally cooled annular fuel geometry is schematically shown in Figure 1-1. Because of the reduced heat conduction resistance in the new geometry, the fuel exhibits substantially lower peak temperature than the solid fuel. In addition, due to the larger heat transfer area of the annular fuel, the DNBR margin is increased allowing for significant power uprate.

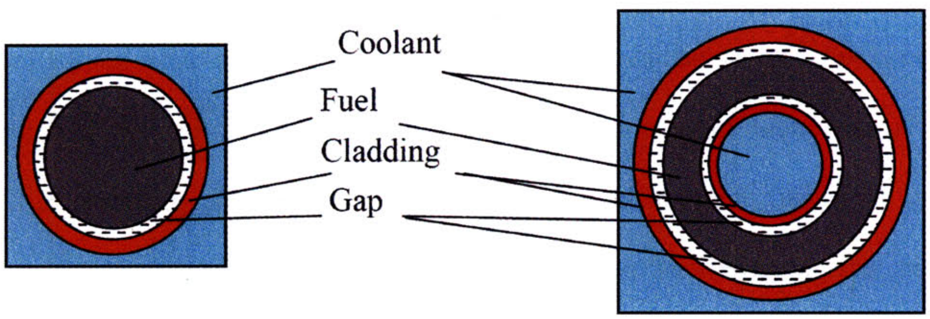

Figure 1-1: Schematic of solid fuel and internally and externally cooled annular fuel (not to scale) (from [Kazimi et al., 2005])

The Center for Advanced Nuclear Energy Systems (CANES) at MIT has proposed an annular fuel design suitable for uprating a reference design of a typical Westinghouse 4-loop with an initial 3411MWt core power. The size and number of fuel assemblies in the core were kept fixed. Coolant inlet and outlet temperatures of the annular design were also kept the same as the solid fuel design, while the mass flow rate was increased proportionally to the power uprate, which can be as high as 50%. It is expected that for this kind of design, an additional balance of plant loop will be constructed to accommodate the increased flow rate, and new steam generators and primary coolant pumps are requisite for higher power and larger flow rate.

Different fuel array sizes were investigated to optimize MDNBR in the inner and outer coolant channels. Results shown in Figure 1-2 indicate that the 13x13 array is the optimum design because of the well balanced MDNBR and the large safety margin for both the inner and outer channels. Table 1-1 compares the annular fuel rod geometry of the 13x13 array with the reference solid fuel of the 17x17 array. To maintain similar fuel volume and heavy metal to moderator ratio, the control rod guide tubes were reduced from 24 to 8, and the dimensions were adjusted accordingly with each array size. In addition, higher enrichment of 8.7w/o was necessary to maintain the same 18 month cycle length. Much larger MDNBR with the annular fuel allowed an increase from the nominal 3411MWt power by 50% to the higher value of 5117MWt. The MDNBR for this uprated condition is 1.74 for the hot inner channel and 1.61 for the hot outer channel, both of which are larger than the 1.58 MDNBR for the solid fuel at 100% power. However, the pressure drop of the annular fuel design at 150% power is about 0.242MPa, which is much larger than that of the standard solid fuel at 100%, 0.138MPa [Feng et al, 2007].

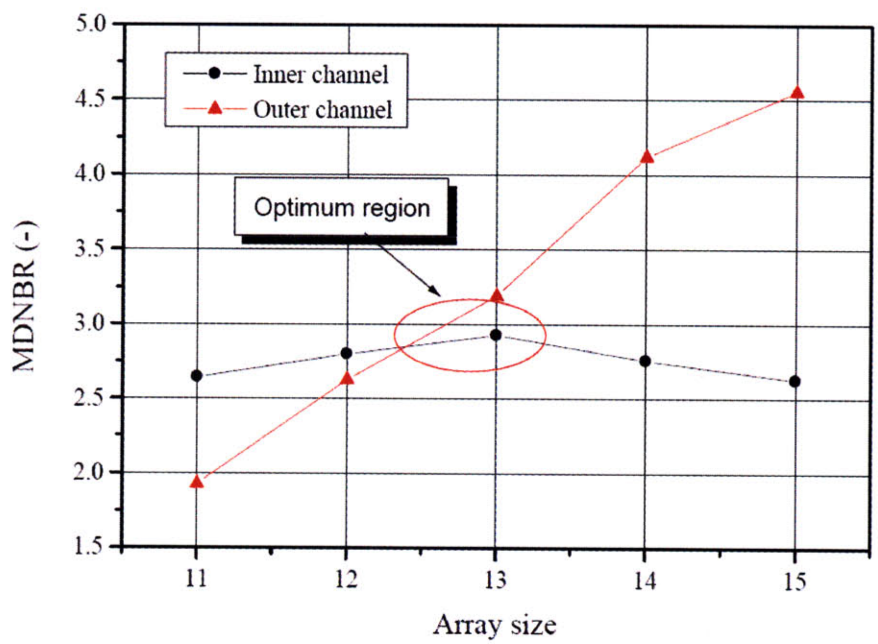

Figure 1-2: Inner and outer channel MDNBR for different Westinghouse array designs at 100% power (from [Feng et al, 2007])

Table 1-1: Dimensions (mm) of annular fuel elements compared to solid pins for Westinghouse design (from [Feng et al, 2007])

Array	Inner clad in. dia.	Inner clad out. dia.	Fuel inner dia.	Fuel outer dia.	Outer clad in. dia.	Outer clad out. dia.	Pitch
Annular 13x13	8.61	9.753	9.877	14.225	14.349	15.492	16.51
Solid 17x17	--	--	--	8.26	8.38	9.52	12.63

Note: dia = diameter, in. = inner, out. = outer

1.2. Objectives and Scope

Currently, Korea Atomic Energy Research Institute (KAERI) is pursuing the development, including irradiation and testing, of this annular fuel for Generation III Korean OPR-1000 reactor. The OPR-1000 reactor has different dimensions of the fuel assembly, different fuel lattice (16x16 versus 17x17) and different operating conditions than the standard Westinghouse PWR considered in previous MIT analyses. Moreover, the new fuel design was developed under the additional constraint of preserving control rod positions and a limited increase in the coolant flow rate. Thus, instead of proportionally increasing the flow rate, the core outlet temperature is kept constant while reducing the core inlet temperature by about 10°C. Also, the power uprate target is smaller than that strived for in the MIT design for the Westinghouse reactor. Therefore, this power uprate is aimed for the plant without major componenet modifications.

The overall objective of this project is to evaluate feasibility of the high power density annular fuel for the OPR-1000 reactor, which operates under different constraints and conditions than the standard Westinghouse PWR used in earlier MIT analyses. The evaluation work involves several tasks, as described below.

A. Steady-state Thermal-Hydraulic Analysis

KAERI has developed a conceptual design of a 12x12 annular fuel assembly to achieve 20% power uprate while increasing DNBR margin and remaining compatible with current control rod positions. In the first place, steady-state thermal-hydraulic analyses of KAERI design for the OPR-1000 reactor with both solid fuel and annular fuel will be performed to evaluate, and optimization the proposed design will be undertaken.

B. Assessment of the Impact of Partial Blockage of the Inner Channel

Because the inner channel is isolated from other channels, there is no lateral flow and mixing and questions are often raised about potential channel blocking and its consequences. Both the partial debris blockage at the inlet and blockage due to oxide growth, which can occur along substantial axial section of the inner channel, will be evaluated.

C. Reactor physics performance of OPR-1000 core

Reactor physics performance of OPR-1000 core with solid fuel and annular fuel will be evaluated, to determine if the key three core design targets of (1) prescribed cycle length (2) peak critical boron concentration; and (3) the hot channel and hot spot factors can be satisfied within given enrichment and other constraints.

2. Description of Reference Solid and Annular Fuel Design

Geometric configuration of OPR-1000 assembly with conventional solid fuel is shown in Figure 2-1, and assemblies with the proposed annular fuel designs are shown in Figure 2-2 and 2-3. All geometrical data were provided by KAERI. It should be noted that the annular fuel design is fully compatible with the conventional solid fuel design in terms of structure, fuel to moderator ratio, amount of fissile material and coolant flow area [Yang et. al., 2007]. Moreover, the guide tubes for the annular fuel design are of annular shape and their positions are compatible with the reference design to match vessel head penetrations. The outer tube is sized to reduce the large flow area around the original tube, reducing the bypass flow as compared to the original design.

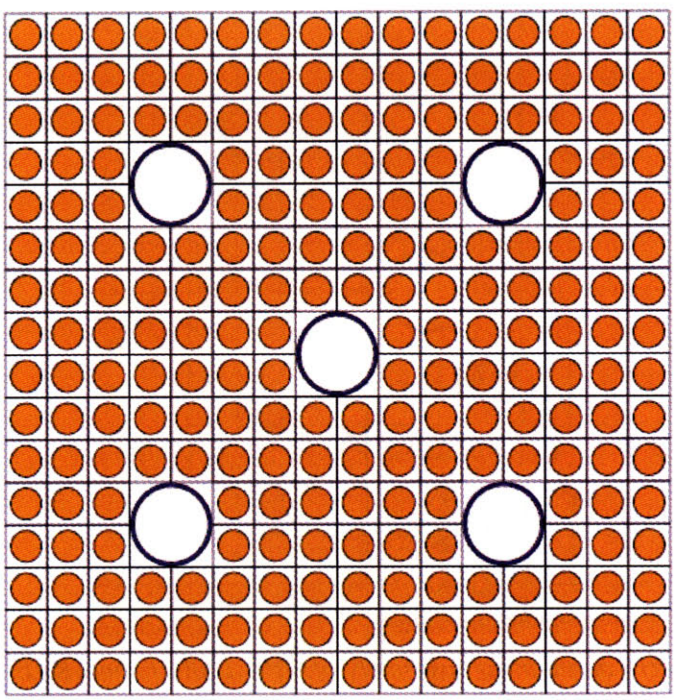

Figure 2-1: Conventional 16x16 solid fuel assembly of OPR-1000 (From [KAERI, 2008])

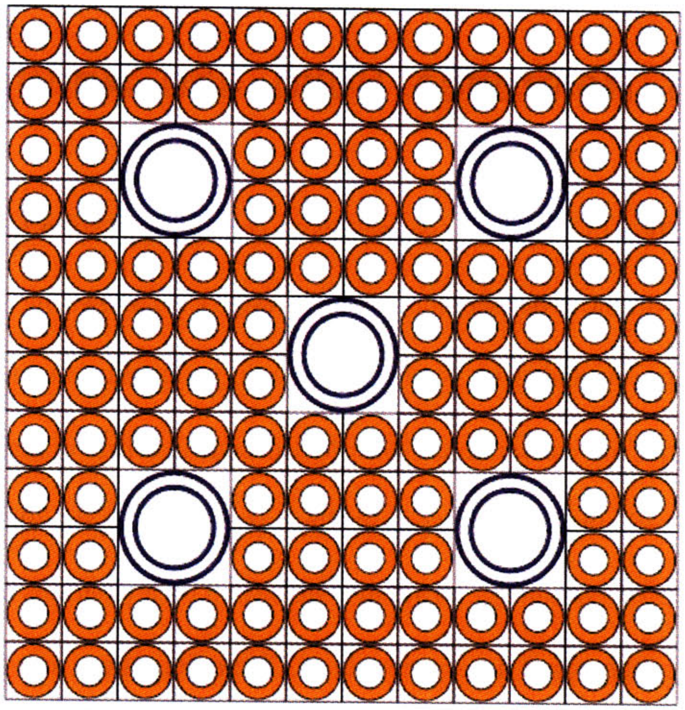

Figure 2-2: Proposed 12x12 annular fuel assembly of OPR-1000 (From [KAERI, 2008])

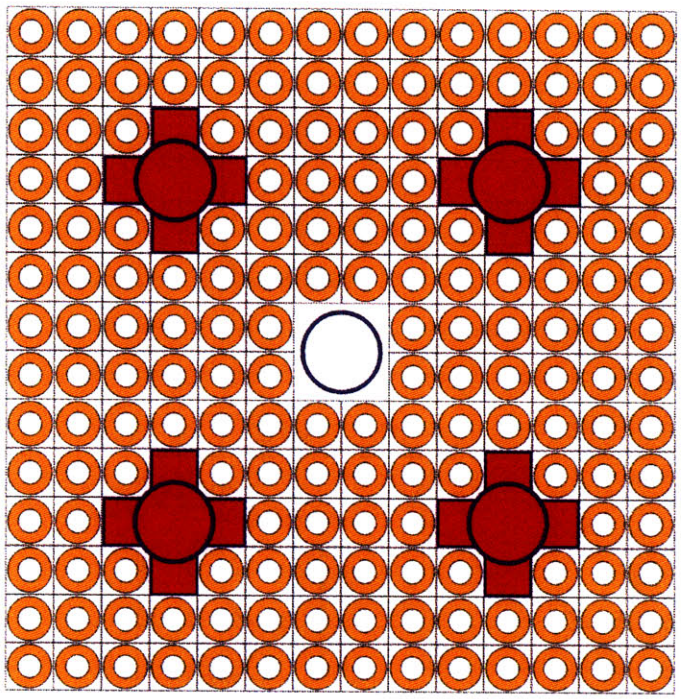

Figure 2-3: Proposed 14x14 annular fuel assembly of OPR-1000 (From [KAERI, 2008])

The geometrical parameters of three fuel types are given in Table 3-1. Note that these parameters are used as hot dimensions in VIPRE-01, CASMO-4, and MCODE-2.2.

Table 2-1: Cold geometric data of the current and proposed OPR fuel assemblies

Fuel Assembly	**Solid Fuel**	**Annular Fuel**	
Rod array	16 x 16	12 x 12	14x14
Fuel rods number	236	124	172
Guide tube number	4		
Instrument tube number	1		
Assembly pitch (mm)	207.8		
Rod pitch (mm)	12.85	17.13	14.68
Fuel volume per assembly (cm^3)	47369	40527	35409
Rod			
Rod inner diameter (mm)	--	8.80	7.10
Inner clad thickness (mm)	--	0.57	0.39
Inner clad outer diameter (mm)	--	9.94	7.88
Inner gap thickness (mm)	--	0.07	0.06
Fuel inner diameter (mm)	--	10.08	8.00
Fuel outer diameter (mm)	8.19	14.52	11.85
Outer gap thickness (mm)	0.085	0.07	0.06
Outer clad inner diameter (mm)	8.36	14.66	11.97
Outer clad thickness (mm)	0.57	0.62	0.74
Rod outer diameter (mm)	9.50	15.90	13.45
Guide tube			
Guide tube clad thickness (mm)	1.0		
Inner guide tube outer diameter (mm)	--	24.90	(cross shape, see Fig.3-14)
Outer guide tube outer diameter (mm)	24.9	33.50	

3. Thermal Hydraulic Analysis

Thermal hydraulic analysis is a critical part of annular fuel design since it determines the dimensions of the fuel that allow achievement of the power uprate within acceptable MDNBR margins. Because the option space of the thermal hydraulic design is constrained by assembly dimensions and control rod guide tube positions, it is important to assure thermal hydraulic feasibility before proceeding with full core neutronic design. Therefore, the effort in this chapter was focused on the verification and optimization of the annular fuel design within acceptable thermal hydraulic constraints, e.g., MDNBR should be no less than 1.3 using the W-3 correlation.

3.1. Thermal Hydraulic Analysis Tools

VIPRE-01 (Versatile Internals and Component Program for Reactors; EPRI) is a thermal-hydraulic analysis code to evaluate reactor core safety limits. It is a finite-volume sub-channel analysis code capable of three-dimensional modeling of reactor cores and other similar geometries in steady and transient states. It can perform very detailed nuclear reactor thermal-hydraulic calculations to obtain the minimum departure from nucleate boiling ratio (MDNBR), critical power ratio (CPR), fuel and cladding temperatures, and coolant state [EPRI, 1985]. VIPRE-01 is approved by US Nuclear Regulatory Commission (USNRC), and is widely used by several U.S. utilities and international organizations.

3.2. Thermal Hydraulic Analysis of Reference and 12x12 Annular Fuel

This section summarizes the steady state thermal hydraulic analysis model and results of reference fuel and 12x12 annular fuel. The thermal-hydraulic calculation is carried out mostly using VIPRE-01 code. Results show that the original KAERI design of annular fuel does not satisfy MDNBR requirement for 120% power. Therefore, the design was modified to obtain well balanced and acceptable MDNBR margin. Using the modified design, the impact of partial blockage of the inner channel, including both the partial debris blockage of the inlet of the inner channel and blockage due to oxide growth and crud along the axial length, is evaluated.

3.2.1. VIPRE-01 Model of Reference and 12x12 Annular Fuel

VIPRE-01 was used for detailed steady state thermal-hydraulic calculations of both solid fuel and annular fuel. To obtain realistic and conservative MDNBR and account for core-wide cross flow, it was essential to model the whole core or its symmetric section. Because of the symmetry of the core, an octant of the core was modeled by VIPRE-01, in which all the rods and channels were well represented.

3.2.1.1. Thermal Conditions

The thermal operating conditions were assumed to be similar for the reference solid fuel and annular fuel at the same power level. If annular fuel design had a 20% power uprate, the coolant inlet temperature was assumed to be reduced to maintain the same core outlet temperature. For all cases, analyses were performed with 18% overpower to allow for transients. In addition, inlet coolant temperature was increased by 2°C to account for possible non-uniformities of the core inlet temperature due to imperfect coolant mixing in the lower plenum. All assumptions and values of parameters are summaried in Table 3-1.

The radial pin power distribution in the solid fuel hot assembly with one-eighth symmetry is shown in Figure 3-1. The radial peaking factors for the one-eighth assembly were taken from the averages of power distribution for the one-fourth hot assembly provided by KAERI. One and a half burnable poison pins with power distribution of 0.816 and 0.909 are placed in this one-eighth hot assembly. It can be seen that the maximum radial peaking factor is 1.550, and the average radial peaking factor in the hot assembly is taken as 1.436. Note that this nodial factor accounts for both the core-wide neutronic condition as well as the intra-assembly conditions.

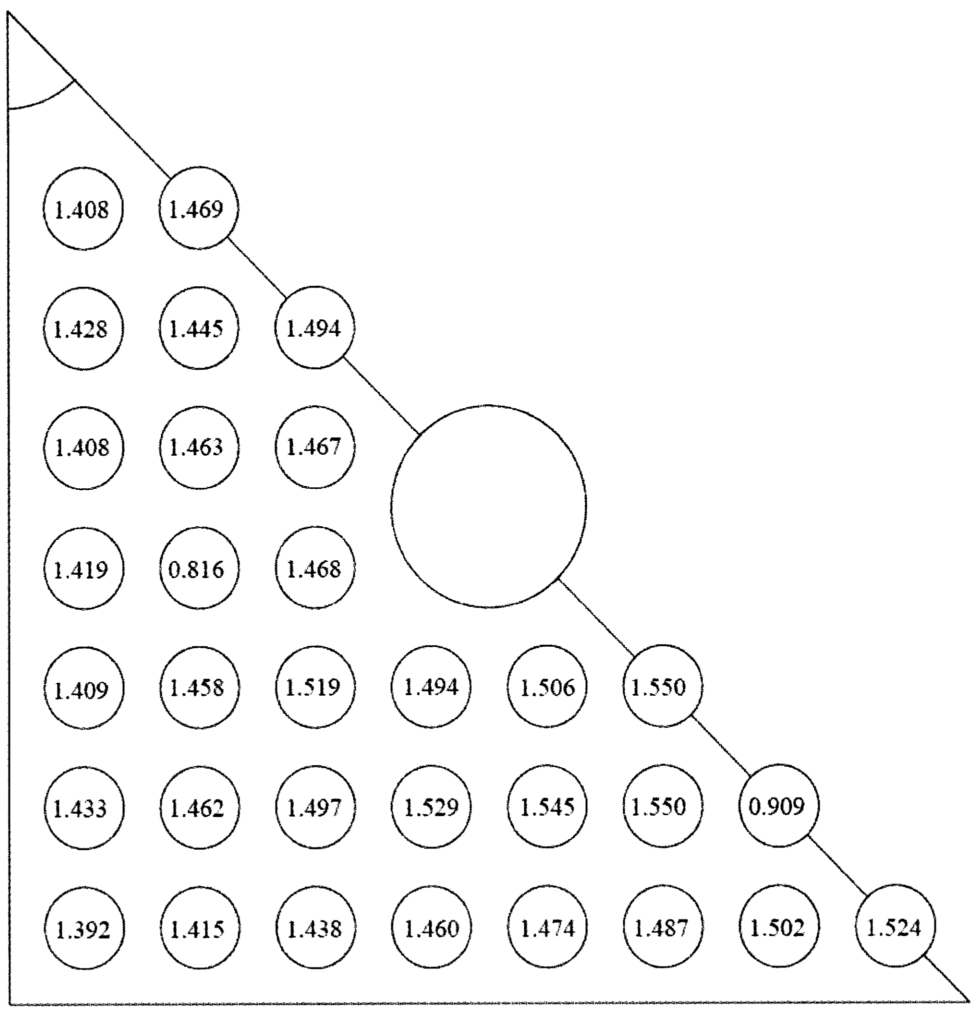

Figure 3-1: Pin power distribution in the hot assembly with one-eighth symmetry (solid fuel)

For the whole core modeling, the hot assembly was moved into the center of the core, and then surrounded by assemblies with the same peaking factor to minimize the effects of mixing among the adjacent assembly channels to obtain conservative MDNBR. Assembly power peaking for the whole core model for the solid fuel case is shown in Figure 3-2. Power levels of the outer assemblies were decreased gradually moving progressively away from the central hot assembly. Power peaking in the core periphery was adjusted to normalize the average power to 1.0. Notice that one quarter of the assembly nearest to the hot assembly is divided into two parts. The main reason is that the data of power distribution in the hot quarter assembly from KAERI shows that the upper half of the quarter has a larger average peaking factor (1.442) than the lower half of the quarter (1.429). Most hot assembly channels near the location where the MDNBR is expected to occur are modeled as individual subchannels and the subchannels few pitches away from the hot channel are gradually lumped. This is the same approach as used in the VIPRE-01 model of PWR cores studied at MIT [Feng et al, 2007].

Calculations for the proposed PWR with annular fuel design are also performed by VIPRE-01 based on finite-volume sub-channel analysis. It has already been verified by [Feng et al., 2007] that annular fuel can be successfully modeled as heat generating tubes with five material regions using the hollow tube option in VIPRE-01. The five regions include the inner cladding, inner gap, fuel meat, outer gap, and outer cladding. Because VIPRE-01 cannot automatically calculate heat transfer across a gap for the hollow tube option, it is necessary to model the gaps as heat conductors having an effective thermal conductivity that matches the gap conductance [Feng et al., 2007].

The maximum radial peaking factor of the annular fuel assembly is assumed to be the same as that of the reference PWR, i.e., 1.550. The pin power normalized distribution in a model of one-eighth assembly was calculated using MCNP code under a reflective boundary and poison free condition. The pin power distribution in the hot assembly, shown in Figure 3-3, was obtained by multiplying the normalized pin power distribution by a factor that gives the same core-wide maximum radial peaking factor as the reference solid fuel. Therefore, the average radial peaking factor of the hot assembly for the annular fuel is 1.363, which is lower than that for the solid fuel (1.436). It is assumed that refined neutronic analyses using burnable poison can reduce intra-assembly peaking and allow for increased core-wide assembly-to assembly peaking. The axial power distribution for both cases is assumed to be a chopped cosine shape with a peaking factor of 1.55.

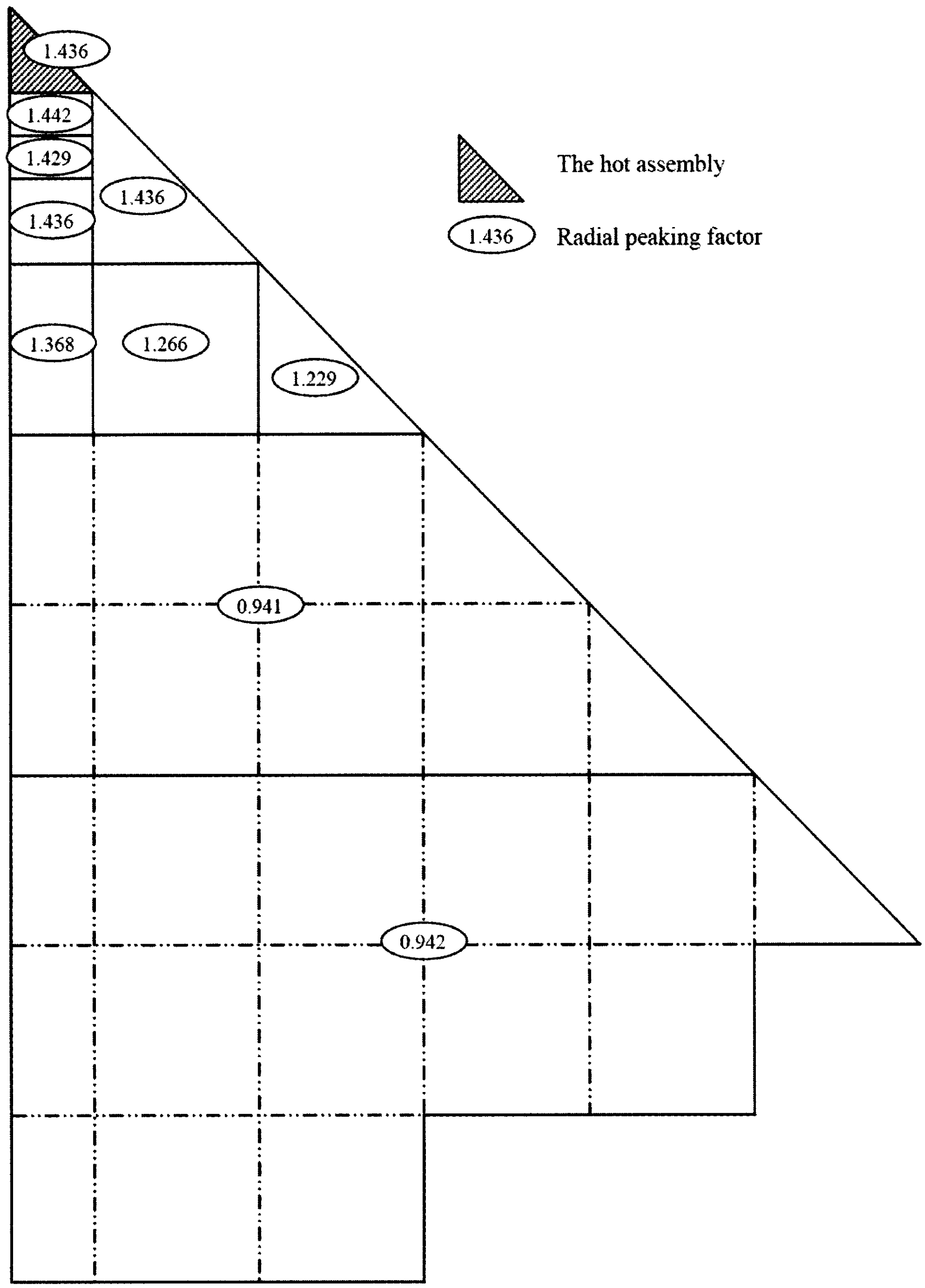

Figure 3-2: Assumed assembly power distribution in the octant of core (solid fuel)

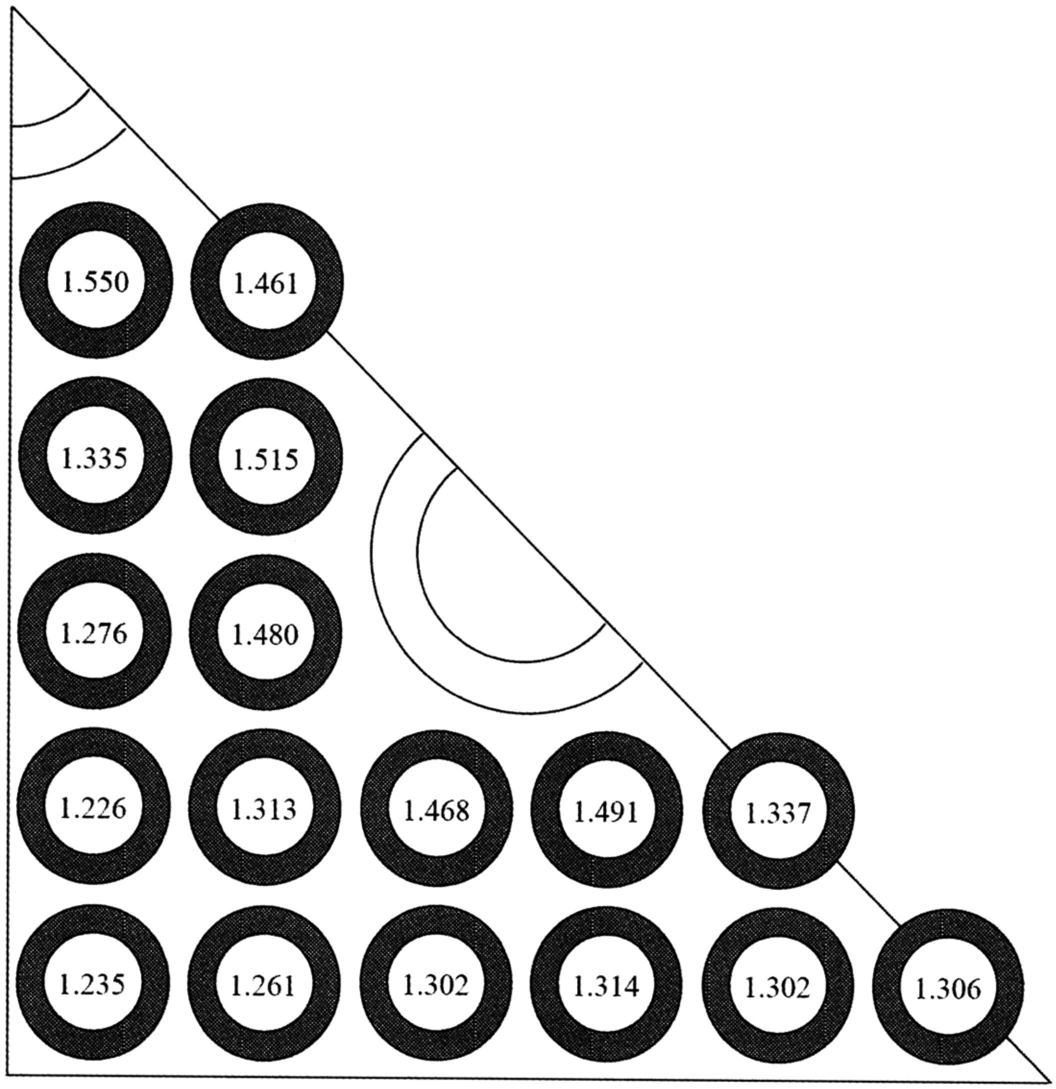

Figure 3-3: Pin power distribution in the hot assembly with one-eighth symmetry (annular fuel)

Similar to the radial peaking factors in the solid fuel case, the assembly power distribution in the one-eighth core is adjusted to normalize the core average power to unity, as shown in Figure 3-4.

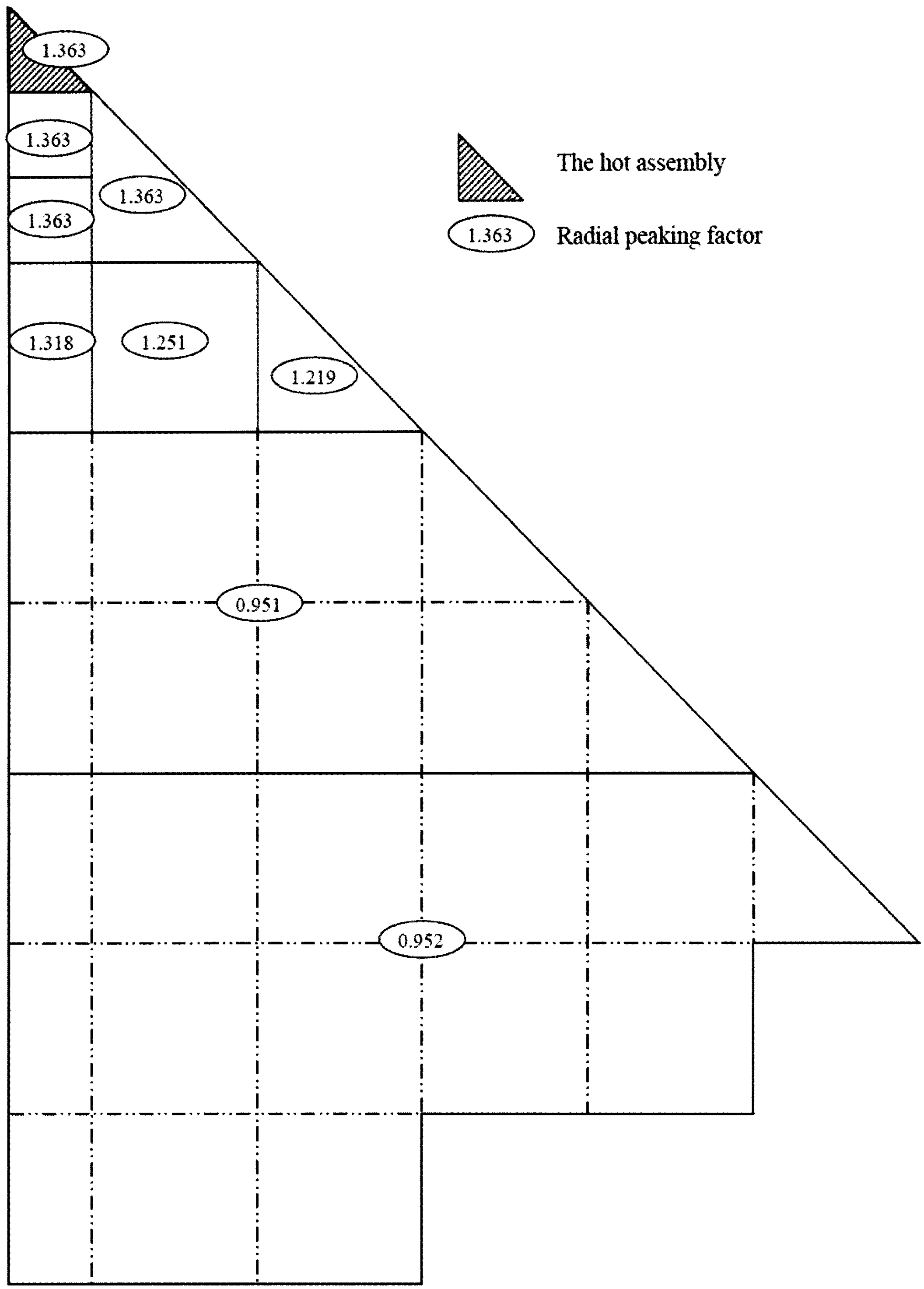

Figure 3-4: Assumed assembly power distribution in the octant of core (annular fuel)

3.2.1.2. **VIPRE-01 Models of Core Geometry**

One-eighth of the core is modeled by VIPRE-01 to minimize computation time. Moreover, certain groups of fuel rods, channels, and assemblies that are away from the hot rod and channels are lumped together for further simplification. For the hot region of the core, detailed flow channels and rods are represented individually. Thus, the extent of lumping depends on the power distribution.

Figure 3-5 shows the numbering scheme of channels and rods in the hot assembly for the whole core VIPRE-01 model with the solid fuel. Rods No.17 and 18 are the hottest rods, so the channels around them are modeled with high resolution. Channels that are away from the hottest rods, e.g., channels 1, 2, 5, and 6, are lumped to minimize the total number of channels in order to speed the calculations. The numbering of channels and rods for the whole core model can be found in Figure 3-6.

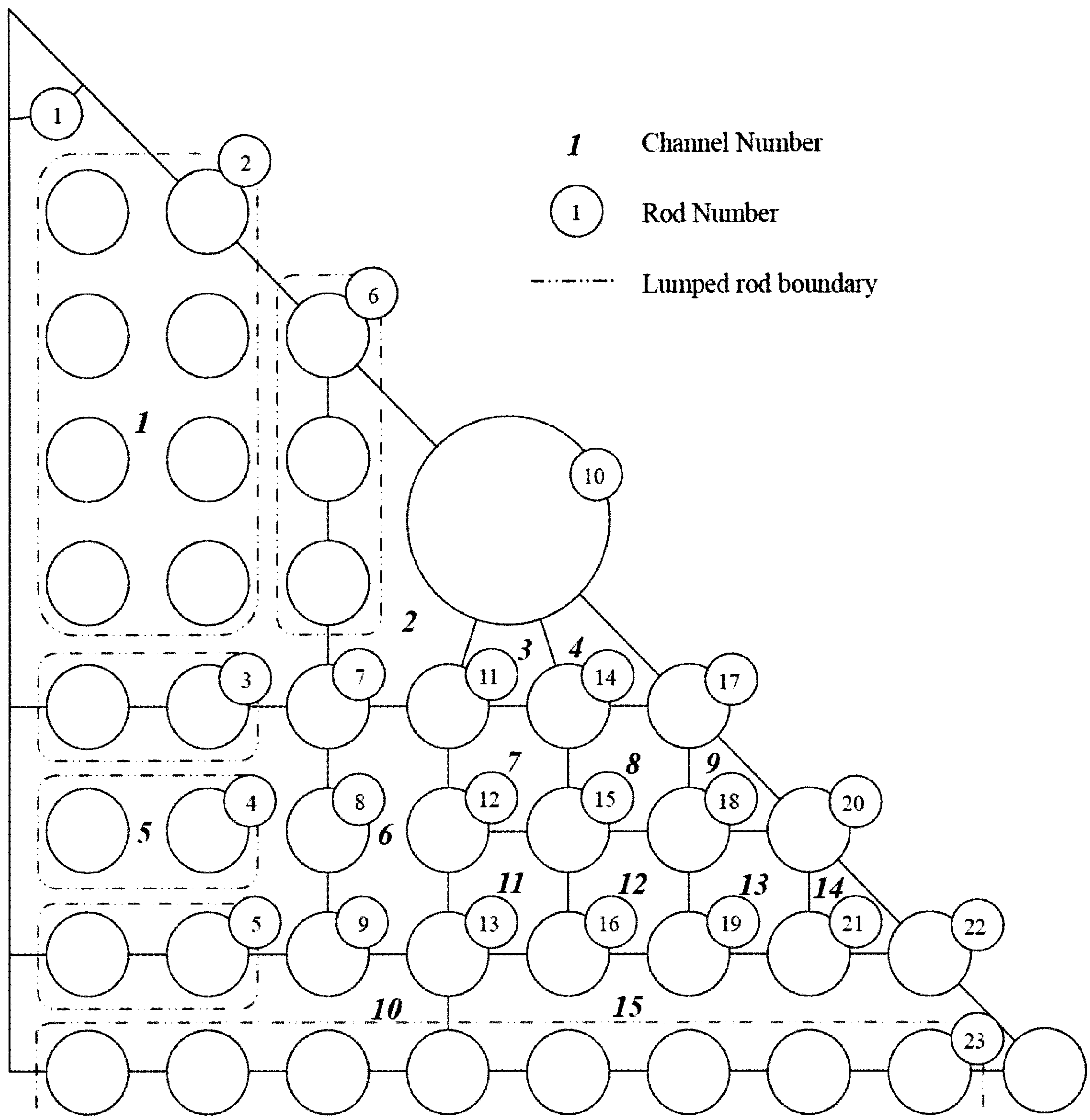

Figure 3-5: Numbering scheme of channels and rods in the hot assembly (solid fuel)

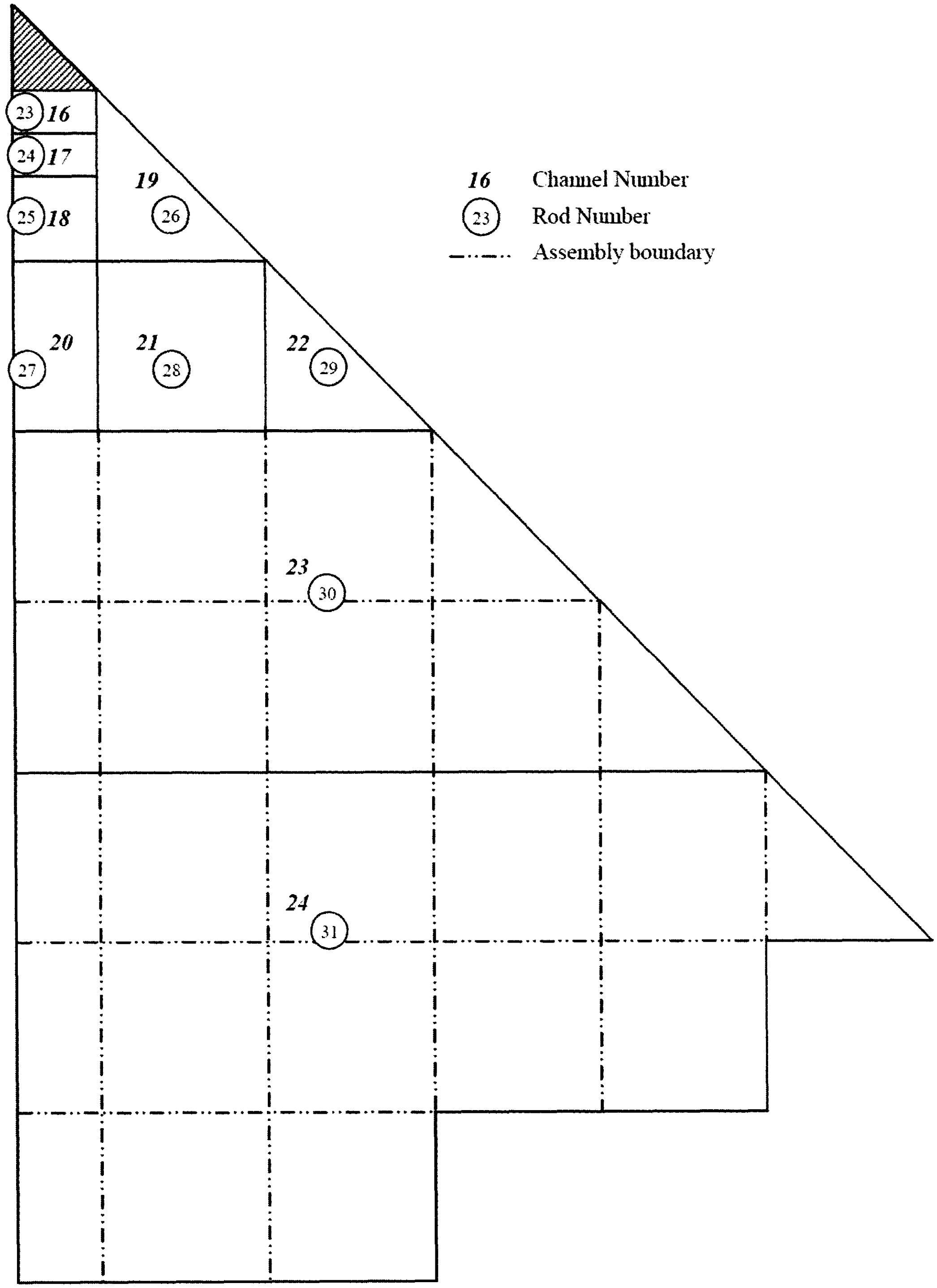

Figure 3-6: Numbering scheme of channels and rods in the one-eighth core (solid fuel)

Total number of channels and rods for the solid fuel design is 24 and 31, respectively. All channels are designated using a certain pattern to minimize the largest difference between adjacent numbers to increase computational efficiency [EPRI, 1985].

For annular fuel design, the designation of sub-channels and rods in the hot assembly is shown in Figure 3-7. Flow in the inner channels does not experience mass or energy exchange with other channels, while flows in the outer channels have mass and energy exchanges with the adjacent outer channels through the pin-to-pin gaps. Note that all channels in the hot assembly are treated individually. The original largest channel next to the guide tube was divided into two sub-channels (channel 11 and 12). This is because the rods along the guide tubes have larger peaking factors than those away from the guide tubes.

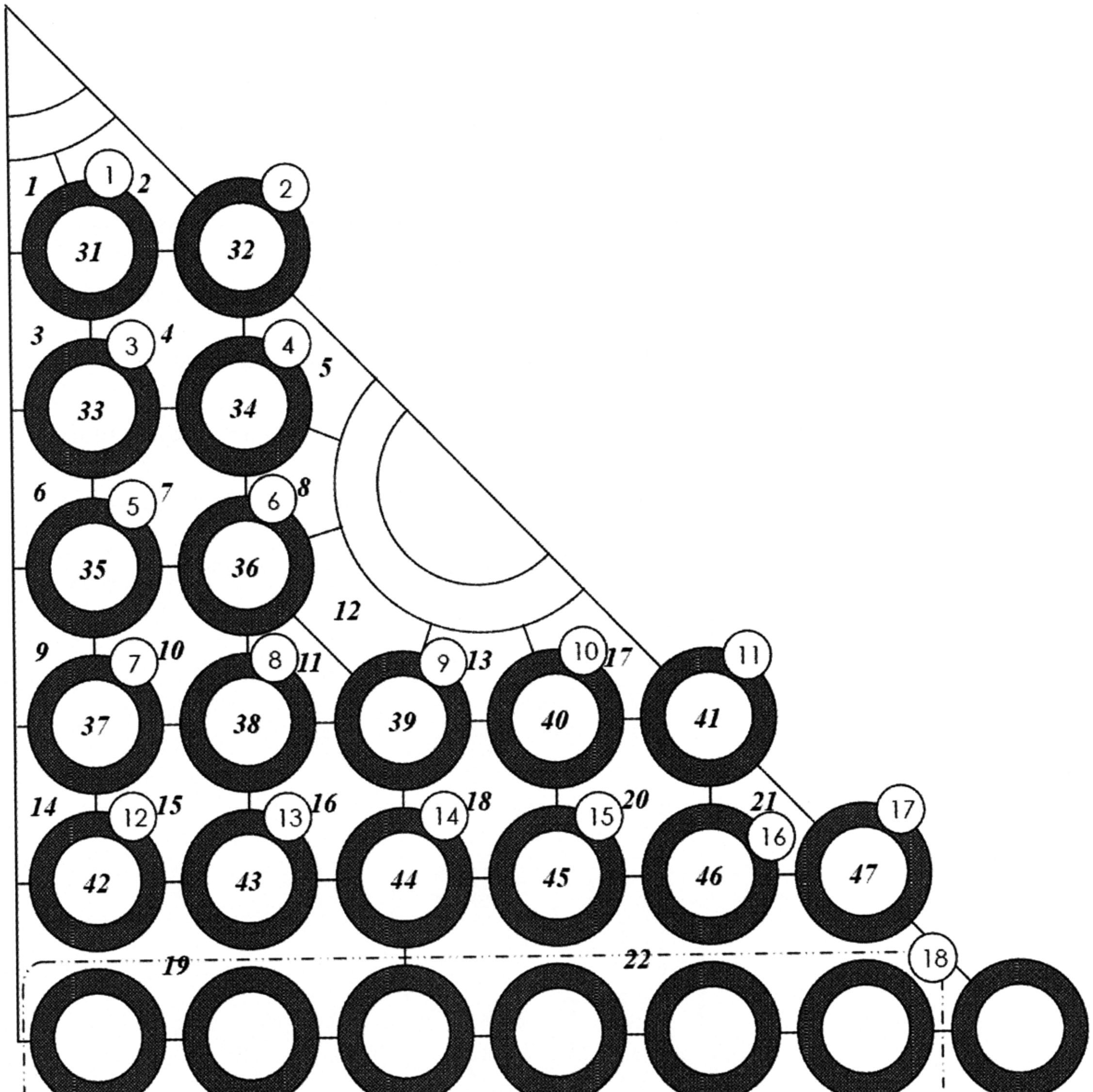

Figure 3-7: Numbering scheme of channels and rods in the hot assembly (annular fuel)

The numbering scheme of the lumped channels and rods in the one-eighth core of the annular fuel is shown in Figure 3-8. The total number of channels in the whole core model of annular fuel is 55, much more than that of the solid fuel case. Thus, the annular fuel model is more challenging for numerical convergence. In fact, the maximum number of axial nodes to satisfy the convergence criteria is 20 for the annular fuel model. Both models use 20 axial nodes for consistent comparison.

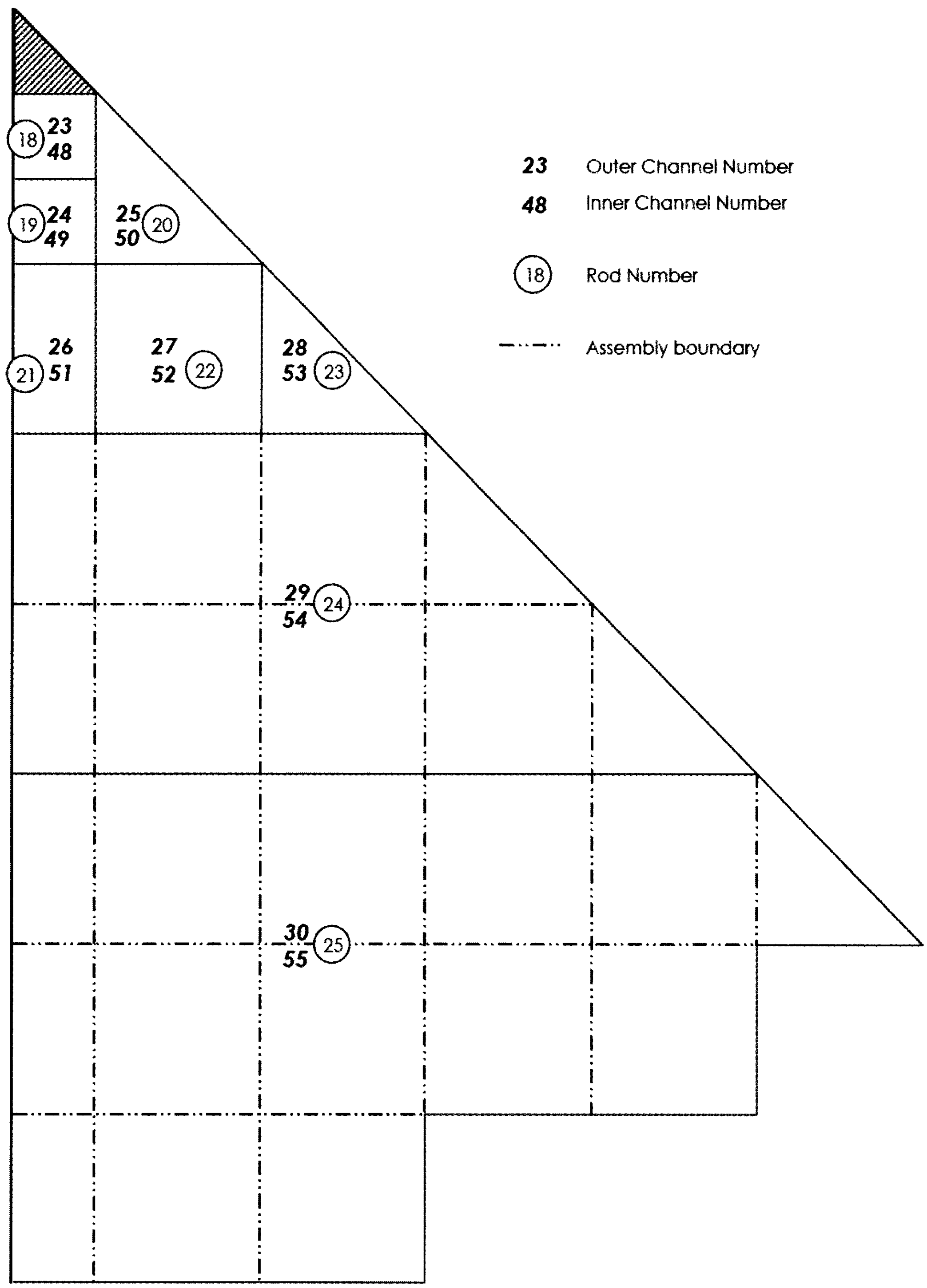

Figure 3-8: Numbering scheme of channels and rods in the one-eighth core (annular fuel)

Because VIPRE-01 does not automatically calculate the channel flow areas and distances between the centroids of adjacent channels, they must be all supplied in the input. Fuel rods contribute to both the heated and wetted perimeters of their adjacent channels, while guide tubes account for the wetted perimeter only and have no effect on heat transfer in the system. The flow through the guide tube was considered as fully blocked, assuming that highly effective flow restrictors are used. Ten grids, with 0.4 m axial spacing, are distributed along the active length of each fuel rod.

3.2.1.3. **Thermal Hydraulic Correlations of the Models**

To evaluate the lateral heat and mass exchange among the outer channels, a turbulent mixing model can be used to define the cross flow $w'(kg/m \cdot s)$ from an average axial mass velocity $\bar{G}(kg/s \cdot m^2)$ in adjacent channels over a gap width $s(m)$ with a turbulent mixing coefficient β:

$$w' = \beta s \bar{G}.$$

A larger β value indicates a greater amount of turbulent mixing among adjacent channels, which means the tendency to decrease the enthalpy peaking and increase the flow rate and MDNBR in the hot channel. To yield conservative results the turbulent mixing coefficient is assumed to be zero [Feng et al., 2007]. Additionally, the turbulent momentum factor FTM is also chosen to be zero, which implies that turbulence does not mix momentum from two adjacent channels.

The pressure drop between adjacent channels that drives the cross flow is defined as:

$$\Delta p_{cross} = K_G \frac{|w| w v'}{2s^2},$$

where K_G is the lateral resistance coefficient, w is the cross flow in $(kg/m \cdot s)$, v' is the specific volume for momentum in (kg/m^3), and s is the gap width in (m). A typical value for the lateral flow resistance coefficient between two rods is on the order of 0.5 [Feng et al., 2007]. A more accurate correlation can be used for the cross flow across the tube bundle on a square pitch [Idelchik, 1993]. For conventional OPR-1000 solid fuel design, a pitch of 12.85 mm and a rod diameter of 9.5 mm, the appropriate value is:

$$K_G = 3.031\,\mathrm{Re}^{-0.2}.$$

For annular fuel design, the pitch is 17.13 mm and rod outer diameter is 15.9 mm, thus the correlation becomes

$$K_G = 6.472\,\mathrm{Re}^{-0.2}.$$

The Re number is based on lateral velocity and rod diameter. The form loss coefficients for inlet, grids, and outlet are assumed to be 0.4, 0.6, and 1.0 respectively. For critical heat flux calculation, W-3L CHF correlation with grid mixing factor 0.0, grid spacing factor 0.066, and grid factor leading coefficient 0.986, is used for all the channels in the core of solid fuel. The same W-3L correlation is adopted for the outer channels of annular fuel model. Note that W-3L correlation has a cold wall factor incorporated automatically. For the inner channels of annular fuel model, W-3S CHF correlation with grid mixing factor 0.0 is used to calculate the critical heat flux where there are no grids. As for heat transfer correlations, Dittus-Boelter correlation is used for single phase flow, and Thom correlation is used for both subcooled and saturated nucleate boiling in both the solid fuel and the annular fuel models [Feng et al., 2007]. Table 3-1 summarizes the details of the VIPRE-01 model for both cases.

Unless specified, it is assumed that the conductances for both the inner and outer gaps are constant over the entire rod length and equal to 6000 W/m^2-K.

Table 3-1: Summary of the VIPRE-01 whole-core model of PWR with solid fuel and annular fuel (100% power)

Parameters	Solid fuel	Annular fuel
Model region	One-eighth core with full axial length	
Fuel rod inner diameter	---	8.8 mm
Fuel rod outer diameter	9.5 mm	15.9 mm
Guide tube diameter	24.9 mm	33.5 mm
Rod pitch	12.85 mm	17.13 mm
Rod array	16x16	12x12
Assembly pitch	207.8 mm	
Active core height	3.81 m	
Number of axial nodes	20	
Number of channels	24	55
Number of rods	31	25
Name of channels and rods	Figure 3-5 & 3-6	Figure 3-7 & 3-8
Axial power profile	Chopped cosine with peak-to-average ratio 1.55	
Radial Power distribution	Figure 3-1 & 5.2	Figure 3-3 & 3-4
Reactor power	3321.7 MWt (18% overpower)	
Power per rod	79.52 kW/rod	151.34 kW/rod
1/8 Core mass flow rate	1855.125 kg/s	
Core inlet temperature	298 C (increased by 2C)	
Turbulent mixing model	$\beta = 0$	
Turbulent momentum factor	$FTM = 0$	
Cross flow resistance coefficient (turbulent)	$K_G = 3.031\,\mathrm{Re}^{-0.2}$	$K_G = 6.472\,\mathrm{Re}^{-0.2}$
Cross flow resistance coefficient (laminar)	$K_G = 0.5$	
Axial friction coefficient (turbulent)	$f_{ax} = 0.316\,\mathrm{Re}^{-0.25}$	$f_{ax} = 0.32\,\mathrm{Re}^{-0.25}$
Axial friction coefficient (laminar)	$f_{ax} = 64\,\mathrm{Re}^{-1}$	
dor rep sdirg fo rebmuN	10	
Grid spacing	0.4 m	
Form loss coefficient for inlet	0.4	
Form loss coefficient for mixing vane grids in outer channels	0.6	
Form loss coefficient for outlet	1.0	
CHF correlations for inner channels	---	W-3S, grid mixing factor 0.0
CHF correlations for outer channels	W-3L, grid mixing factor 0.043, grid spacing factor 0.066, grid factor leading coefficient 0.986	
Void correlations	Subcooled: EPRI void model Bulk void quality: Zuber-Findlay drift flux equation Two-phase friction multiplier: Columbia/EPRI	
Heat transfer correlations	Single-phase flow: Dittus-Boelter correlation Subcooled and saturated nuclear boiling: Thom correlation	

3.2.2. Thermal Hydraulic Results of Whole Core Model

3.2.2.1. Reference Solid Fuel and Annular Fuel at 100% Power

Figure 3-9 shows the DNBR profile in hot channels for both cores. The values of DNBR that are greater than 10 are assumed to be 10. For the reference PWR with solid fuel, MDNBR is 1.582 which satisfies the 1.3 limit with margin, as expected. For annular fuel model at 100% power, MDNBR of the inner hot channel is 1.625 and that of the outer hot channel is 2.793. It can be observed that the annular fuel design has larger MDNBR than the conventional solid fuel design. The main reason is that the fuel surface of annular fuel is significantly larger due to internal cooling. Thus, at the same power level, annular fuel design has thermal hydraulic advantages because of the larger safety margin.

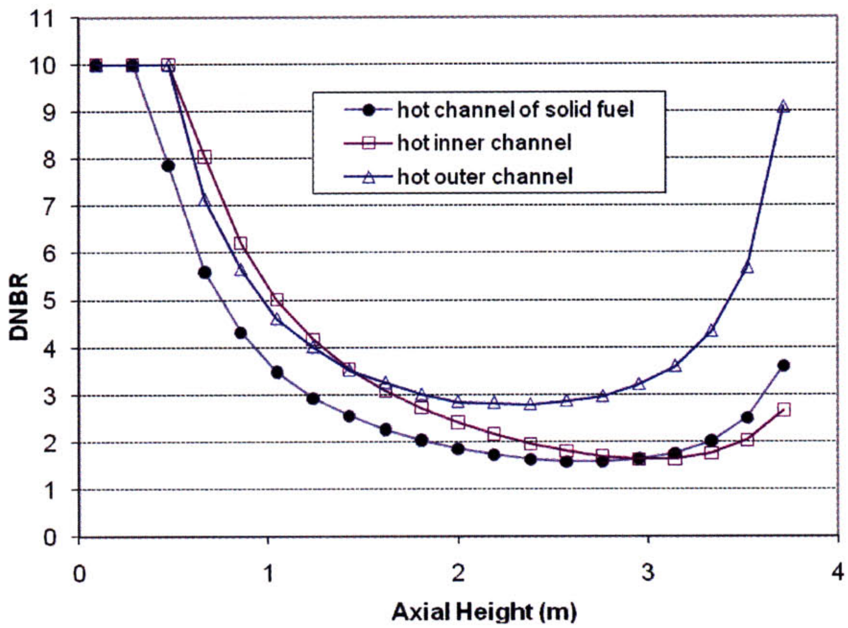

Figure 3-9: DNBR profile along the axial height in hot channels (100% power)

However, it should be noted that for annular fuel, MDNBR of the outer hot channel is much larger than that of the inner hot channel. The highly imbalanced MDNBR suggests that the original design is not well optimized.

Figure 3-10 shows the surface heat flux profile in the hot channels for both cases at 100% power. As expected, the heat flux is smaller for annular fuel due to larger fuel surface area. The higher heat flux of the inner hot channel is partially responsible for lower MDNBR, compared to the hot outer channel. Figure 3-11 compares the equilibrium quality in all three hot channels. It can be seen that the hot inner channel is the hottest channel because of highest equilibrium quality. But since it has the highest mass flux at the same time, shown in Figure 3-12, its MDNBR is still larger than that of the hot channel of the solid fuel.

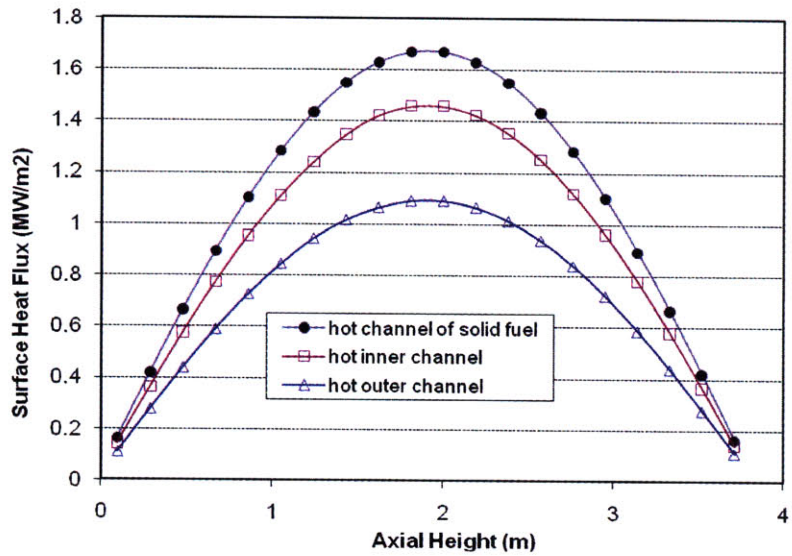

Figure 3-10: Surface heat flux profile along the axial height in hot channels (100% power)

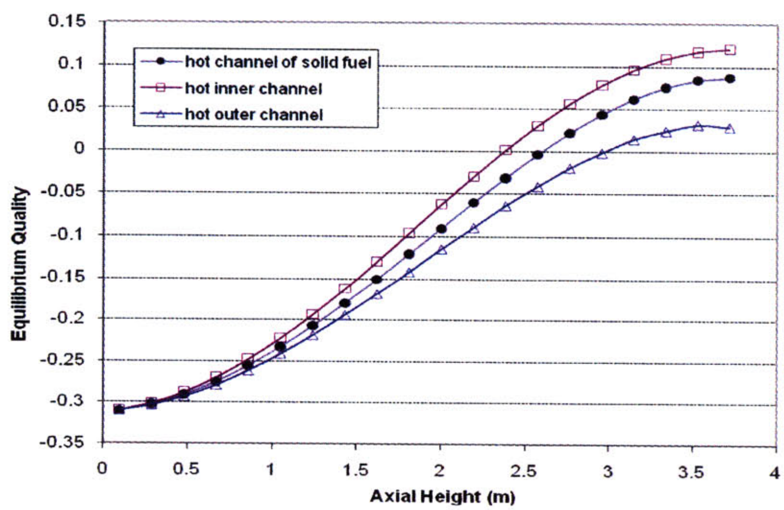

Figure 3-11: Equilibrium quality along the axial height in hot channels (100% power)

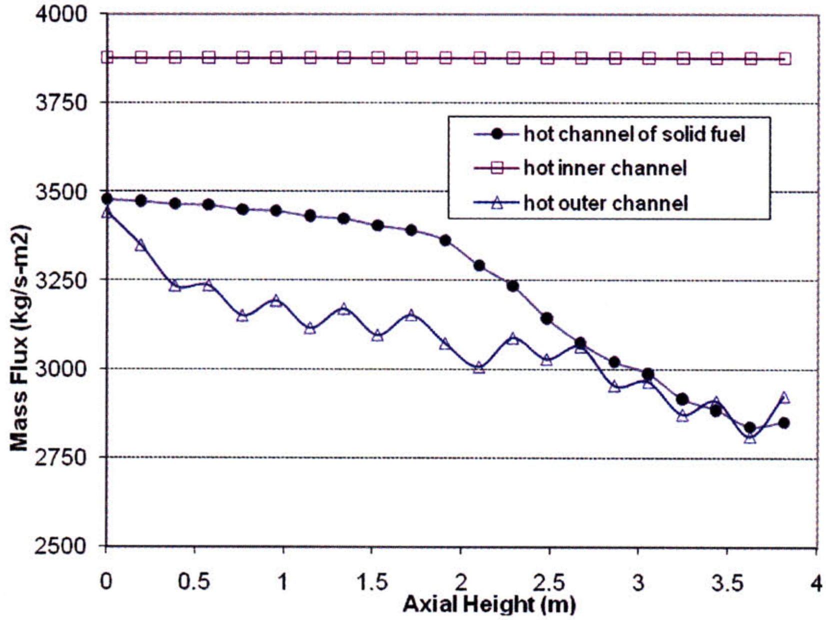

Figure 3-12: Mass flux profile along the axial height in hot channels (100% power)

3.2.2.2. **Annular Fuel at 120% Power**

VIPRE-01 results for the annular fuel show that at 120% power case, MDNBR of the inner channel is only 0.665, which is less than 1 and not acceptable. Moreover, the MDNBR in the outer channel is 2.110, confirming the high imbalance of DNBR between the inner and outer channels, as shown in Figure 3-13.

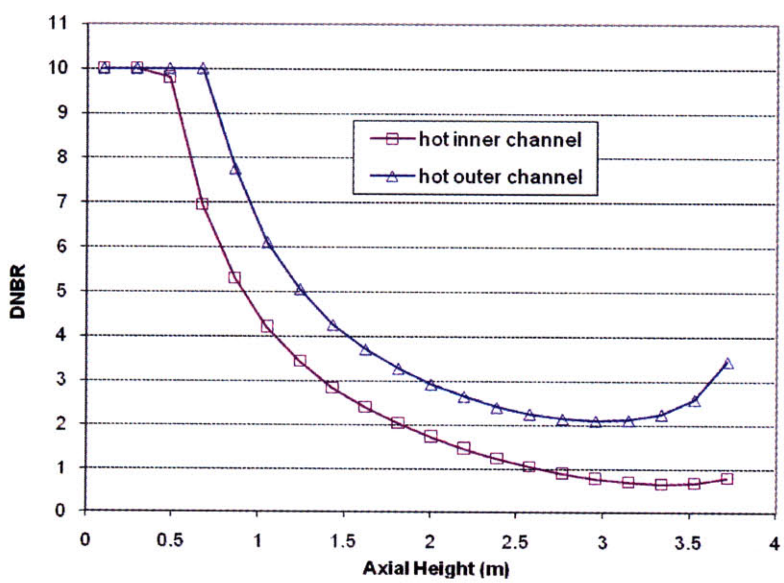

Figure 3-13: DNBR profile along the axial height in hot channels (120% power)

To maintain the same coolant outlet temperature, the inlet temperature has to be decreased from 298°C (568.4°F) to 289.7°C (553.5°F) for the 120% power case. Other conditions such as mass flow rate are unchanged.

The locations of hot channels and hot rods, MDNBR and exit equilibrium quality in both models are summarized in Table 3-2. The original annular fuel design, although it has thermal hydraulic merits compared to the conventional solid fuel, cannot achieve desirable 20% power uprate because of the imbalance of MDNBRs.

Table 3-2: Results of VIPRE-01 whole core models of solid fuel and 12x12 annular fuel

	Solid fuel	**12x12 Annular fuel**			
		100% power		**120% power**	
		Inner channel	**Outer channel**	**Inner channel**	**Outer channel**
Hot channel No.	12	31	1	31	4
Hot rod No.	18	1	1	1	1
MDNBR	1.582	1.625	2.793	0.665	2.110
Exit equilibrium quality	0.0871	0.1207	0.0293	0.2125	0.175

3.3. Thermal Hydraulic Analysis of the 14x14 Annular Fuel

3.3.1. VIPRE-01 Model description

The proposed 14x14 annular fuel design is similar to the 12x12 annular fuel assembly. The major difference is the replacement of the circular guide tubes with cruciform guide tube in the corners. The VIPRE-01 calculation of 14x14 annular fuel design adopts the same physical model as the previous 12x12 annular fuel design. The dimensions, pin power distribution, and subchannel arrangement of hot assembly needed to be changed. The pin peaking factors shown in Figure 3-14 are derived from the pin power distribution calculated by MCNP using energy deposition tally with maximum core-wide peaking factor of 1.55, which is the same value for the 12x12 annular fuel and solid fuel design. The dimensions of fuel pins and guide tubes are summarized in Chapter 2. The width and height of the corner cruciform guide tube (as defined in Figure 3-14) are 14.2 mm and 14.6 mm, respectively.

The sub-channel and rod numbering scheme of hot assembly with one-eighth symmetry is shown in Figure 3-14. It is assumed that there is no bypass flow into the guide tube along the axial direction.

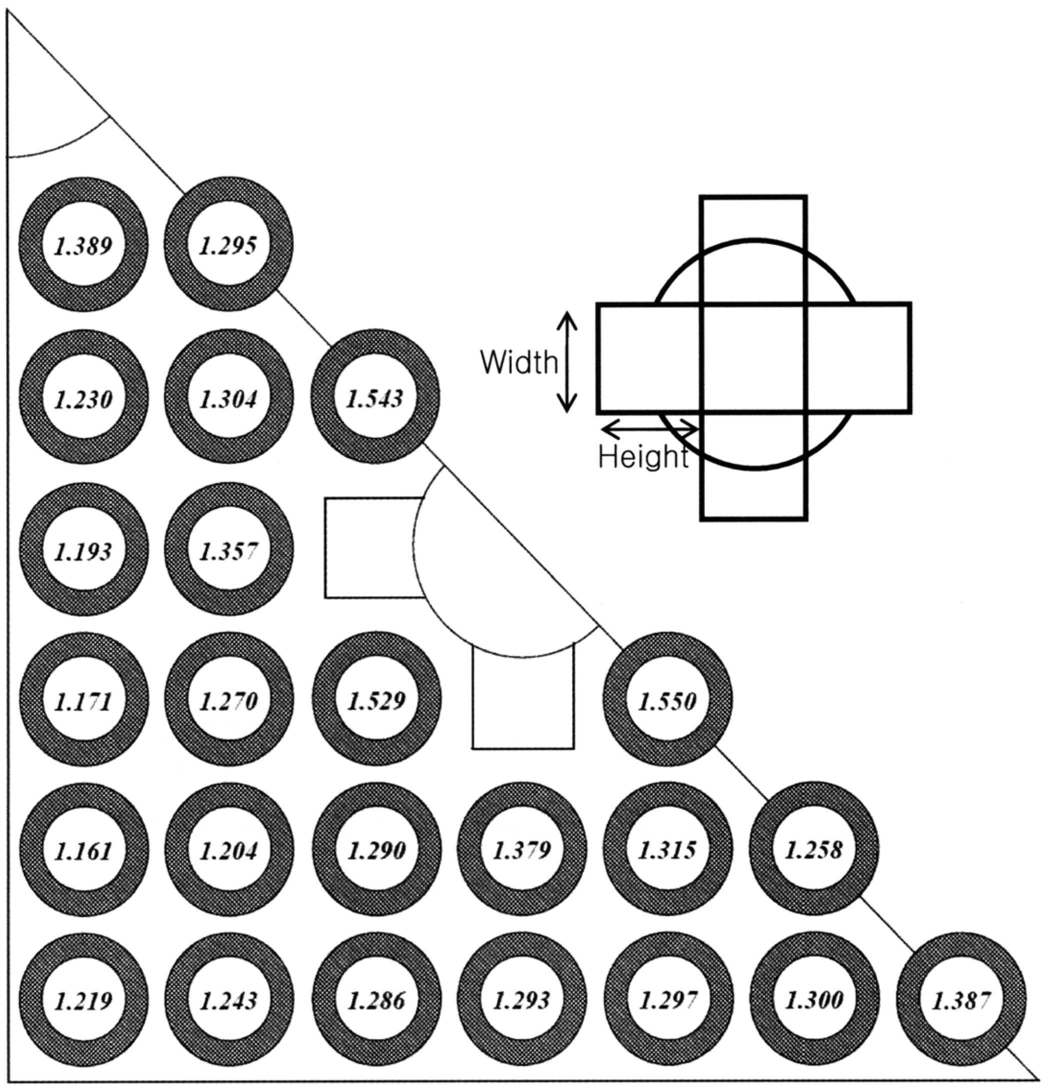

Figure 3-14: Pin power distribution in the hot assembly of 14x14 annular fuel design

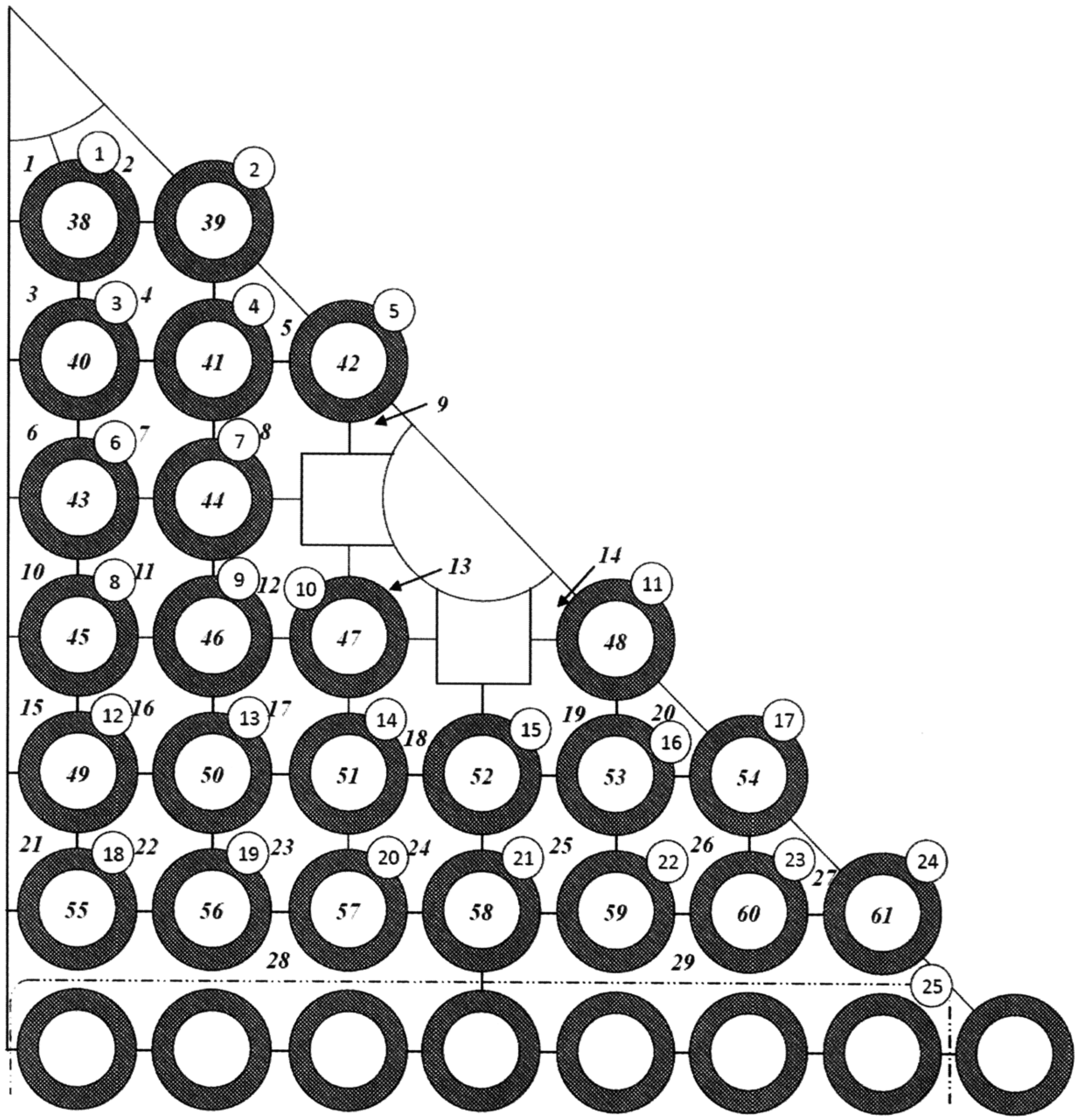

Figure 3-15: Numbering scheme of channels and rods in the hot assembly of 14x14 annular fuel design

3.3.2. **Thermal Hydraulic Results**

The results show that the MDNBR of the outer hot channel (Channel Number 14) is well below 1.3 for 100% power, which means this design cannot offer sufficient safety margin to allow the power uprate. By locating burnable poison rods at pins facing the inner corner of each cruciform guide tube, one would reduce the power peaking, which could possibly accommodate higher power rating. As shown in Table 3-3, two other power peaking have also been investigated: peaking factor of pin No. 5 changed to that of pin No. 2, 1.295, and peaking factor of pin No. 11 replaced by that of No. 17, 1.258 (Type 1); peaking factor of pins No. 5, 10, and 11 all changed to that of pin No. 17, 1.258 (Type 2). Results show that for the 14x14 original geometry, even after reducing the peaking factors, power uprating still cannot be obtained. MDNBR either fails in the outer channel No. 9, 13, or 14, or it fails in the inner channel 42, 47, or 48. For power peaking of Type 2, the inner MDNBR is below the 1.3 limit in Channel 52 for 6000/6000 W/ m^{2}-K (inner/outer) gap conductance when the power is over 100%. VIPRE-01 results show that the inner channel of the proposed 14x14 annular fuel design cannot provide sufficient flow for 20% power uprating, even if the MDNBR of the outer channel is satisfied. Basically, it can be concluded that the inner channel of the 14x14 annular fuel design is not large enough to accommodate sufficient flow to cool the inner surface of the annular fuel. Thus, the 14x14 annular fuel design is not promising for potential power uprate and the major focus should be on the more promising 12x12 array.

Table 3-3: MDNBR for the original proposed 14x14 annular fuel assembly

Power peaking	Gap conductance W/ m^{2}-K	Average power/rod (kW/rod)	MDNBR inner	MDNBR outer	Compared to reference power
Original	3500/7000	80	6.456	**0.625**	73.32%
	6000/6000	90	2.424	**0.577**	82.49%
Type 1	3500/7000	95	4.551	**0.642**	87.07%
	6000/6000	105	**0.352**	1.708	96.23%
Type 2	3500/7000	95	5.780	2.169	87.07%
		97	6.669	**1.107**	88.90%
	6000/6000	105	1.687	2.932	96.23%
		110	**1.204**	1.600	100.82%

3.4. Optimization Study

As discussed above, the original 12x12 annular fuel design cannot satisfy the MDNBR margin for 20% power uprate due to high imbalance of DNBRs between the inner and outer channels. Thus, an optimization study was performed to eliminate this imbalance and improve the original 12x12 annular fuel design.

The first possible option to optimize the design is to identify a better rod array configuration within an assembly. However, the requirement of keeping the large guide tube positions fixed offers fewer choices than for the MIT redesign of the Westinghouse 17x17 array, where the size and number of guide tubes was open for optimization. In the OPR1000 design, the assembly pitch is fixed as well as the locations of five guide tubes in the assembly. The central guide tube is located at the center of the whole assembly, and the other four are located at the center of their quadrants. Therefore, the array sizes should be multiples of 4, namely 8, 12, and 16. However, for an 8x8 assembly array, the guide tube would take up more than 30% volume of the whole assembly, which means the fuel volume would be too small. The 16x16 array would require very small inside channel (even the 14x14 array has insufficient inner channel flow), which is undesirable. Thus, the only available assembly array for a possible annular fuel design is the 12x12, as proposed by KAERI.

The second way to improve the design is to adjust the rod geometry for MDNBR balance. The goal is to obtain a well-balanced and acceptable MDNBR for the hot inner and outer channels. In addition, to maximize the fuel cycle length, it is desirable to maximize the fuel volume. Moreover, the moderator-to-fuel ratio should be kept the same as for the reference solid fuel design, to keep reactor physics parameters near the conventional OPR-1000.

For all calculations of different annular fuel rod dimensions, the cladding thickness and gap width were unchanged. Because the heat split between the inner and outer surface of the annular fuel is largely dependent on the gap conductance, which is still not very clearly understood in the literature, the optimization is investigated based on two different pairs of inner and outer gap conductances.

3.4.1. Inner/Outer Gap Conductance (6000/6000)

Nine different cases were examined with the dimensions shown in Table 3-4 with inner/outer gap conductance of 6000/6000 W/m^2-K. All cases are assumed at hot dimensions. Note that V_{fa}/V_{fs} is the fuel volume ratio of annular and solid fuel, V_c/V_f is the coolant to fuel ratio. Basically, we want larger fuel volume ratio between annular fuel and solid fuel, V_{fa}/V_{fs}, for neutronics reasons; and higher surface ratio between annular fuel and solid fuel, S_a/S_s, for heat transfer consideration; and similar coolant to fuel ratio, V_c/V_s, to maintain similar neutron spectrum to the solid fuel.

Table 3-4: Geometries of Alternative Designs of 12x12 Array Size

	$\frac{V_{fa}}{V_{fs}}$	$\frac{(V_c/V_f)_a}{(V_c/V_f)_s}$	$\frac{S_a}{S_s}$	**D_{coo}**	**D_{coi}**	**D_{fo}**	**D_{fi}**	**D_{cio}**	**D_{cii}**
				cm	cm	cm	cm	cm	cm
1	0.856	1.0557	1.366	1.590	1.466	1.452	1.008	0.994	0.880
2	0.883	1.0049	1.374	1.603	1.479	1.465	1.0094	0.9954	0.8814
3	0.885	1.0010	1.376	1.605	1.481	1.467	1.011	0.997	0.883
4	0.885	1.0006	1.379	1.607	1.483	1.469	1.014	1.000	0.886
5	0.884	1.0018	1.380	1.608	1.484	1.470	1.016	1.002	0.888
6	0.884	1.0015	1.383	1.610	1.486	1.472	1.019	1.005	0.891
7	0.850	1.0594	1.395	1.610	1.486	1.472	1.040	1.026	0.912
8	0.857	1.0463	1.397	1.613	1.489	1.475	1.040	1.026	0.912
9	0.858	1.0451	1.392	1.610	1.486	1.472	1.035	1.021	0.907

Case 1 is the original KAERI 12x12 array design. The inner and outer rod diameters are gradually increased while the thickness of the fuel is decreased from case 2 to case 8. All cases have a fixed pitch of 1.713 cm, i.e., the same as for the KAERI design. Increasing rod dimensions results in a reduced gap between the rods. Case 8 has the smallest gap between the rods of 1 mm. It was assumed that 1mm gap size is the smallest for which the grids can be manufactured. Case 9 is calculated as a reference for case 8 with smaller rod diameter and larger grid form loss coefficient.

The one rod model is first used to identify the best design because the dimension adjustments are much simpler than the whole core model. The results of MDNBR calculation can be found in Table 3-5. The single rod model shows that Case 4 yields the best balanced MDNBRs. A whole core model is then used to obtain more accurate results for selected cases. The core flow redistribution provides smaller MDNBRs as in earlier MIT studies of the Westinghouse design. Cases 6 through 8 show that as inner and outer rod diameters increase, MDNBR of the inner channel would be increased and that of the outer channel would be decreased. Moreover, even Case 8 having minimum gap of 1mm does not yield fully balanced MDNBR. This is because the large guide tubes allow more bypass flow through guide tube subchannels reducing the MDNBR margin. In reality, the guide tubes will have very tight inlet orifices to allow very small flow for cooling, but this was not modeled, since the details of the orifice design were not available.

Table 3-5: MDNBR Values of Alternative Designs at 120% power

	MDNBR single rod model		**MDNBR whole core model**		**Average Pressure drop (KPa)**
	Outer	**Inner**	**Outer**	**Inner**	
1	2.377	1.815	2.110	**0.665**	(failed)
2	2.247	2.058			(failed)
3	2.212	2.108			(failed)
4	2.160	2.166	1.897	**1.048**	(failed)
5	2.120	2.209			(failed)
6	2.075	2.258	1.826	**1.159**	(failed)
7	1.867	2.405	1.675	1.347	135.015
8	1.813	2.453	1.623	1.421	136.404

Case 8 was taken as the new base case since it yields the best performance in terms of well balanced and acceptable MDNBRs for both inner and outer channels. It is also noted that because during irradiation the annular pellets tends to expand towards the outer cladding, closing the outer gap earlier and increasing outer heat flux, the larger outer MDNBR is desirable since it provides larger margin to accommodate heat flux increase due to this repositioning.

Table 3-6: MDNBR Values of Case 9 at 120% power

	Grid form loss coefficient	MDNBR whole core model		Average Pressure drop (KPa)
		Outer	Inner	
9	0.60	1.708	1.299	136.2873
	0.65	1.652	1.387	138.2634
	0.70	1.589	1.474	140.1574
	0.75	1.527	1.560	142.0589

If a 1 mm gap is found to be too small from a manufacturing perspective, an alternative design with slightly increased gap would be needed. This was also evaluated, as shown in Table 3-6. To force more flow in the inner channel, the grid form loss coefficient was gradually increased. When it reaches the value of 0.70 ~ 0.75, well balanced MDNBRs were achieved. In addition, the results of MDNBR are better balanced than Case 8. It is easy to manufacture grids with higher loss coefficient. The penalty is a slightly higher core pressure drop.

3.4.2. Inner/Outer Gap Conductance (3500/7000)

It has been found using FRAPCON-ANNULAR model that the annular fuel pellet would expand outwardly when heated up [Yuan et al., 2007]. Thus, the outer gap conductance would tend to be larger than the inner gap conductance. KAERI proposed to use the value 3500 W/m^2-K as the inner gap conductance and 7000 W/m^2-K for the outer gap. The same optimization procedure is done to search the best design. Table 3-7 lists two additional cases (case 1 is for the original geometry) that are investigated to get better MDNBR in the inner and outer channels in the whole core model. Note that the rod-to-rod gap slightly increases because of the reduction of the rod outer diameter. Thus, manufacture of spacer grids should be feasible for these smaller rods.

Table 3-7: Geometries of alternative pin designs for 12x12 annular fuel assembly

	$\frac{V_{fa}}{V_{fs}}$	$\frac{(V_c/V_f)_a}{(V_c/V_f)_s}$	$\frac{S_a}{S_s}$	**Rod gap**	**D_{coo}**	**D_{coi}**	**D_{fo}**	**D_{fi}**	**D_{cio}**	**D_{cii}**
				cm	cm	cm	cm	cm	cm	cm
1	0.8560	1.0557	1.366	0.123	1.590	1.466	1.452	1.008	0.994	0.880
2	0.8765	1.0228	1.345	0.133	1.580	1.456	1.442	0.980	0.966	0.852
3	0.8843	1.0126	1.328	0.143	1.570	1.446	1.432	0.960	0.946	0.832

Results of the alternative designs are shown in Table 3-8. MDNBRs of the inner channel and outer channel in case 2 and 3 are all above the 1.3 limit for 20% power uprating, while the values of pressure drop are very close in these three cases. Therefore, the goal of power uprate of 120% can be reached with 12x12 designs, assuming the 3500/7000 W/m^2-K conductance imbalance. Case 2 is preferred because it has larger margin in the outer channels.

Table 3-8: MDNBR and pressure drop of alternative designs for 12x12 annular fuel assembly

	Gap conductance Inner/outer (W/m2-K)	**MDNBR whole core model**		**Average Pressure drop (KPa)**
		Outer	**Inner**	
1	3500/7000	1.058	2.444	140.8599
2		1.453	1.871	139.3431
3		1.658	1.361	140.2394

3.4.3. Sensitivity to Manufactoring Tolerance

It can be seen from Tables 3-5 and 3-6 that MDNBR results are relatively sensitive to diameter changes. The main reason is that both the inner and outer rod diameters had to be increased or decreased at the same time to keep the same fuel volume. The sensitivity would be smaller if only the inner or the outer diameter was changed, or if they were changed in opposite directions. This large sensitivity to dimensional changes raises a potential concern that manufacturing tolerance could possibly deteriorate the MDNBR margin.

Table 3-9: MDNBR sensitivity to manufacturing tolerance

	D_{coo}	D_{coi}	D_{fo}	D_{fi}	D_{cio}	D_{cii}	**MDNBR Whole core model**			
	cm	cm	cm	cm	cm	cm	Outer	changes	Inner	changes
8	1.613	1.489	1.475	1.040	1.026	0.912	1.623	--	1.421	--
--	1.610	1.486	1.472	1.037	1.023	0.909	1.633	0.6%	1.407	-1.0%
+	1.616	1.492	1.478	1.043	1.029	0.915	1.456	-10.3%	1.598	12.5%

Therefore, a sensitivity study was performed to quantify this effect. It is reported that the achievable manufacturing tolerance for the rod diameter is between ±0.002 and ±0.003 cm [Feng et al., 2007]. Two extreme cases with increasing and decreasing both the inner and outer diameters by 0.003 cm were calculated. MDNBR results shown in Table 3-9 are all acceptable and well balanced. Moreover, in reality the sensitivity should be smaller due to the random distribution of plus and minus tolerances of the inner and outer channels.

3.4.4. Sensitivity to Gap Conductance

During normal operation, the annular fuel pellet would expand, crack, swell, and relocate, which might fail to agree with the assumption made about the gap conductances. It is expected that after thermal expansion, the annular fuel would contact the outer cladding, which would increase the outer gap conductance [Yuan et al., 2007]. Sensitivity to gap conductance has been investigated by increasing the outer gap conductance while keeping the same value for the inner gap, which is 6000 W/m^2-K. Results show that MDNBR of the inner hot channel increases with the outer gap conductance, while that of the outer hot channel decreases. Both of them change linearly with the outer gap conductance. It can be seen that MDNBR is very sensitive to the asymmetry of gap conductance. This is because thermal resistance to the outer channel decreases as the outer gap conductance increases, which leads to higher heat flux through the outer surface of the annular fuel rod. This heat split becomes more serious if the gap conductance difference rises further. Figure 3-16 shows that MDNBR of the hot outer channel will decrease below 1.3 if the outer gap conductance increases to 7150 W/m^2-K. In other words, the outer gap conductance is only able to increase by less than 20% and still meet the thermal hydraulic safety requirement.

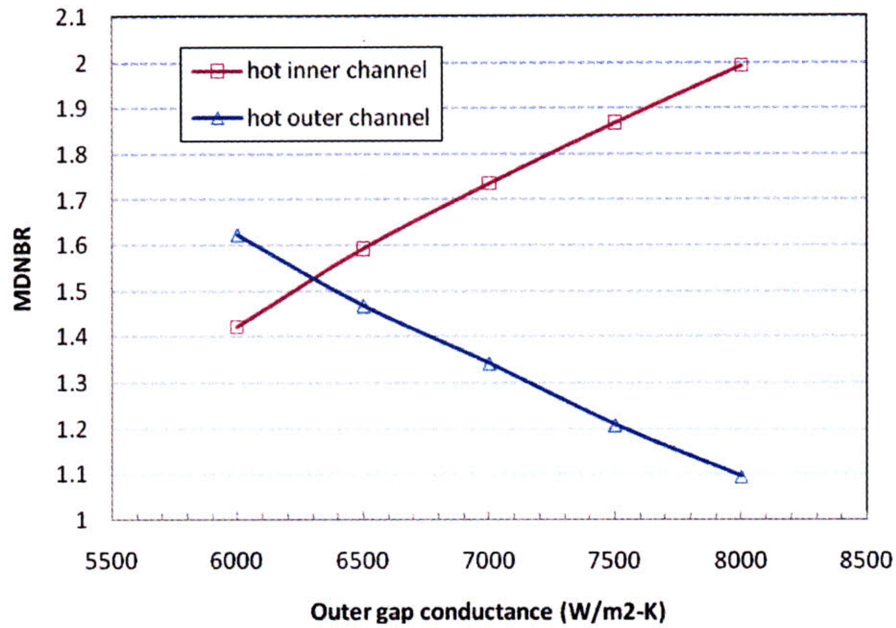

Figure 3-16: MDNBR sentivitity to outer gap conductance

3.5. Partial Blockage of Inner Channel

Due to the absence of lateral flow and mixing, the isolated inner channel raises questions about potential channel blockage and its consequences. This is a hypothetical scenario since all current PWRs are equipped with debris filters, which have typically a mesh size of 3mm, i.e., much smaller than the inner channel diameter of 9.1mm. Nevertheless, it is still important to evaluate the impact of partial blockage, which might involve two categories: blockage due to oxide and crud growth along axial length, and partial debris blockage at the inlet. All calculations are based on the optimized design (Case 8 with 6000/6000 gap conductance).

3.5.1. Corrosion and Crud model

To model the impact of corrosion and crud, a uniform layer of crud and zirconium oxide is added on the inner and outer cladding surfaces of the hottest rod. It is a conservative model because [Feng, 2008]:

A. The level of corrosion that is modeled does not develop until the EOC, and it was assumed that the corroded hot rod would still have a BOC power density.

B. The corrosion layer will decrease the flow areas inside the hot rod resulting in a decrease in local coolant flow, consequently a significant rise in the coolant temperature.

C. The corrosion occurs along the entire height of the hot rod which is unlikely due to the non-uniform axial power profile.

D. The corrosion occurs only on the hot rod, increasing flow resistantce in the subchannels around it. Corrosion occurring on all fuel rods of the hot assembly would lead to more uniform flow and increased flow in the hot subchannels.

In the model, the oxide layer is assumed to be developed first and then a crud layer of equal thickness to be developed on top of it. This was done to simplify the VIPRE-01 input since the only required values were the thickness and thermal conductivity of each layer. Although the ZrO_2 and crud may form a homogeneous layer simultaneously, the thermal conductivity of this mixed layer is assumed to be the weighted average of the two compositions and thus would not change the heat conduction through this layer.

Because ZrO_2 has larger molecular mass (123 g/mol) and lower density (5.9 g/cm^3) than Zr metal (91 g/mol and 6.4 g/cm^3), the corroded part of the cladding will increase in volume. Assuming that the corrosion thickness is δ_{Zr}, the original outer diameter is D_0, and D_1 is the diameter inside the ZrO_2 layer, then the outer cladding, they satisfy:

$$D_1 = D_0 - 2\delta_{Zr}.$$

Assume that D_2 is the cladding diameter after corrosion, V, M, A and ρ represent the volume, mass, molecular mass, and density respectively. For the outer cladding the conservation of the mass of Zr leads to:

$$\frac{\pi}{4}(D_0^2 - D_1^2)\rho_{Zr} = \frac{\pi}{4}(D_2^2 - D_1^2)\rho_{ZrO_2}\frac{A_{Zr}}{A_{ZrO_2}},$$

or

$$D_2 = \sqrt{D_1^2 + (D_0^2 - D_1^2)\frac{\rho_{Zr}A_{ZrO_2}}{\rho_{ZrO_2}A_{Zr}}}.$$

Similarly, for the inner cladding, we can get:

$$D_1 = D_0 + 2\delta_{Zr}$$

and

$$D_2 = \sqrt{D_1^2 - (D_1^2 - D_0^2)\frac{\rho_{Zr}A_{ZrO_2}}{\rho_{ZrO_2}A_{Zr}}},$$

where the meaning of each variable is similar to that in the expression for the outer cladding, except now D_0 is the inner diameter of the inner cladding. The labeling scheme is illustrated in Figure 3-17.

Another important value is the total thickness of the zirconium oxide layer t:

$$t = \frac{|D_2 - D_1|}{2}.$$

It should be noted that the inner t and outer t values will be different but extremely close for δ_{Zr}, less than 100μm. For example, assuming a corrosion thickness of 20μm, the values of the various diameters D_0, D_1, and D_2 are shown in Table 3-10.

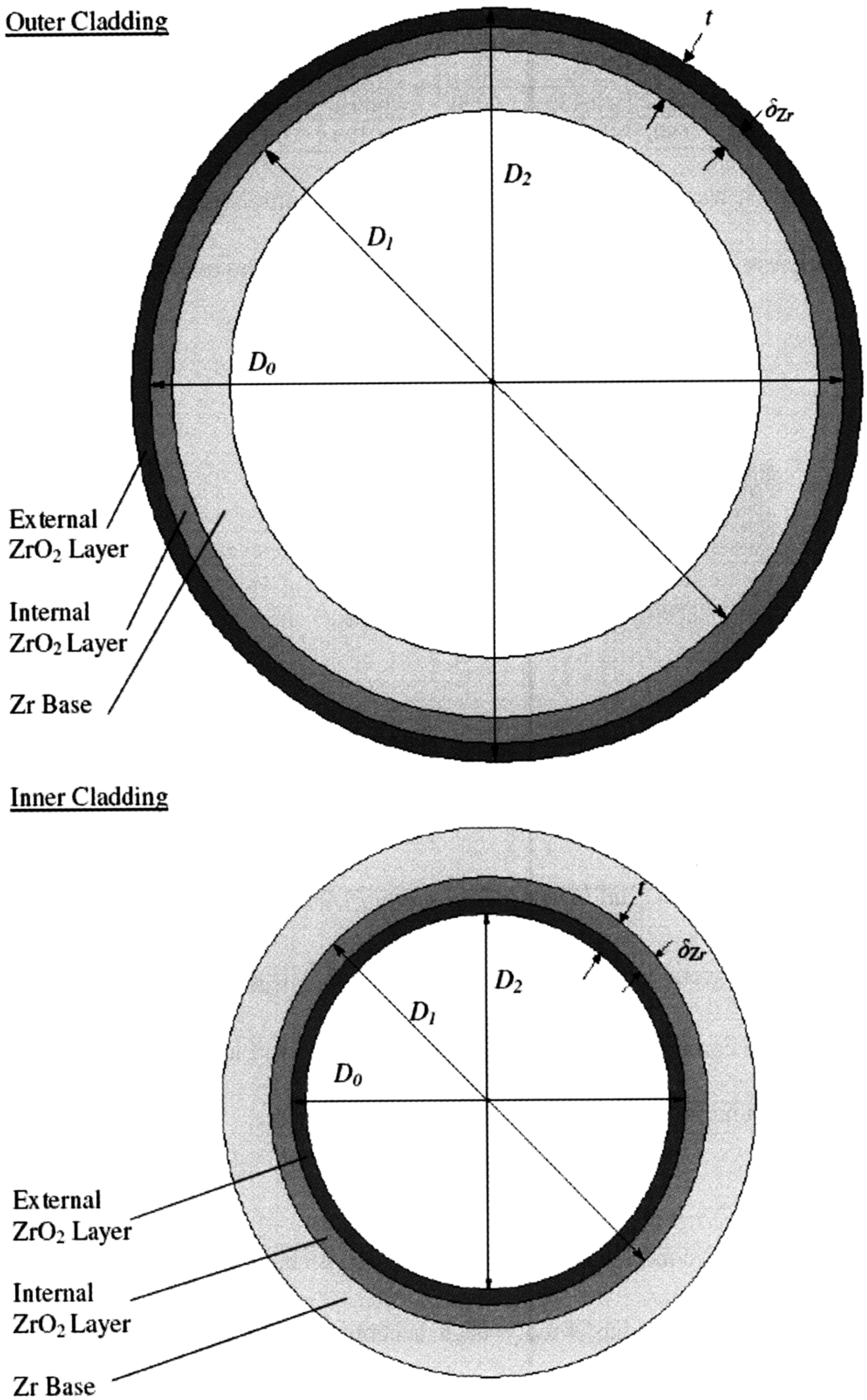

Figure 3-17: Outer and Inner cladding labeling scheme for ZrO_2 development (not drawn to scale) (from [Feng, 2008])

Table 3-10: Diameter changes after zirconium oxidation

	δ_{Zr}	D_0	D_1	D_2	t
Outer cladding (cm)	0.002	1.6130	1.6090	1.614861	0.002931
Inner cladding (cm)	0.002	0.9120	0.9160	0.910129	0.002935

In the VIPRE-01 model, it was assumed that on top of this zirconium oxide layer was an additional crud layer of thickness δ_C which was equal to δ_{Zr}. The profile of the crud/oxide layer is illustrated in Figure 3-18.

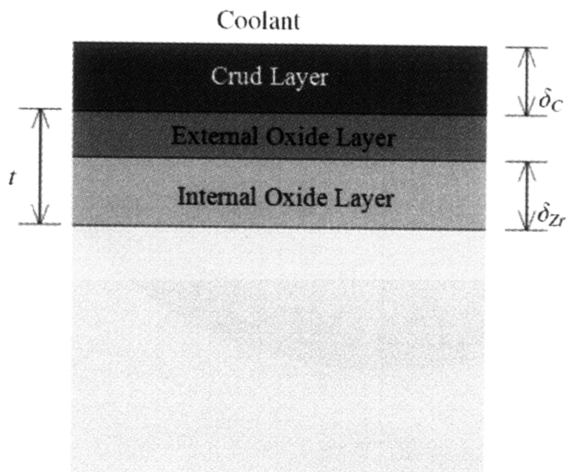

Figure 3-18: Profile of ZrO_2 and crud layers (not to scale) (from [Feng, 2008])

For this study, δ_C and δ_{Zr} were varied simultaneously in the VIPRE-01 model from 10μm to 50μm, but ultimately the combined thickness L of the ZrO_2 and crud layers correspond to the thickness of the deposits found in PWR cladding surface scrapes where:

$$L = t + \delta_C .$$

So for the case of δ_C being 20μm, the combined corrosion thickness L is about 49μm.

The thermal conductivity of ZrO_2 has widely been accepted to be about 2 W/m-K. However, the thermal conductivity of crud from reactors has never been measured in its purest form. Due to its complex structure and the uncertainty of its composition varying from different reactors, the thermal properties can only be estimated or partially measured. For the purpose of this study, various thermal conductivities ranging from 0.75 to 2 W/m-K were used to account for this uncertainty. The conductivity of crud is assumed to be lower than that of ZrO_2 because of its greater porosity.

MDNBR results for the inner and outer channels at different corrosion levels and various crud conductivities are shown in Table 3-11 and 3-12. The position of MDNBR is at channel No. 31 for the inner channel, and channel No. 3 for the outer channel. It can be found from Figure 3-19 that the MDNBR margin would be below its limit for the optimized design for a combined corrosion thickness above about 74μm~94μm. As the corrosion thickness grows, the inner channel tends to have lower MDNBR at low crud thermal conductivities (less than 1W/m-K), while for high crud thermal conductivity the outer hot channel MDNBR would fall below the limit of 1.3 earlier than the inner hot channel.

Table 3-11 MDNBR of the inner channel as a function of combined corrosion thickness and crud thermal conductivity

δ_C (μm)	L (μm)	Crud thermal conductivity (W/m-K)			
		0.75	**1**	**1.5**	**2**
10	24.66945	1.414	1.403	1.392	1.387
20	49.35394	1.395	1.376	1.356	1.346
30	74.05351	1.372	1.345	1.318	1.304
40	98.7682	1.346	1.313	1.279	1.261
50	123.4981	1.317	1.279	1.238	1.217

Table 3-12: MDNBR of the outer channel as a function of combined corrosion thickness and crud thermal conductivity

δ_C (μm)	L (μm)	Crud thermal conductivity (W/m-K)			
		0.75	**1**	**1.5**	**2**
10	24.66945	1.553	1.558	1.563	1.566
20	49.35394	1.473	1.479	1.488	1.493
30	74.05351	1.378	1.393	1.41	1.418
40	98.7682	1.27	1.29	1.307	1.318
50	123.4981	1.154	1.176	1.201	1.215

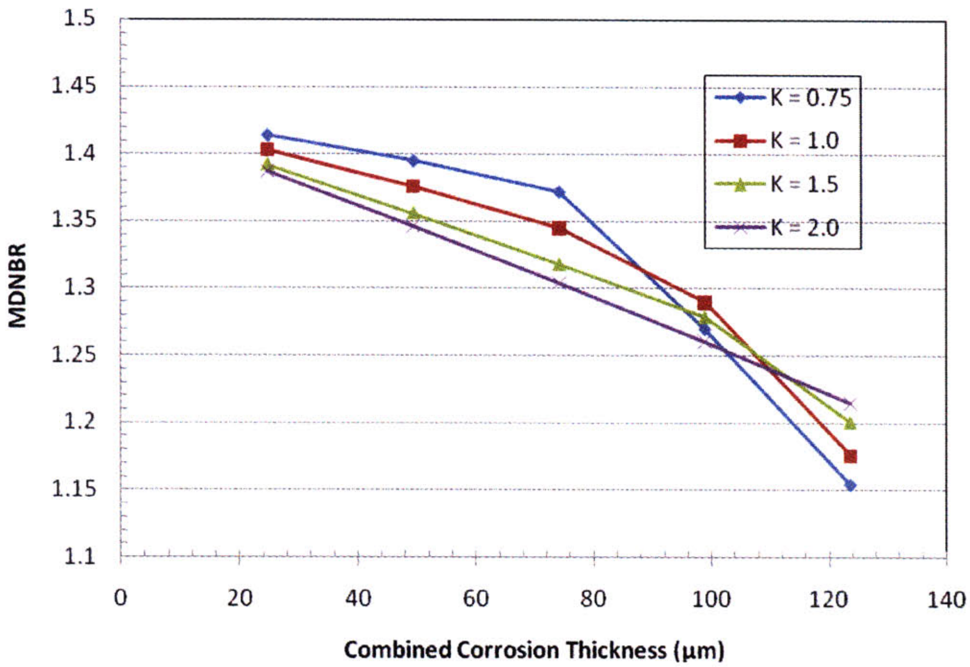

Figure 3-19: MDNBR as a function of combined corrosion thickness

As expected, the MDNBR for all cases occur at the same axial location as that for the corrosion-free case. It is interesting to note that as the crud thermal conductivity increases, the inner MDNBR decreases while the outer MDNBR slightly increases. This is attributed to the unequal heat split due to the annular geometry. An increase in crud thermal conductivity leads to a greater decrease in the thermal resistance of the inner cladding than that of the outer cladding. This is because the outer cladding has a smaller ratio of cladding outer diameter to cladding inner diameter in the thermal resistance equation. Thus, as the crud thermal conductivity increases, more heat from the fuel is conducted through the inner cladding.

As the combined corrosion thickness increases, the flow area of the hot inner and outer channels decreases, which results in an increase in the local pressure drop. To maintain the same pressure drop, the flow through the hot channel is redistributed to other parts of the core, thus decreasing the mass flux, as shown in Figure 3-20. Overall, increasing the thickness will decrease the MDNBR for any value for thermal conductivity.

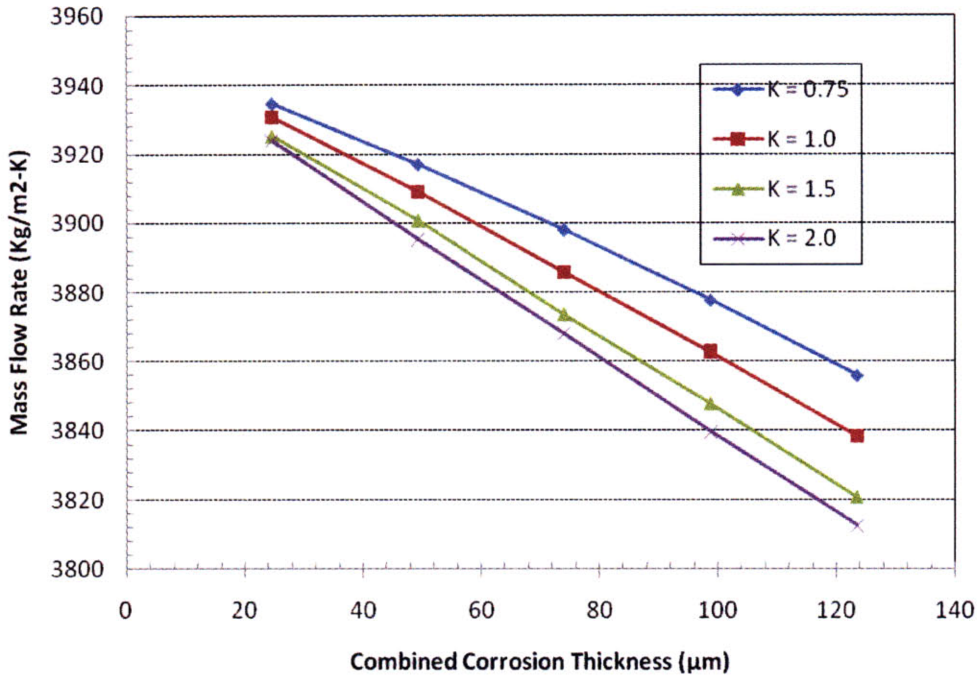

Figure 3-20: Mass flow rate of hot inner channel as a function of corrosion thickness

3.5.2. Partial blockage at the Inlet

For the case of inner channel blockage, it was assumed that, in the unlikely event that inlet debris filters failed in a PWR, a hypothetical large particle would partially block the inner channel of the hot rod. The VIPRE-01 model was again used to simulate this event to determine the largest fractional channel blockage that can be allowed. All assumptions and parameters from the optimized model were kept the same except for the overpower transient factor that is used to approximate DNBR under loss of flow transient in steady state calculations. This factor was reduced from 118% to 105% since a blockage accident and loss of flow event are highly unlikely to occur simultaneously.

The entrance blockage was modeled as an increase in the entrance form loss coefficient K_0 using a correlation for flow through an orifice plate at a pipe entrance from [Idelchik, 1993]. The geometry is described in Figure 3-21 and the calculated values for K_0 as a function of the orifice area to channel area ratio, f are shown in Table 3-13 and Figure 3.22. The relationship between K_0 and the channel pressure drop can be described as

$$\Delta P = K_0 \frac{\dot{m}}{2\rho A_c^2}$$

where ΔP is the pressure drop of hot channel, $\dot{m}$ is the mass flow rate through the channel, ρ is the coolant density, and A_c is the flow area of the channel.

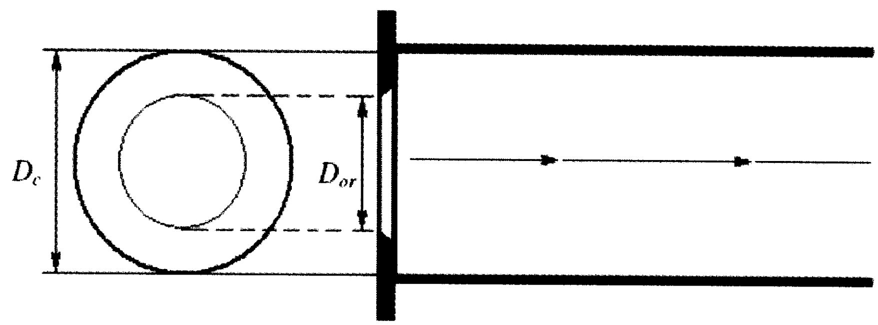

$$f = \frac{A_{or}}{A_c},\ A_{or} = \frac{\pi D_{or}^2}{4},\ A_c = \frac{\pi D_c^2}{4}$$

Figure 3-21: Geometry of correlation used for entrance channel blockage (from [Feng, 2008])

Table 3-13: Entrance form loss coefficient as a function of ratio between orifice and channel areas [Idelchik, 1993]

f	0.05	0.1	0.15	0.2	0.25	0.3	0.35	0.4	0.45
K_0	1100	258	98	57	38	24	15	11	7.8

f	0.5	0.55	0.6	0.65	0.7	0.75	0.8	0.9	1
K_0	5.8	4.4	3.5	2.6	2	1.7	1.3	0.8	0.4

This was the preferred approach as opposed to decreasing the entrance channel area in the VIPFRE-01 model, because to simulate the effects of an entrance flow constriction, the area decrease must be modeled in the axial node after the entrance. This is because VIPRE-01 uses the hydraulic properties of the preceding node in order to calculate the velocity and mass flow for the current node. This would assume that the flow constriction occurs at the end of the first node which would be inaccurate. Thus, the additional form loss resulting from the entrance blockage was calculated outside of the code to ensure that the VIPRE-01 model captures the desired change correctly.

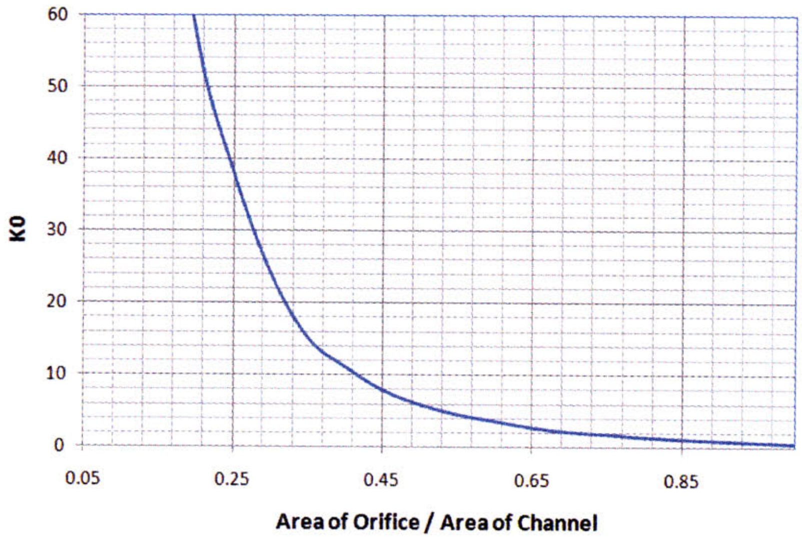

Figure 3-22: Regression function of Idelchik's entrance form loss correlation

The entrance form loss coefficient was gradually increased from 0.4 (no blockage) until the MDNBR dropped below 1.3, and then the corresponding f was approximated using Figure 3-22 and Table 3-13. The results are shown in Table 3-14:

Table 3-14: Effect of entrance blockage on MDNBR

K_0	f	hot inner channel		hot outer channel		
		MDNBR	mass flux (kg/s-m^2)	MDNBR	inlet mass flux (kg/s-m^2)	outlet mass flux (kg/s-m^2)
0.4	1	2.64	4443.239	2.722	3370.406	2408.789
1.3	0.8	2.18	4005.154	2.721	3370.406	2407.433
2.6	0.65	1.696	3579.276	2.72	3370.406	2407.433
3.5	0.6	1.431	3363.624	2.712	3370.406	2406.076
4	0.572	1.305	3264.614	2.712	3370.406	2406.076
4.1	0.567	1.281	3246.982	2.712	3370.406	2406.076

As the blockage increases, the mass flux decreases due to the whole core flow redistribution to accommodate equal pressure drops across each channel. The decreased mass flux was unable to remove as much heat from the inner channel, thus decreasing the MDNBR. The maximum blockage allowed under the assumed conditions was calculated to be about 43%. It can be inferred from Figure 3-22 that it becomes exponentially more difficult to accommodate blockages with area restriction greater than 45% regardless of the power level.

3.6. Summary

Whole core VIPRE-01 models for OPR-1000 with conventional solid fuel and with the proposed annular fuel design were developed. VIPRE-01 whole core results showed that the initial 12x12 KAERI annular fuel design has larger MDNBR margin than the solid fuel at 100% power. However, the whole core model show that the initial design could not achieve power uprate to 120% for fixed core flow rate and reduced core inlet temperature, due to lower than desirable MDNBR in the inner channel. Furthermore, the design had an imbalanced MDNBR between the inner and outer channels, as the diameter of the inner channel does not allow sufficient flow rate through the inner channel. The thermal hydraulic feasibility of an alternative design option having an array of 14x14 annular fuel was then explored. This optionwas conclude to be an unpromising design because of insufficient flow in the inner channel. The thermal hydraulic results of the 14x14 annular fuel design with asymmetric gap conductance are more promising since the MDNBR of the inner and outer channel are more balanced. However, 20% uprate still cannot be achieved through this geometry and its performance is inferior to that of the 12x12 design.

A search was then performed to identify a better optimized 12x12 design that would achieve 20% power uprate under two different pairs of assumed inner and outer gap conductances. This was accomplished through fine-tuning of the rod dimensions by slightly increasing the inner channel diameter and outer channel diameter, while keeping the fuel to moderator ratio fixed. The new dimensions of the OPR1000 annular fuel that can achieve sufficient MDNBR at 120% power are given in Table 3-4 and Table 3-7. Moreover, calculation of 12x12 annular fuel design with reduced inner gap conductance and increased outer gap conductance has been performed. In addition, MDNBR sensitivity to manufacturing tolerances was also investigated, showing that the new proposed design could accommodate typical manufacturing tolerances. Overall, rod geometry adjustment was shown to achieve a better MDNBR balance between the inner channel and outer channel with assymetrical gap conductance which can accommodate 20% power uprate. However, an important issue is the sensitivity of MDNBR to the gap conductance, and this was also investigated. Results show that MDNBR is very sensitive to the gap conductance and it needs further investigation.

Partial inlet blockage of the inner channel by debris and the impact of corrosion and crud growth along the entire axis were analyzed. Although an inner channel blockage is a hypothetical scenario due to the much smaller mesh size of the inlet debris filter than the inner channel diameter, it has been shown that the inner channel can accommodate a blockage of up to 43% of its flow area before MNDBR falls below the 1.3 limit. MDNBR results for the corrosion and crud growth show that the impact of crud and ZrO_2 buildup does not reduce MDNBR margin below the 1.3 limit, as long as the thickness is less than 74µm~94µm.

4. Reactor Physics Analysis

In order to complete the evaluation of OPR-1000 with annular fuel, the neutronic behavior needs to be assessed. Section 4.1 describes the tools used for the nuclear analyses. Section 4.2 describes the challenges of analyzing annular fuel, Section 4.3 presents the assembly-level benchmark calculations for both the solid fuel and annular fuel. Then, steady state whole core analysis of OPR-1000 with traditional solid fuel was performed using SIMULATE-03. The refueling strategies of Cycle 1 to Cycle 4 of Ulchin Unit 5, provided by KAERI, were analyzed as a benchmark for further annular fuel core analysis. The models and results of basic core physics parameters, e.g., critical boron concentration and power distribution, are documented in Section 4.4.

4.1. Reactor Physics Assessment Tools

Nowadays, many industrial LWR analysis codes are able to predict existing core performance accurately. One such tool is the core management system (CMS) code package developed by Studsvik, which consists of CASMO-4, TABLES-3, and SIMULATE-3. This code package adopts the deterministic, multi-group approach, and can accurately perform the whole core calculations in a relatively short time period. However, as found in earlier studies of annular fuel at MIT [Kazimi et al., 2001], CASMO-4 without modification cannot accurately calculate the annular fuel design. Thus, a Monte Carlo based method, which is realistic but computationally time-consuming, is needed to benchmark the results from the deterministic codes and determine adjustments needed to reproduce rigorous results. An in-house burnup code, MCODE-2.2, coupling MCNP-4C developed at Los Alamos National Laboratory and ORIGEN-2.2 developed at ORNL, is used for benchmark burnup analyses.

4.1.1. **CASMO-4**

CASMO-4 is a multi-group two dimensional transport theory code for burnup calculations of LWR lattices. As a deterministic lattice physics code, it is used for a geometry consisting of cylindrical fuel rods of varying composition in a square or hexagonal lattice with different conditions [Edenius et al., 1995]. CASMO is user friendly and is widely used in industry. Many default values are set for input quantities. Although the print-out is usually succinct, options for very detailed print-outs are provided.

In the first part, macroscopic group cross sections are directly calculated from input data, i.e. densities, geometries, for the next micro group calculations. The effective cross sections in the resonance energy region, which is defined to lie between 4 eV and 9118 eV, are calculated using an equivalence theorem which relates the particular heterogeneous problem to a simpler homogenous problem.

Using the macroscopic group cross sections, each type of pin can be associated with an individual neutron energy spectrum to be used for energy condensation by micro group calculations. Then, a 2D macro group calculation is performed, following the micro group calculation, which provides flux spectra for energy condensation for 2D calculation.

Based on the above steps, the generated data constitute the input to the 7 energy groups two-dimensional transport calculation, which yields the eigenvalue and the flux distribution. For a single assembly, a fundamental buckling mode which considers the leakage effect is used for updating the results that were obtained from the transport calculation. For each fuel pin and each region containing a burnable poison, isotopic depletion is performed.

For the burnup calculation, a predictor-corrector approach is adopted. For each burnup step, depletion is calculated twice, first using the neutron spectrum at the beginning of the step, and then using the updated neutron spectrum at the end of the step. For the next burnup step, values that are the average number densities from these two depletion calculations are used.

4.1.2. TABLES-3

A lot of CASMO runs are needed for a fuel segment under various core conditions. TABLES-3 is used to link those CASMO results to SIMULATE via reading CASMO card image files and producing a master binary library for SIMULATE use. The type of data processed by TABLES-3 include two group cross sections, discontinuity factors, fission product data, detector data, pin power reconstruction data, kinetics data, and isotopic data. Each type of data except the last three is expressed as a summation of partials from the base condition value, where each partial can be a function of three variables.

4.1.3. SIMULATE-3

SIMULATE-3 is an advanced three dimensional two group commercial code for LWR steady state core analysis. A coupled neutronics and thermal hydraulics iteration can be performed to obtain the detailed core power distribution.

In SIMULATE-3, the reactor core is represented by a number of nodes with homogenized parameters that are constructed from the lattice physics code, i.e., CASMO-4. Discontinuity factors were introduced as an additional artificial parameter to allow more degrees of freedom for simultaneous preservations of reaction rates and currents. The transverse-integrated flux distribution within a node was assumed to be able to be expressed as a fifth-degree polynomial with base functions given according to the moment weighting. In addition, it is assumed that the transverse leakage term can be represented by quadratic polynomials to preserve the average transverse leakage in each of three neighboring nodes. A non-linear iteration scheme is used to solve the coarse mesh finite difference equations. Then, assuming the global flux (homogeneous intra-nodel flux) and local flux (heterogeneous form functions) are separate, a pin power reconstruction can be performed by SIMULATE-3 [Cronin et al., 1995].

In a core analysis, feedback effects such as fuel temperature feedback and thermal hydraulic feedback have to be considered, since the reactor power, fuel temperature, and coolant density distributions are closely coupled together. In SIMULATE-3, the relation between the fuel temperature and power in a node is assumed to be quadratic,

$$T_{fuel} = T_m + a + b \cdot \hat{P} + c \cdot \hat{P}^2$$

where T_{fuel} is the average fuel temperature in the node, T_m is the average moderator temperature in the node, $\hat{P}$ is the fraction of rated node-average power, and a, b, c are temperature-fitting coefficients. For different burnup steps, a burnup dependent array of corrections to temperature-fitting coefficients is used. The thermal hydraulic feedback model in SIMULTATE is based on four assumptions: (1) the coolant inlet temperature and flow distributions are given as boundary conditions; (2) the power produced in a node is deposited in the local coolant node; (3) cross flow is ignored, and the exit coolant remains subcooled; (4) pressure drop across the core is negligible so that water properties can be evaluated at a single pressure [Cronin et al., 1995].

In addition, SIMULATE-3 can be used to perform transient analysis which is usually based on one point or one dimensional model. It is significant for these reduced dimensional models to preserve the kinetics parameters of three dimensional core model.

4.1.4. MCNP-4C

MCNP is a general-purpose Monte Carlo N-Particle code used for coupled neutron/photon/electron transport problems developed at Los Alamos National Laboratory (LANL) [Briesmeister, 2000].

By treating a 3D configuration in geometric cells bounded by first- and second-degree surfaces and fourth-degree elliptical tori, MCNP can model any arbitrary 3D geometric structure without any approximations.

After defining the geometric configuration, the continuous-energy Monte Carlo solves the integral transport equation by simulating particle histories. The trajectory of each neutron is tracked according to interaction laws. Random numbers are used to sample and determine the probability of a specific interaction. For reactor physics interest, the neutron criticality calculation, i.e., kcode problems, is of major importance to our analyses. Source neutrons are distributed throughout fissionable materials, and are emitted isotropically with sampled fission spectrum. The same number of neutrons is tracked in each cycle. After enough time, all those neutrons either escape or are absorbed. When fission is induced, the location is stored for the next generation or cycle of neutrons. At the end of each cycle, the eigenvalue is calculated as the ratio of the number of fission neutrons to that of source neutrons. Reaction rates in the fuel can be obtained by track length estimators. All MCNP calculations, unless specifically noted, were performed using the JEF3.1 libraries.

4.1.5. **MCODE2.2**

A Monte Carlo based burnup code, MCODE-2.2, is a linkage program developed at MIT [Xu et al., 2002, 2008]. MCODE2-2 combines MCNP-4C and one-group depletion code, ORIGEN2.2. MCNP can provide neutron flux distribution and reaction rates at predefined locations. On the other hand, ORIGEN2.2 carries out depletion calculations and updates material composition in each region defined by the user. MCODE also follows the predictor-corrector approach that was described in CASMO-4. For each burnup step, the material compositions at the end of time step are predicted by ORIGEN2.2 using the neutron flux at the beginning of time step. Then, neutron flux at the end of time step can be obtained by MCNP using the calculated material compositions. The new neutron flux is used to correct the compositions. The average of the results from the predictor and corrector steps is taken as the final end-of-timestep material compositions.

4.2. Challenges of Annular Fuel Analysis

For LWRs with typical solid fuel, CASMO-4 provides very close results, i.e., eigenvalue and the ratio of U-238 capture to U-235 fission rate (C^*), to those of Monte Carlo code. However, previous calculations at MIT have shown that CASMO-4 cannot be used to calculate the annular fuel correctly unless adjustments are made [Xu, et al, 2004]. Both the eigenvalue and conversion ratio, C^*, were shown to be different from the MCNP results. This is because CASMO-4 resonance calculations underestimate the U-238 resonance capture on the inner surface of the annular fuel. For typical solid cylindrical rods, CASMO-4 assumes that epithermal U-238 captures are driven by the outer surface of the fuel. This is not the case for dually cooled annular fuel. Thus, equivalence relations for heterogeneous resonance calculations for solid fuel are inadequate for modeling the annular fuel. Following the approach established during earlier annular fuel work at MIT that showed it was possible to modify CASMO-4 input to match U-238 resonance captures in MCNP results, the first task will be to determine these modifications for the OPR-1000 annular fuel.

4.3. Initial Assembly-Level Calculations

This section summarizes initial neutronic analyses which were focused on reactor physics analysis of the OPR-1000 fuel assemblies. For the OPR-1000 assembly with solid fuel and annular fuel, CASMO-4 was benchmarked against the Monte-Carlo based burnup code, MCODE-2.2. All cases studied are poison-free, i.e., neither burnable poison nor soluble boron is considered. It is expected that CASMO-4 and MCODE produce the same results for the OPR-1000 assembly with the solid fuel. However, for the assembly with the annular fuel, the results exhibit slight discrepancy due to resonance capture treatment of CASMO-4, which is tailored to traditional solid fuel. Adjustments are performed for CASMO-4 input to match MCODE rigorous results, and validity of CASMO-4 for the annular fuel cases is investigated.

4.3.1. MCNP and CASMO Model of Reference Assembly

For all cases considered, the fuel is UO_2 at 4.5 w/o enrichment and 95% theoretical density (10.4 g/cm^3). Reflective boundary conditions are imposed on the three edge surfaces of one octant of assembly because of the mirror symmetry. Figure 4-3 shows the geometric configuration of solid fuel built by MCNP-4C. A slice of 10 cm thickness is used as 3D configuration in MCNP with reflective boundary conditions on both the top and the bottom surface.

For both MCNP and CASMO-4 calculations of solid fuel, the cladding temperature is 583K, and the temperatures of the fuel pellet and the coolant are assumed to be 900K and 585K respectively. Spacers and burnable poisons are not considered in both cases. The results of CASMO-4 and MCODE-2.2 are shown in Figure 4-4. As expected, the results of CASMO-4 and that of MCODE-2.2 are in satisfactory agreement for a typical PWR solid fuel.

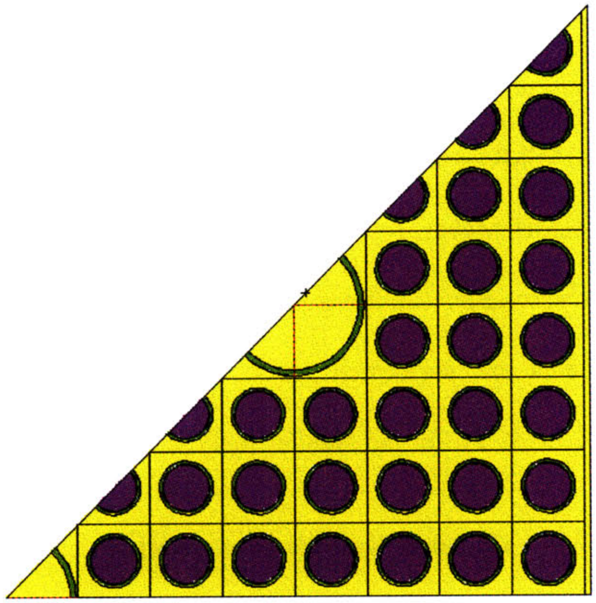

Figure 4-1: Schematic 1/8 assembly with solid fuel built by MCNP-4C

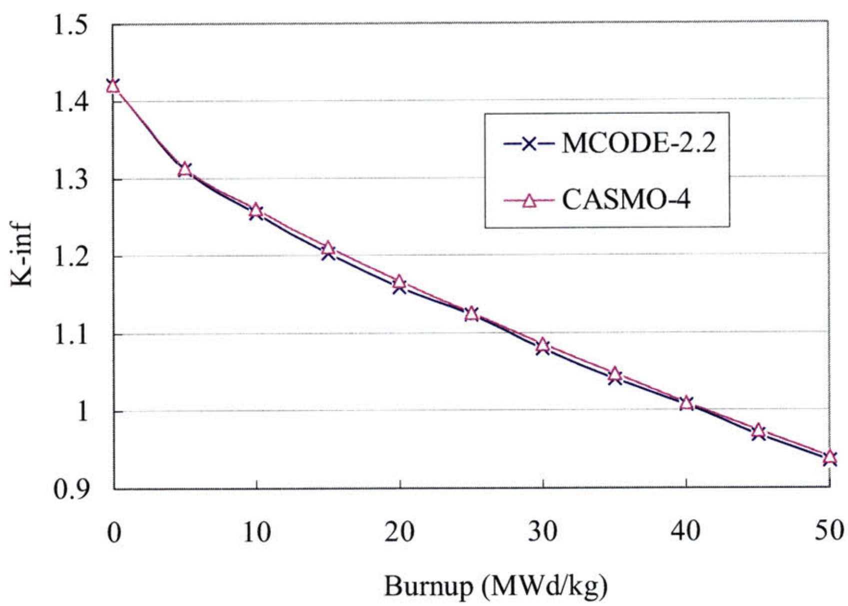

Figure 4-2: Benchmark of CASMO-4 against MCODE-2.2 for the solid fuel

4.3.2. MCNP and CASMO Model of Annular Fuel Assembly

Similar to the solid fuel calculation, MCNP and CASMO are also used to compare the annular fuel cases. Figure 4.5 illustrates the configuration of 1/8 annular, 12x12 fuel assembly constructed in MCNP-4C. For both MCODE-2.2 and CASMO-4 calculations, the fuel pellet temperature is changed from 900K to 600K to reflect lower temperatures of annular fuel, and specific power is increased from 36.574 W/gHM to 42.748 W/gHM, because the fuel volume per assembly is decreased in the annular fuel design.

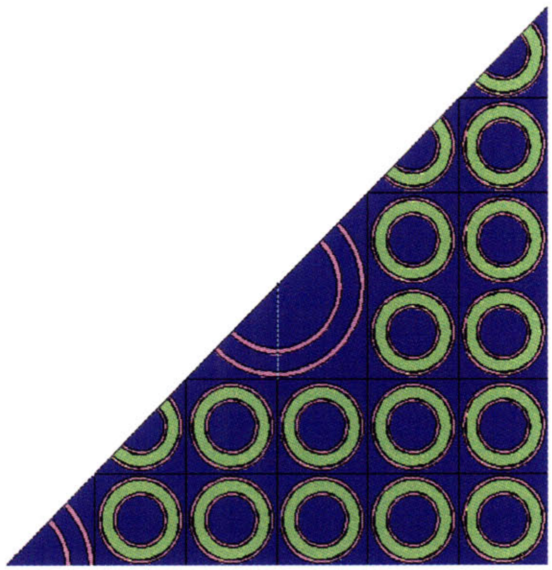

Figure 4-3: 1/8 assembly with the annular fuel modelled in MCNP-4C

The eigenvalues calculated by CASMO-4 and MCODE-2.2 for the annular fuel at different burnups are shown in Figure 4-4. It can be seen that the eigenvalue difference is much larger than that of solid fuel. Larger CASMO-4 eigenvalues than the MCODE-2.2 results are expected, because CASMO-4 code underestimates the U-238 resonance capture of the annular fuel based on the earlier analysis.

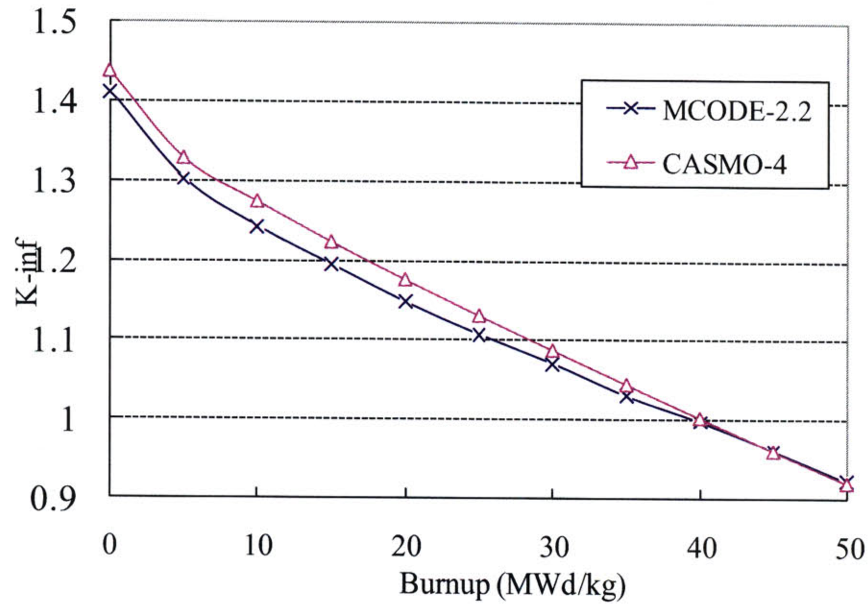

Figure 4-4: Benchmark of CASMO-4 against MCODE-2.2 for the annular fuel

Since CASMO-4 underestimates epithermal U-238 capture rate, the reactivity is overestimated at the beginning of life (BOL). Thus, it is necessary to reduce the reactivity predicted by CASMO-4 to better match MCODE results. Several ideas were explored during previous MIT studies of a Westinghouse PWR with the annular fuel. The best option appeared to be an artificial increase of the U-238 number density in CASMO-4 input to recover partial epithermal U-238 captures [Xu, et al, 2004]. These studies concluded that increasing the amount of U-238 by 20% can best match MCODE-2.2 results for the proposed Westinghouse PWR with the annular fuel design. Because surface to fuel volume ratio is different for the OPR-1000 fuel, the results of the earlier study cannot be used directly and the optimum increase of U-238 number density needs to be determined specifically for the OPR-1000 fuel.

4.3.3. **Modeling Annular Fuel Assembly using CASMO-4**

The OPR-1000 design is different from the typical Westinghouse PWRs: it has different dimensions of the assembly, different rod array, and different operating conditions. Therefore, it is necessary to determine the proper U-238 number density adjustment to reach a satisfactory agreement between the two methods.

Figure 4-5 compares eigenvalue differences between the CASMO-4 and MCODE-2.2 at different levels of increased U-238 number densities. It can be observed that an increase of the amount of U-238 by 10% yields the best agreement with the results of MCODE-2.2.

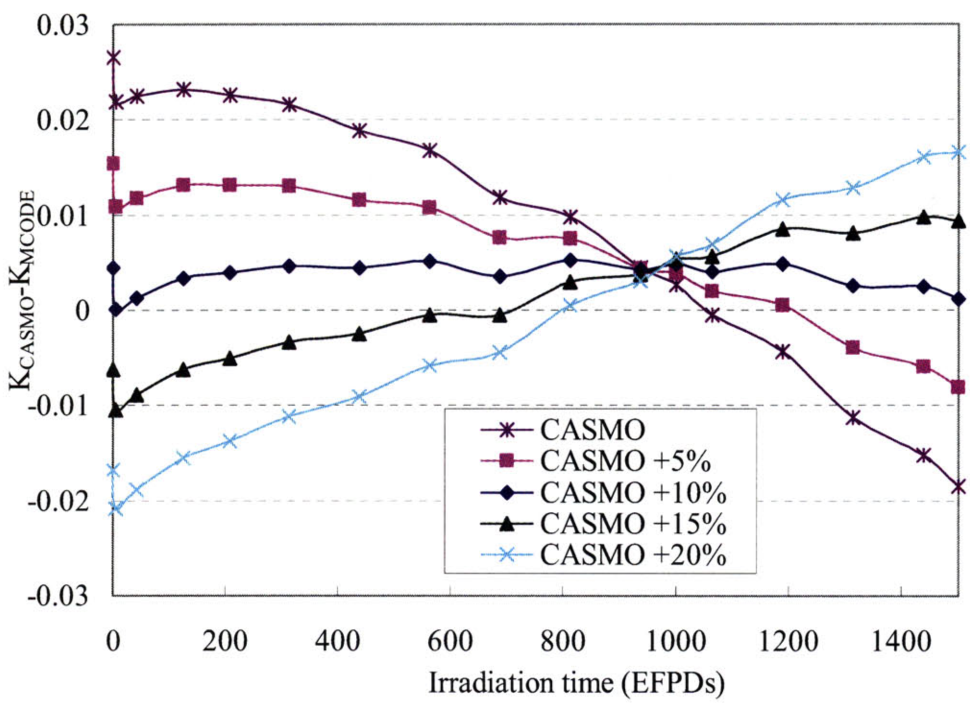

Figure 4-5: CASMO-4 input correction by increasing the U-238 content

For the Westinghouse PWR with the annular design evaluated by MIT, the surface to volume ratio is $2/(R-r)=2/(0.7685-0.4315)=5.9347cm^{-1}$, (where R and r are radii of the outer and inner cladding, respectively). For the OPR-1000 of the annular fuel design with the dimensions provided by KAERI, the surface to volume ratio is $2/(R-r) = 2/(0.795-0.44) = 5.6338 cm^{-1}$. As expected, the smaller surface to volume ratio of OPR-1000 annular fuel design requires smaller increase of U-238 content (+10%) compared to the result of Westinghouse PWR with the annular fuel (+20%).

Reducing the reactivity at BOL is not the only requirement, since plutonium buildup through cycle length needs to be also matched. To further examine the validity of the +10% U238 adjustment, plutonium composition changes with burnup are shown in Figure 4-6. It can be observed that the case with artificially 10% higher U-238 number densities exhibits a relatively good agreement along the entire burnup range. Therefore, artificial increase of U-238 number density by 10% will be used for unpoisoned fuel assemblies of OPR-100 in further studies to obtain data for the whole core analysis using the SIMULATE computer code.

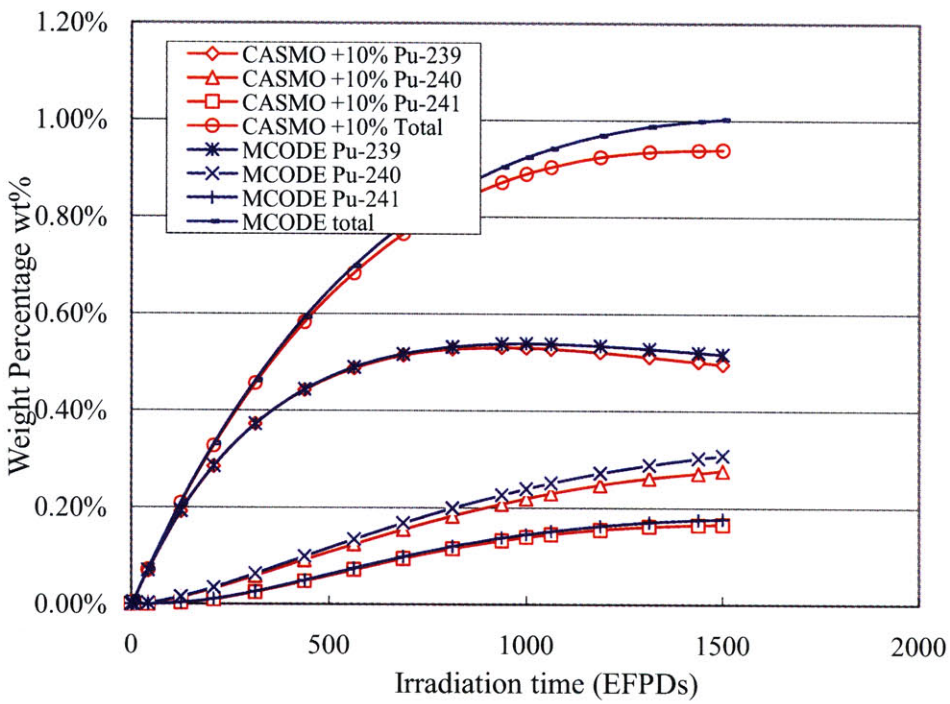

Figure 4-6: Plutonium composition changes with burnup for 10% higher U-238 content

4.3.4. **Benchmarking with TRITON**

There are other options of deterministic tools that can be potentially used for reactor physics analysis besides the CMS package. One of such deterministic codes is TRITON which is part of the SCALE5.1 package (Standardized Computer Analyses for Licensing Evaluation) developed by the Oak Ridge National Laboratory (ORNL) [ORNL, 2006]. TRITON can do multi-material depletion in 2-D using discrete ordinates method with the module NEWT or in 2-D and 3-D using the Monte Carlo module KENO. In this study, the 2-D depletion capabilities using NEWT were compared to MCODE.

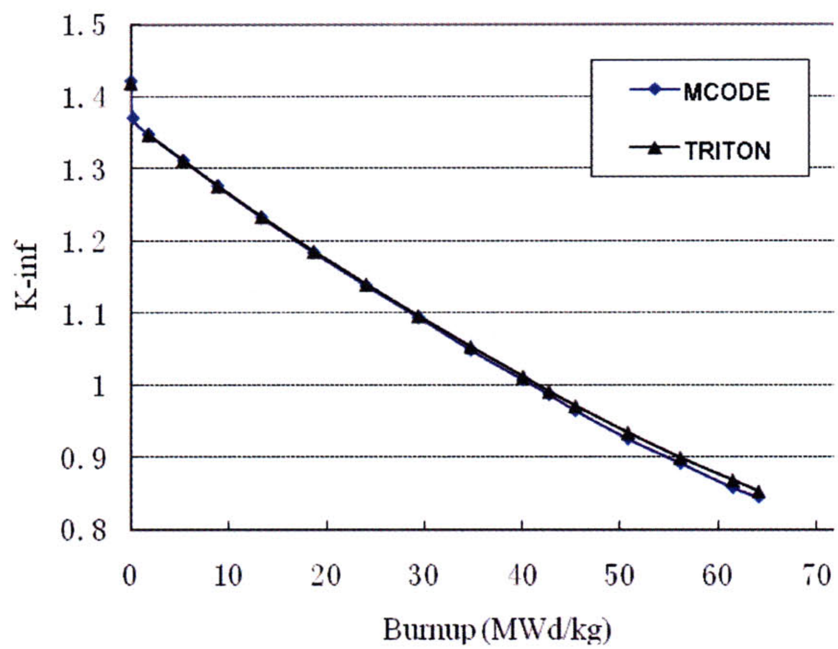

Figure 4-7 Eigenvalues of MCODE codes compared with that of TRITON

Two runs were performed to evaluate TRITON capability against MCNP-based MCODE-2.2. Both used the ENDF-6 cross section libraries. The temperatures of all the materials inside the core, i.e., fuel pellet, coolant, and cladding, are assumed to be all 300K because of limited availability of ENDF6 libraries at elevated temperature. Figure 4-7 compares the eigenvalues obtained by TRITON and MCODE at different burnups. Although the differences slightly increase with burnup, a good agreement is achieved between the results of the two codes. Figure 4-8 further proves that the two results match very well because the amount of plutonium is in very good agreement at different burnup levels.

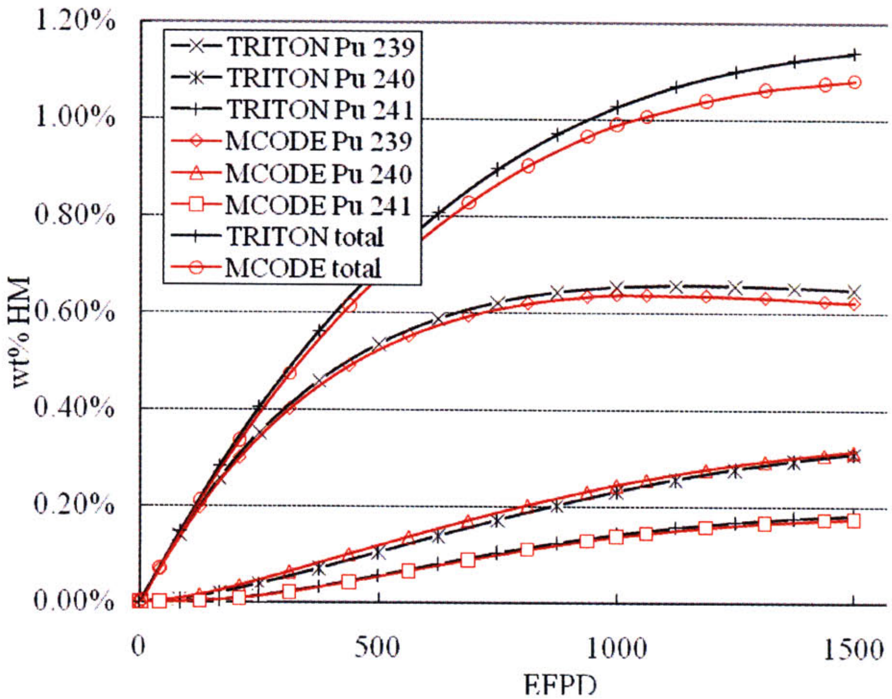

Figure 4-8: Plutonium composition changes with burnup for TRITON and MCODE

4.4. Whole Core Analysis of the Reference OPR-1000 Design

4.4.1. Core Description

The core analysis of the reference design in this section is based on the data provided by KAERI of Ulchin Nuclear (UCN) Unit 5, which is a Combustion Engineering type PWR with 2815 MW thermal power and 177 fuel assemblies. The objective of this section is to calculate the first four cycles of UCN unit 5. The loading patterns and the information of materials and dimensions are from [KAERI, 2008]. Table 4-1 summarizes the basic core description of fuel rod, control rod, burnable poisons, and spacer grids of UCN Unit 5. To simplify the calculation, the control rod is assumed to be B_4C along the active length.

Table 4-1: Summary of basic UCN unit 5 core description [KEARI, 2008]

Core performance	
Total thermal power, MW	2815
Heat generated in fuel, %	97.5
Specific power, kW/kgU	36.91
Volumetric power density, kW/ltr	96.26
Inlet temperature, °C	296.11
Average temperature, °C	312.22
Fuel rod	
Pellet material	UO_2
Pellet theoretical density, g/cc	10.96
Pellet density, g/cc	10.44
Active length, cm	381
Pellet diameter, cm	0.826
Cladding material	ZIRLO
Clad inner diameter, cm	0.843
Clad outer diameter, cm	0.970
Clad thickness, cm	0.064
Control rod	
Poison material	B_4C
Diameter, cm	1.872
Density, g/cc	1.84
Clad material	Inconel 625
Clad thickness, cm	0.089
Clad outer diameter, cm	2.073
Burnable absorber	
Absorber material	Gd_2O_3-UO_2
Theoretical density, Gd_2O_3, g/cc	7.41
Spacer grid	
Material	Zircaloy-4
Number per assembly (active region)	10
Grid spacing, cm	39.93

During the four cycles, fourteen different assembly types are utilized, as shown in Table 4-2. Each assembly except the first one, A0, has mixed fuel pins with two different enrichment levels. All burnable poison rods are comprised of 6.0 wt% of Gd_2O_3 admixed homogenously in uranium oxide with natural U-235 enrichment. Note that the burnable absorber active length is in the center of the active core, where in the top and bottom of the burnable poisons, there are axial cutback regions with no gadolinia mixed. The technique of using enrichment split and burnable poison is to reduce the power peaking.

Table 4-2: Summary of assembly types from Cycle01 to Cycle04 [KEARI, 2008]

Assembly type	Fuel Enrichment (wt% U-235)	No. of fuel rod per assembly	No. of Gd poison rod per assembly	Cutback regions (cm)
A0	1.42	236	---	---
B0	2.92/2.42	184/52	---	---
B1	2.92/2.43	176/52	8	27.95
B2	2.92/2.43	128/100	8	27.95
C0	3.43/2.93	184/52	---	---
C1	3.43/2.93	124/100	12	27.95
D0	4.42/3.93	184/52	---	---
D2	4.43/3.93	172/52	12	19.05
E0	4.50/4.00	184/52	---	---
E1	4.50/4.00	176/52	8	19.05
E2	4.50/4.01	172/52	12	19.05
F0	4.50/4.01	184/52	---	---
F1	4.50/4.01	176/52	8	15.24
F2	4.50/4.01	172/52	12	15.24

Table 4-3: Summary of the number of various assemblies in each cycle [KEARI, 2008]

Assembly type	Cycle 01	Cycle 02	Cycle 03	Cycle 04
A0	61	1		
B0	24	24	24	
B1	20	20		
B2	16	16	4	
C0	16	16	16	
C1	40	40	9	
D0		28	28	28
D2		32	32	25
E0			16	16
E1			24	24
E2			24	24
F0				12
F1				20
F2				28

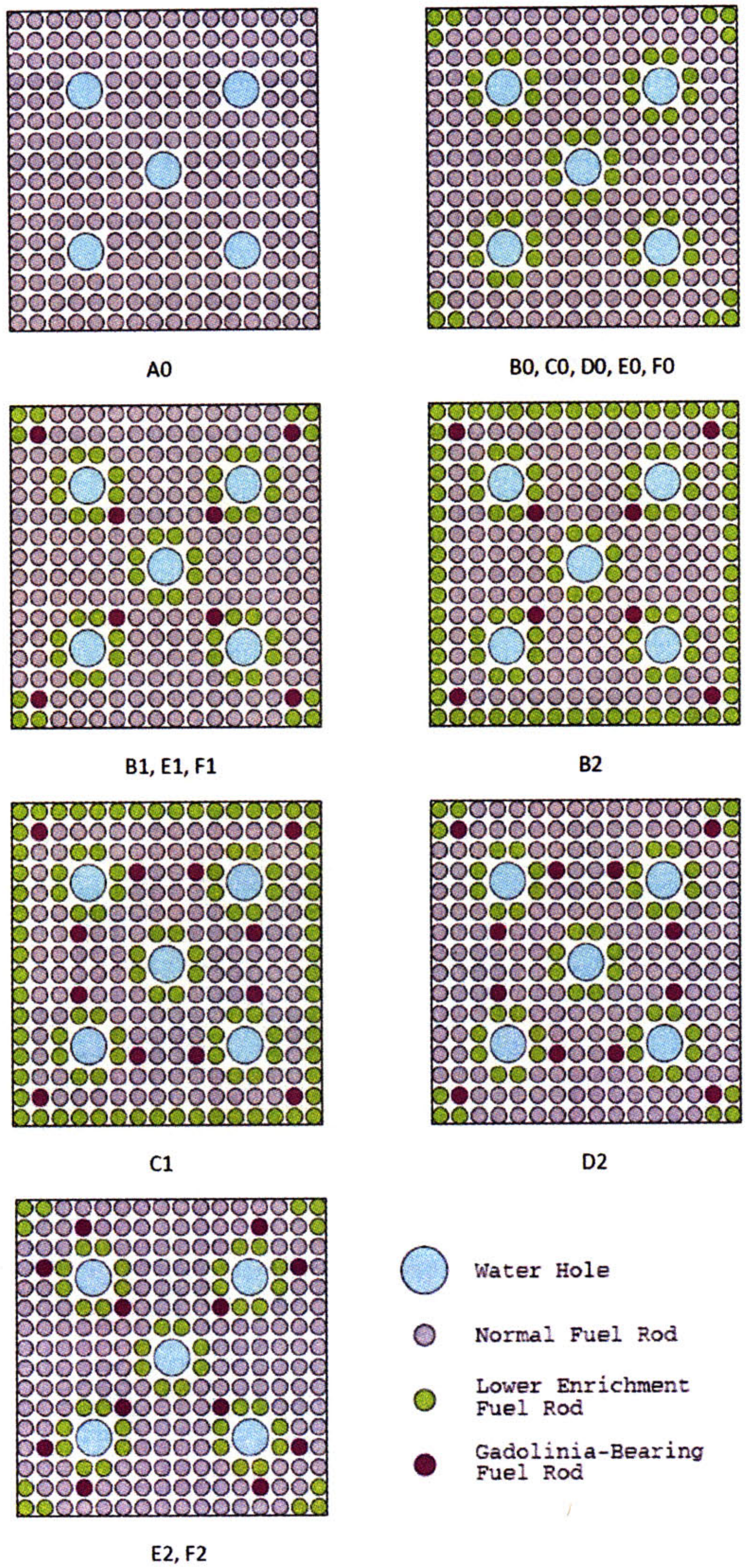

Figure 4-9: Enrichment pattern and burnable absorber arrangement of various assemblies (from [KAERI, 2008])

The enrichment zoning pattern and burnable poison arrangement of different assemblies are shown in Figure 4-9. Note that there is a typo in the assembly layout of E2 provided by KAERI, which shows that E2 has the same pattern as D2 in Cycle03, and E2 is the same as F2 in Cycle04. In this calculation, it is assumed that E2 and F2 have the same pattern.

The assembly loading patterns for the four cycles basically have three-batch, mixed central zone with low leakage. The number of various kinds of assemblies in different cycles is presented in Table 4-3. The first cycle is for transition of the initial core to the equilibrium core. Figures 4-10 to 4.13 show the loading patterns evolving from Cycle01 to Cycle04, as provided by KAERI.

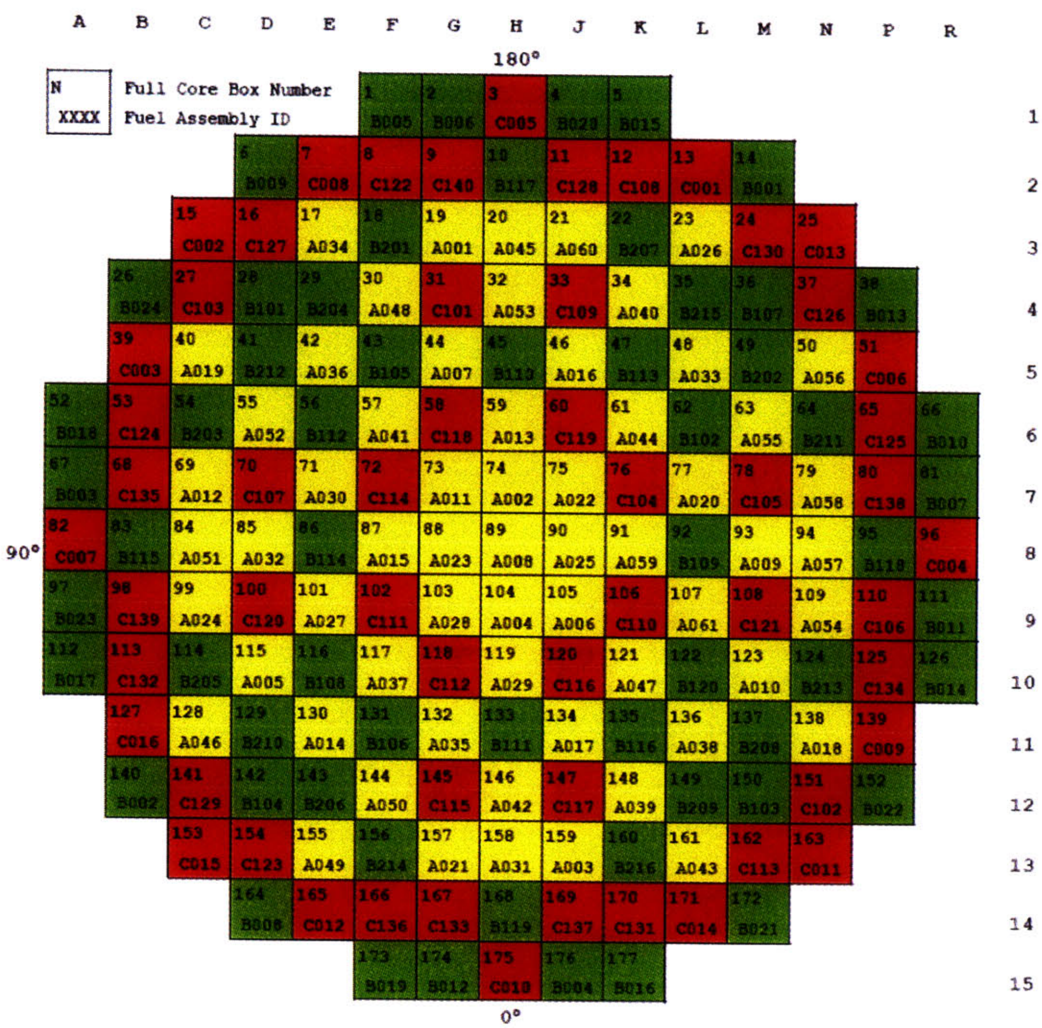

Figure 4-10: Loading pattern for Cycle01 (from [KAERI, 2008])

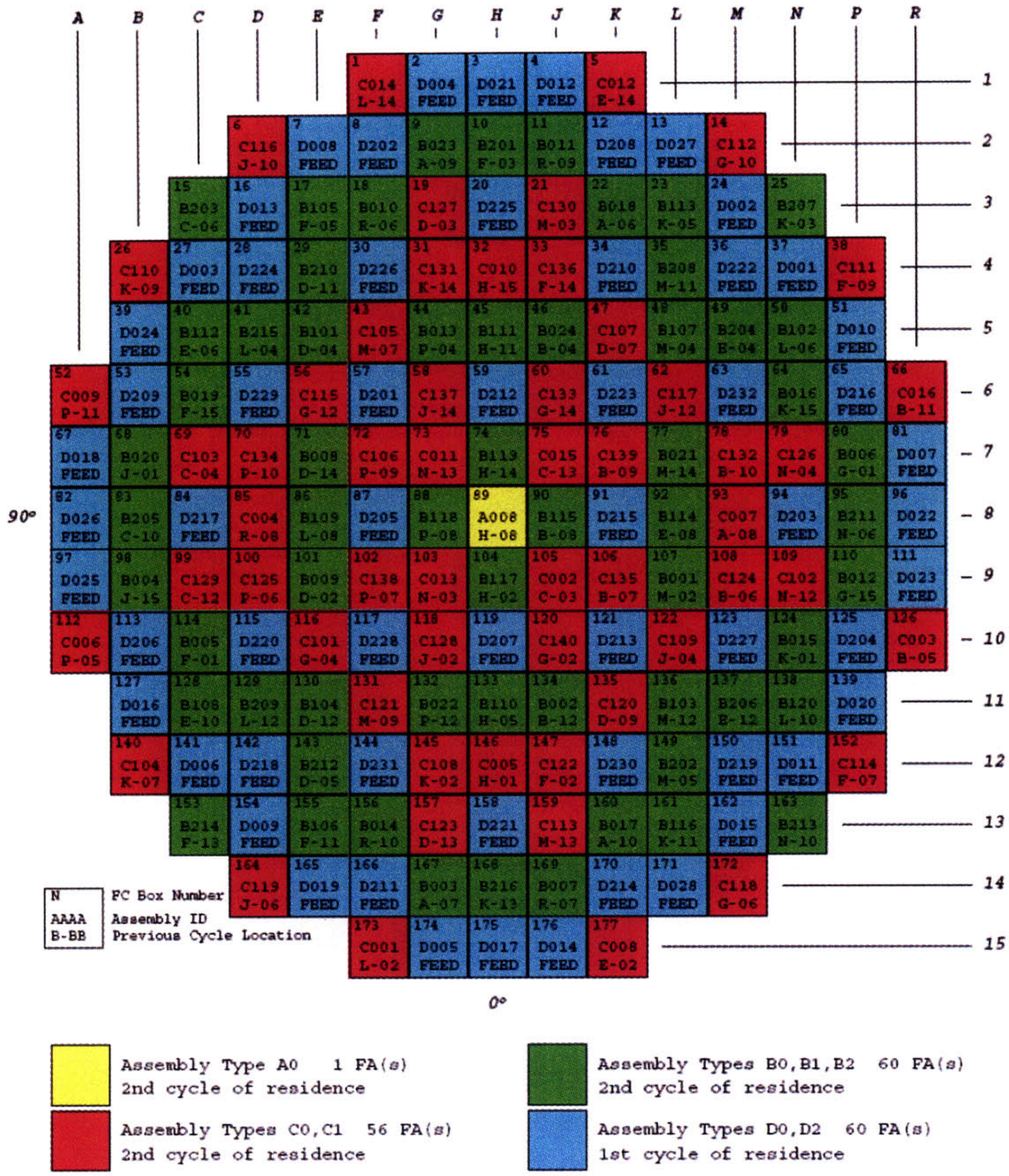

Figure 4-11: Loading pattern for Cycle02 (from [KAERI, 2008])

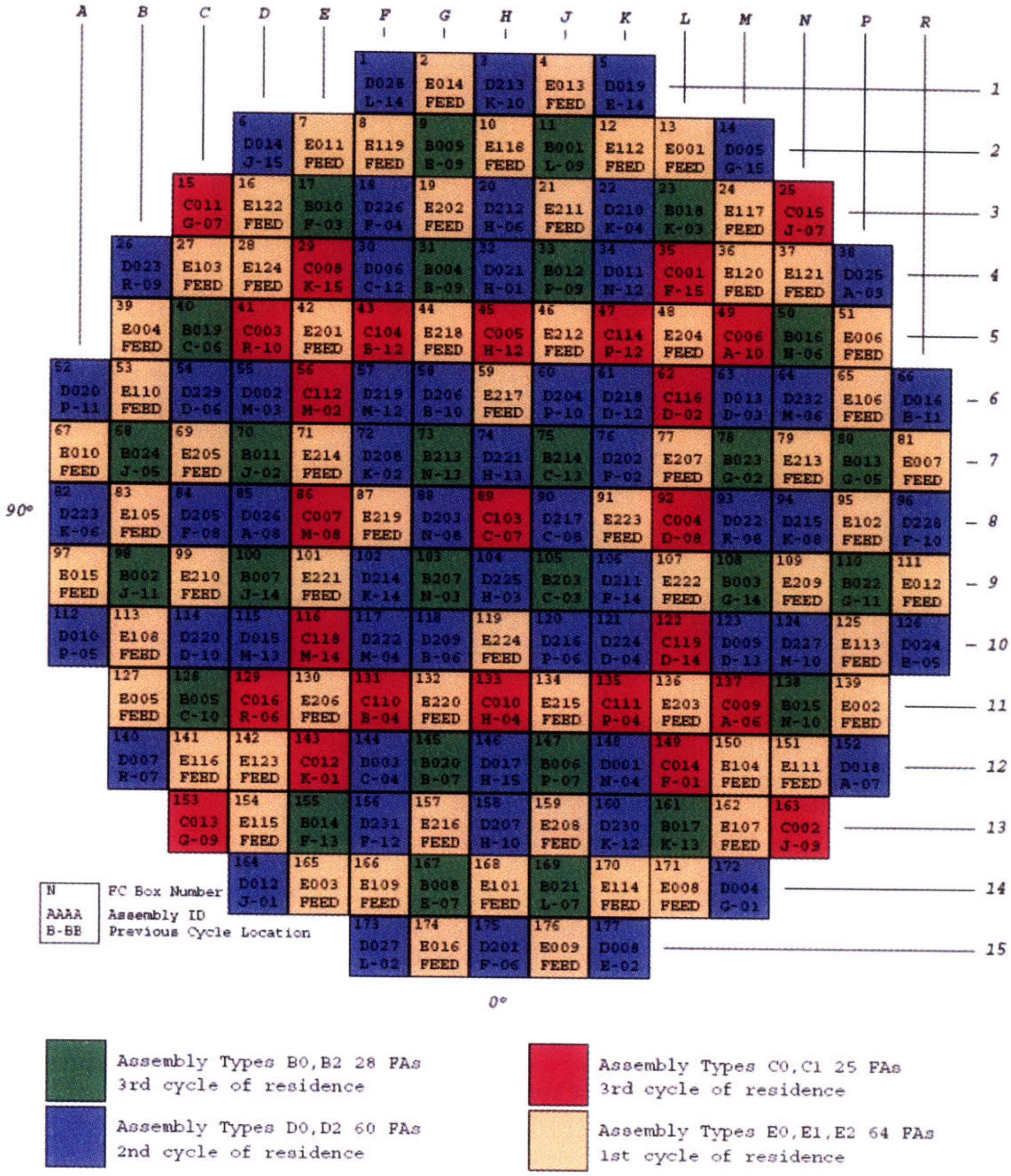

Figure 4-12: Loading pattern for Cycle03 (from [KAERI, 2008])

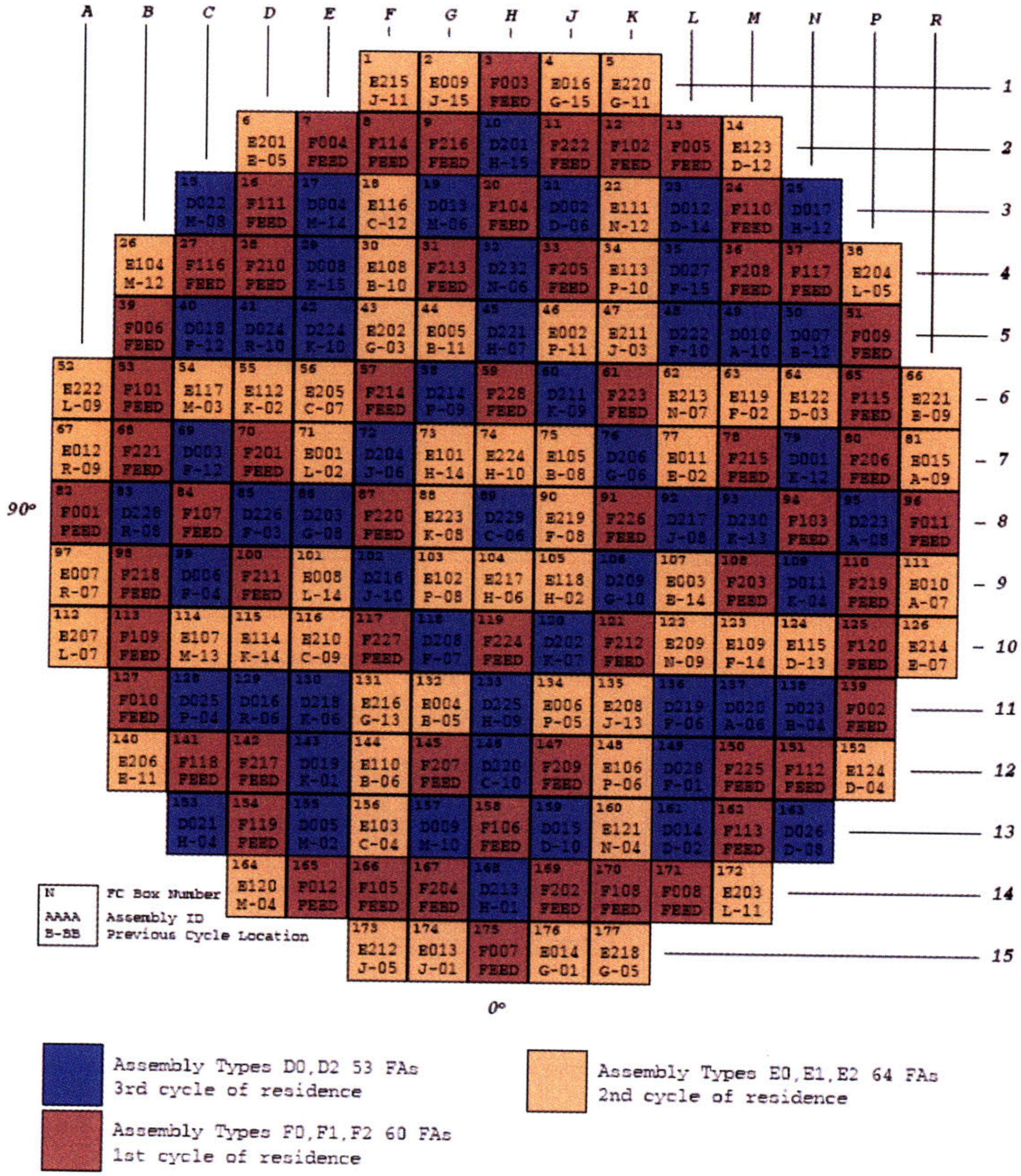

Figure 4-13: Loading pattern for Cycle04 (from [KAERI, 2008])

4.4.2. **SIMULATE-3 Core Models**

Because of the rotational 90-degree symmetry, a quarter core, as shown in Figure 4.16, is modeled in three dimensions, with 24 axial nodes for the fuel and four radial nodes (2x2) for each assembly.

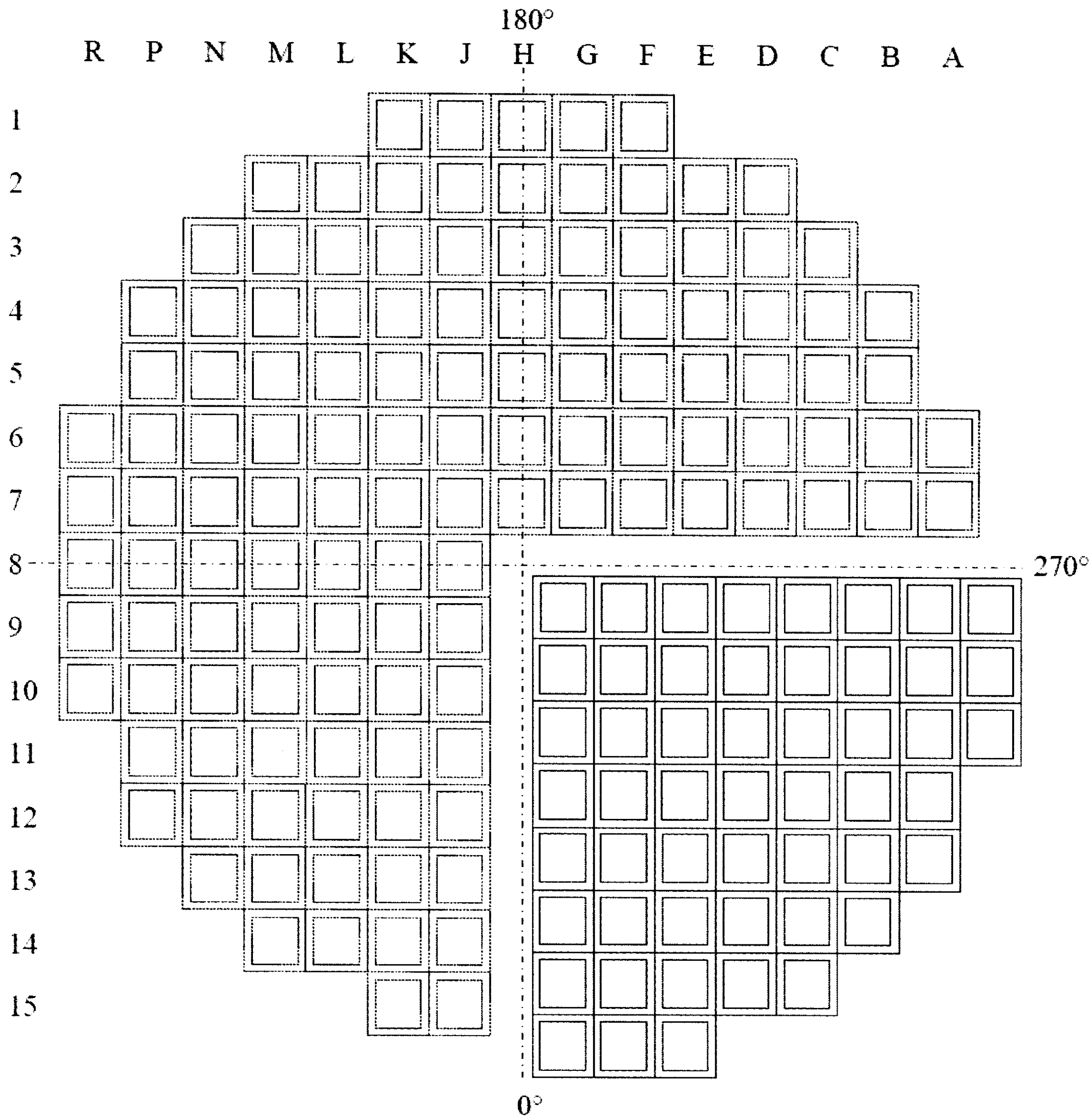

Figure 4-14: Model of quarter core with 52 assemblies

To prepare the master binary library for SIMULATE use, several CASMO-4 runs are needed for the fuel segment under various core conditions. Typical core conditions for CASMO-

4 runs are shown in Table 4-4. After the running of CASMO-4, TABLES-3 produces three dimensional data tables. Then, SIMULATE-3 is used to model the core under steady-state, hot full power operation with all control rods fully withdrawn. During the depletion calculations, critical boron concentration is searched. For the base case, the moderator temperature is a primary variable, which couples with different fuel temperature, boron concentration, and control rod positions.

As introduced in Section 4.1, SIMULATE-3 assumes a quadratic fitting function between the fuel temperature and the local power to consider the fuel temperature feedback. In this report, the coefficients of the quadratic fitting function are chosen to be the same values in [Xu et al., 2004], which is used for the typical Westinghouse PWR. Since the information on the core reflector is unknown for UCN unit 5, the same bottom, top, and radial reflectors as for a Westinghouse core are likewise used in this study.

In the whole core reactor physics analyses, three targets or limitations are desired in the core design [Xu et al., 2004]:

(1) 18-month-cycle with a capacity factor of 90%;

(2) the peak critical boron concentration should be no more than 1750ppm

(3) the power peaking during the cycles satisfies $F_{\Delta h} \leq 1.65$, $F_q \leq 2.5$.

The target capacity factor requires a cycle length of 493.1 effective full power days, which depends on the average reload enrichment. The critical boron concentration is limited in the second target, for primary coolant chemistry and moderator temperature coefficient considerations. For the third target, the typical licensing limit of maximum pin power peaking $F_{\Delta h}$ is 1.65 for the Westinghouse PWR, and the hot spot factor F_q is usually required to be less than 2.5.

Table 4-4: Typical parameters in CASMO-4 runs

Parameters	Base value	Instantaneous branches
Base case		
Fuel temperature (K)	900	293.2 449.8 549.8 569.3 900 1200
Moderator temperature (K)	585.4	293.2 333.2 449.8 505.4 546.8 569.3 585.4 601.15 616.5
Boron concentration (ppm)	600	0 1200 1800 2400
Control rod position	Fully withdrawn	Fully inserted
Low fuel temperature history		
Fuel temperature (K)	565.8	900
Moderator temperature (K)	585.15	—
Boron concentration (ppm)	600	—
Control rod position	Fully withdrawn	—
High fuel temperature history		
Fuel temperature (K)	1200	900
Moderator temperature (K)	585.15	—
Boron concentration (ppm)	600	—
Control rod position	Fully withdrawn	—
Low moderator temperature history		
Fuel temperature (K)	900	—
Moderator temperature (K)	569.3	585.4
Boron concentration (ppm)	600	—
Control rod position	Fully withdrawn	—
High moderator temperature history		
Fuel temperature (K)	900	—
Moderator temperature (K)	601.15	585.4
Boron concentration (ppm)	600	—
Control rod position	Fully withdrawn	—
Low boron concentration history		
Fuel temperature (K)	900	—
Moderator temperature (K)	585.4	—
Boron concentration (ppm)	0	600
Control rod position	Fully withdrawn	—
High boron concentration history		
Fuel temperature (K)	900	—
Moderator temperature (K)	585.4	—
Boron concentration (ppm)	1200	600
Control rod position	Fully withdrawn	—

4.4.3. Steady State Core Performance

During burnup, the core under steady state operation is maintained critical by the combined effects of burnable poisons depletion, fuel burnup, and soluble boron concentration (all control rods are fully withdrawn). The critical boron concentration (CBC) is an important core depletion factor, and is usually calculated at hot full power with equilibrium xenon for steady state core model. Figures 4-15 to 4-18 show the CBC calculated using SIMULATE-3 (SimCal), compared with the results in the report provided by KAERI (KAERI data). Note that results from SIMULATE model are in good agreement with KAERI's data for the first three cycles, compared with a relatively large difference for the fourth cycle. The relative large difference needs further investigation.

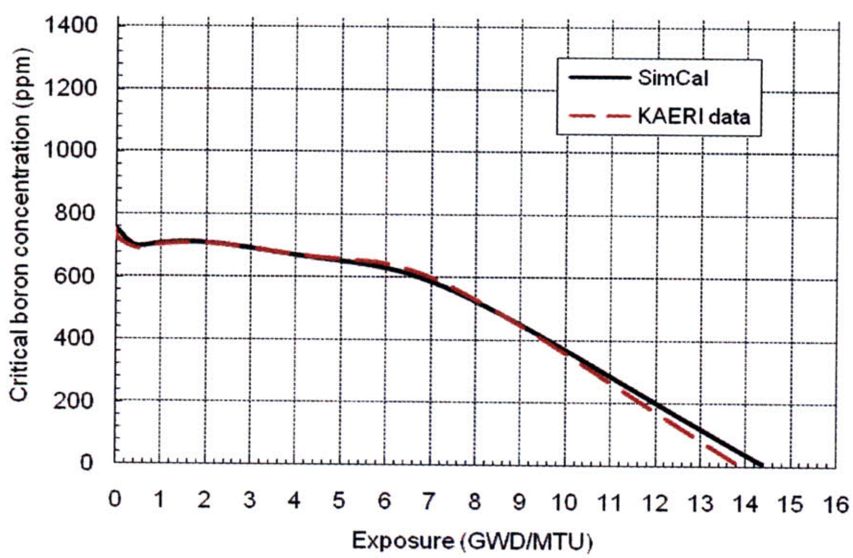

Figure 4-15: Critical boron concentration in Cycle01

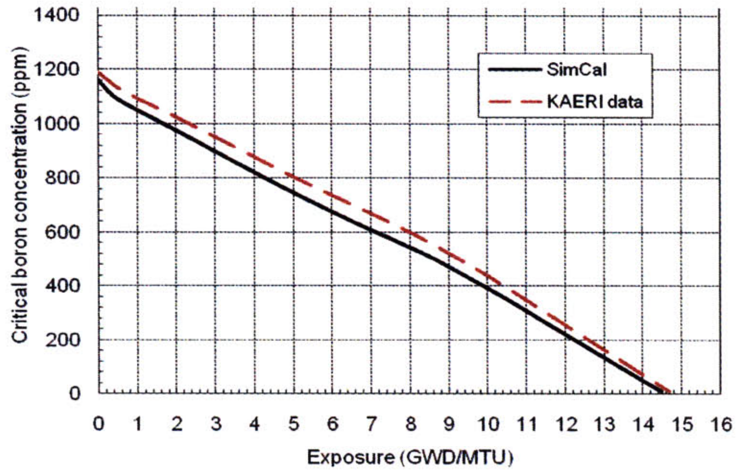

Figure 4-16: Critical boron concentration in Cycle02

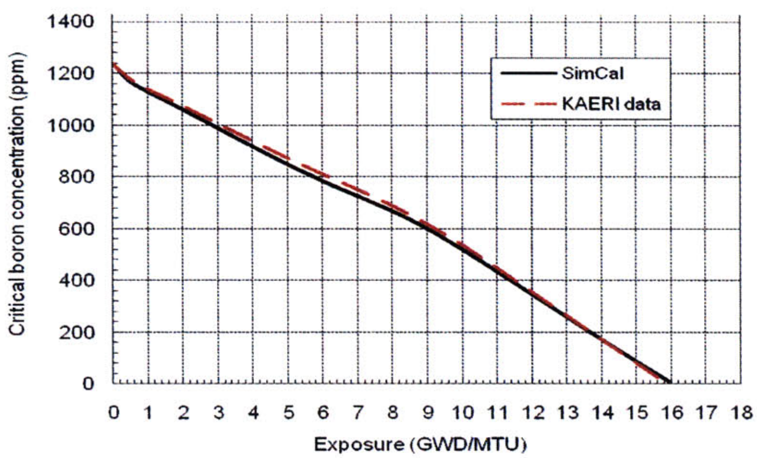

Figure 4-17: Critical boron concentration in Cycle03

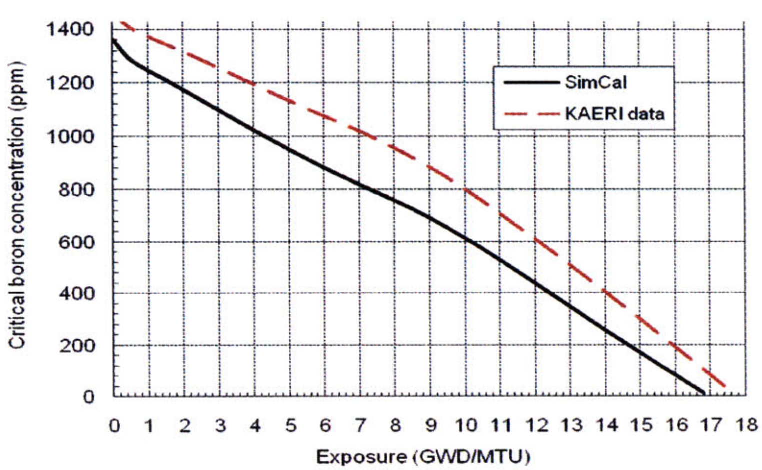

Figure 4-18: Critical boron concentration in Cycle04

During the cycle, the locations of the peak assembly and pin are usually continuously changing as a result of the depletion of the fuel and burnable poison in the core. Typically three states in a cycle are of interest: BOC, MOC, and EOC. The BOC and MOC are defined as when the exposures are 0.15 GWD/MT and 8.0 GWD/MT in each cycle, respectively. The end of cycle is defined as when the CBC is below 6ppm in each cycle. Figures 4-19 to 4-30 show the distribution of assembly power, peak pin power, and assembly burnup at BOC, MOC, and EOC in each cycle. Note that the solid triangle in the upper right corner indicates the maximum assembly power, the one in the lower right corner refers to the maximum pin peaking, and the one in the left corner means the maximum assembly burnup.

	H	G	F	E	D	C	B	A
08	A008 0.671 0.704 0.100	A023 0.724 0.795 0.107	A015 0.814 0.906 0.121	B114 1.182 1.367 0.177	A032 0.901 0.981 0.135	A051 0.937 1.003 0.140	B115 1.252 1.449 0.189	C007 1.084 1.439 0.163
09	A004 0.724 0.795 0.107	A028 0.757 0.846 0.113	C111 1.134 1.356 0.170	A027 0.898 0.995 0.134	C120 1.233 1.423 0.185	A024 0.933 1.019 0.140	C139 1.231 1.460 0.186	B023 0.924 1.297 0.139
10	A029 0.814 0.906 0.121	C112 1.134 1.356 0.170	A037 0.890 0.992 0.133	B108 1.239 1.439 0.186	A005 0.938 1.030 0.140	B205 1.208 1.380 0.182	C132 1.097 1.370 0.165	B017 0.658 1.110 0.099
11	B111 1.182 1.367 0.177	A035 0.898 0.995 0.134	B106 1.239 1.439 0.186	A014 0.956 1.050 0.143	B210 1.236 1.426 0.186	A046 0.902 1.006 0.135	C016 1.023 1.487 0.154	
12	A042 0.901 0.981 0.135	C115 1.233 1.423 0.185	A050 0.938 1.030 0.140	B206 1.236 1.426 0.186	B104 1.200 1.373 0.180	C129 1.039 1.368 0.156	B002 0.625 1.056 0.094	
13	A031 0.937 1.003 0.140	A021 0.933 1.019 0.140	B214 1.208 1.380 0.182	A049 0.902 1.006 0.135	C123 1.039 1.368 0.156	C015 0.749 1.187 0.112		
14	B119 1.252 1.449 0.189	C133 1.231 1.460 0.186	C136 1.097 1.370 0.165	C012 1.023 1.487 0.154	B008 0.625 1.056 0.094			
15	C010 1.084 1.439 0.163	B012 0.924 1.297 0.139	B019 0.658 1.110 0.099	Fuel ID Assembly power Peak pin power Assembly burnup				

Figure 4-19: Assembly power distribution at BOC for Cycle01

	H	G	F	E	D	C	B	A
08	A008 0.719 0.758 5.112	A023 0.780 0.868 5.504	A015 0.903 0.996 6.236	B114 1.244 1.343 8.708	A032 0.950 1.024 6.625	A051 0.926 0.987 6.554	B115 1.183 1.299 8.314	C007 0.889 1.224 6.621
09	A004 0.780 0.868 5.504	A028 0.839 0.957 5.815	C111 1.252 1.411 8.559	A027 0.978 1.047 6.774	C120 1.298 1.428 8.956	A024 0.950 1.021 6.611	C139 1.210 1.370 8.299	B023 0.785 1.124 5.742
10	A029 0.903 0.996 6.236	C112 1.252 1.411 8.559	A037 0.973 1.044 6.755	B108 1.266 1.359 8.994	A005 0.978 1.045 6.846	B205 1.201 1.324 8.385	C132 1.085 1.348 7.420	B017 0.586 1.002 4.184
11	B111 1.244 1.343 8.708	A035 0.978 1.047 6.774	B106 1.266 1.359 8.994	A014 0.995 1.068 7.017	B210 1.244 1.371 8.753	A046 0.894 1.003 6.272	C016 0.891 1.266 6.520	
12	A042 0.950 1.024 6.625	C115 1.298 1.428 8.956	A050 0.978 1.045 6.846	B206 1.244 1.371 8.753	B104 1.234 1.369 8.464	C129 1.040 1.334 7.124	B002 0.565 0.956 4.051	
13	A031 0.926 0.987 6.554	A021 0.950 1.021 6.611	B214 1.201 1.324 8.385	A049 0.894 1.003 6.272	C123 1.040 1.334 7.124	C015 0.707 1.144 4.953		
14	B119 1.183 1.299 8.314	C133 1.210 1.370 8.299	C136 1.085 1.348 7.420	C012 0.891 1.266 6.520	B008 0.565 0.956 4.051			
15	C010 0.889 1.224 6.621	B012 0.785 1.124 5.742	B019 0.586 1.002 4.184	Fuel ID Assembly power Peak pin power Assembly burnup				

Figure 4-20: Assembly power distribution at MOC for Cycle01

	H	G	F	E	D	C	B	A
08	A008 0.863 0.907 10.843	A023 0.897 0.969 11.592	A015 0.964 1.032 13.033	B114 1.205 1.273 17.649	A032 0.963 1.028 13.601	A051 0.940 0.992 13.389	B115 1.132 1.222 16.876	C007 0.866 1.160 13.076
09	A004 0.897 0.969 11.592	A028 0.933 1.022 12.266	C111 1.256 1.356 17.775	A027 0.988 1.044 13.926	C120 1.245 1.340 18.295	A024 0.958 1.017 13.614	C139 1.177 1.305 17.198	B023 0.785 1.085 11.534
10	A029 0.964 1.032 13.033	C112 1.256 1.356 17.775	A037 0.989 1.045 13.892	B108 1.198 1.267 17.972	A005 0.971 1.031 13.955	B205 1.154 1.245 17.065	C132 1.095 1.299 15.587	B017 0.618 1.012 8.642
11	B111 1.205 1.273 17.649	A035 0.988 1.044 13.926	B106 1.198 1.267 17.972	A014 0.977 1.036 14.186	B210 1.171 1.257 17.608	A046 0.912 0.999 12.922	C016 0.907 1.211 13.160	
12	A042 0.963 1.028 13.601	C115 1.245 1.340 18.295	A050 0.971 1.031 13.955	B206 1.171 1.257 17.608	B104 1.178 1.264 17.389	C129 1.071 1.288 15.047	B002 0.613 0.992 8.411	
13	A031 0.940 0.992 13.389	A021 0.958 1.017 13.614	B214 1.154 1.245 17.065	A049 0.912 0.999 12.922	C123 1.071 1.288 15.047	C015 0.752 1.153 10.377		
14	B119 1.132 1.222 16.876	C133 1.177 1.305 17.198	C136 1.095 1.299 15.587	C012 0.907 1.211 13.160	B008 0.613 0.992 8.411			
15	C010 0.866 1.160 13.076	B012 0.785 1.085 11.534	B019 0.618 1.012 8.642	Fuel ID Assembly power Peak pin power Assembly burnup				

Figure 4-21: Assembly power distribution at EOC for Cycle01

	H	G	F	E	D	C	B	A
08	A008 0.637 0.676 10.938	B118 0.887 0.977 17.009	D205 1.292 1.472 0.194	B109 0.974 1.032 17.794	C004 1.151 1.228 13.248	D217 1.334 1.526 0.200	B205 0.916 0.991 17.202	D026 1.072 1.370 0.161
09	B117 0.887 0.977 17.009	C013 1.093 1.155 10.540	C138 1.021 1.100 17.351	B009 1.095 1.193 8.574	C125 1.075 1.188 15.748	C129 1.081 1.202 15.209	B004 1.015 1.134 11.686	D025 0.995 1.354 0.149
10	D207 1.292 1.472 0.194	C128 1.021 1.100 17.351	D228 1.277 1.463 0.192	C101 0.961 1.064 18.439	D220 1.281 1.479 0.193	B005 1.092 1.204 8.805	D206 1.164 1.474 0.175	C006 0.533 0.952 13.239
11	B110 0.974 1.032 17.794	B022 1.095 1.193 8.574	C121 0.960 1.064 18.439	B104 0.862 0.927 17.518	B209 0.871 0.960 17.739	B108 0.886 0.958 18.106	D016 1.006 1.360 0.151	
12	C005 1.151 1.228 13.248	C108 1.075 1.188 15.748	D231 1.281 1.479 0.193	B212 0.871 0.960 17.739	D218 1.280 1.483 0.193	D006 1.229 1.457 0.185	C104 0.438 0.788 17.841	
13	D221 1.334 1.526 0.200	C123 1.080 1.202 15.209	B014 1.092 1.204 8.805	B106 0.886 0.958 18.106	D009 1.229 1.457 0.185	B214 0.473 0.842 17.136		
14	B216 0.916 0.991 17.202	B003 1.014 1.134 11.686	D211 1.163 1.474 0.175	D019 1.006 1.360 0.151	C119 0.439 0.788 17.841			
15	D017 1.072 1.370 0.161	D005 0.994 1.353 0.149	C001 0.532 0.952 13.239	Fuel ID Assembly power Peak pin power Assembly burnup				

Figure 4-22: Assembly power distribution at BOC for Cycle02

	H	G	F	E	D	C	B	A
08	A008 0.704 0.745 15.919	B118 0.928 1.013 23.746	D205 1.387 1.511 10.055	B109 0.974 1.029 24.995	C004 1.111 1.181 21.568	D217 1.362 1.491 10.073	B205 0.877 0.963 23.788	D026 0.949 1.226 7.533
09	B117 0.928 1.013 23.746	C013 1.113 1.180 18.692	C138 1.054 1.126 25.032	B009 1.089 1.157 16.624	C125 1.058 1.137 23.620	C129 1.051 1.140 23.054	B004 0.965 1.089 18.932	D025 0.906 1.221 7.087
10	D207 1.387 1.511 10.055	C128 1.054 1.126 25.032	D228 1.387 1.518 9.986	C101 1.006 1.092 25.710	D220 1.362 1.492 9.881	B005 1.072 1.160 16.733	D206 1.174 1.425 8.725	C006 0.533 0.929 17.140
11	B110 0.974 1.029 24.995	B022 1.089 1.157 16.624	C121 1.006 1.092 25.710	B104 0.916 0.970 24.085	B209 0.913 0.973 24.312	B108 0.882 0.951 24.614	D016 0.968 1.307 7.371	
12	C005 1.111 1.181 21.568	C108 1.058 1.137 23.620	D231 1.362 1.492 9.881	B212 0.913 0.973 24.312	D218 1.323 1.457 9.720	D006 1.159 1.377 8.926	C104 0.443 0.765 21.094	
13	D221 1.362 1.491 10.073	C123 1.050 1.140 23.053	B014 1.072 1.160 16.732	B106 0.882 0.951 24.614	D009 1.159 1.377 8.928	B214 0.477 0.818 20.637		
14	B216 0.877 0.963 23.788	B003 0.964 1.089 18.928	D211 1.174 1.425 8.723	D019 0.968 1.307 7.372	C119 0.443 0.765 21.096			
15	D017 0.949 1.226 7.533	D005 0.905 1.220 7.083	C001 0.533 0.929 17.139	Fuel ID Assembly power Peak pin power Assembly burnup				

Figure 4-23: Assembly power distribution at MOC for Cycle02

	H	G	F	E	D	C	B	A
08	A008 0.753 0.794 20.945	B118 0.932 0.996 30.198	D205 1.345 1.441 19.652	B109 0.957 1.003 31.701	C004 1.077 1.137 29.150	D217 1.336 1.436 19.547	B205 0.893 0.968 29.928	D026 0.951 1.215 14.070
09	B117 0.932 0.996 30.198	C013 1.086 1.144 26.306	C138 1.027 1.086 32.291	B009 1.058 1.118 24.070	C125 1.033 1.099 30.904	C129 1.037 1.119 30.333	B004 0.974 1.095 25.654	D025 0.921 1.213 13.387
10	D207 1.345 1.441 19.652	C128 1.027 1.086 32.291	D228 1.350 1.448 19.626	C101 0.999 1.066 32.723	D220 1.345 1.448 19.418	B005 1.065 1.144 24.173	D206 1.213 1.409 17.127	C006 0.578 0.972 20.994
11	B110 0.957 1.003 31.701	B022 1.058 1.118 24.070	C121 0.999 1.066 32.723	B104 0.933 0.982 30.538	B209 0.933 0.983 30.760	B108 0.900 0.963 30.814	D016 0.989 1.300 14.154	
12	C005 1.077 1.137 29.150	C108 1.033 1.099 30.903	D231 1.345 1.448 19.418	B212 0.933 0.983 30.760	D218 1.316 1.425 19.006	D006 1.142 1.340 16.898	C104 0.476 0.793 24.277	
13	D221 1.336 1.436 19.547	C123 1.037 1.119 30.331	B014 1.065 1.144 24.171	B106 0.900 0.963 30.815	D009 1.142 1.340 16.901	B214 0.506 0.834 24.044		
14	B216 0.893 0.968 29.928	B003 0.974 1.095 25.647	D211 1.213 1.409 17.124	D019 0.989 1.300 14.154	C119 0.477 0.793 24.280			
15	D017 0.951 1.215 14.070	D005 0.920 1.213 13.382	C001 0.578 0.972 20.992	Fuel ID Assembly power Peak pin power Assembly burnup				

Figure 4-24: Assembly power distribution at EOC for Cycle02

	H	G	F	E	D	C	B	A
08	C103 0.682 0.723 30.433	D203 0.986 1.123 19.695	E219 1.290 1.459 0.194	C007 0.917 0.957 29.287	D026 1.240 1.352 14.256	D205 1.220 1.299 19.835	E105 1.302 1.509 0.196	D223 0.717 1.017 19.734
09	D225 0.986 1.123 19.695	B207 0.778 0.844 24.160	D214 1.162 1.256 17.301	E221 1.278 1.440 0.192	B007 0.869 0.929 25.784	E210 1.325 1.491 0.200	B002 0.848 0.917 24.197	E015 0.890 1.229 0.134
10	E224 1.290 1.459 0.194	D209 1.162 1.256 17.298	D222 1.123 1.197 19.174	C118 0.899 0.990 24.412	D015 1.142 1.220 17.069	D220 1.119 1.220 19.586	E108 1.196 1.419 0.180	D010 0.596 1.035 14.243
11	C010 0.917 0.957 29.287	E220 1.278 1.440 0.192	C110 0.899 0.990 24.415	E206 1.268 1.414 0.190	C016 0.967 1.039 21.138	B005 0.808 0.912 24.294	E005 1.020 1.346 0.153	
12	D017 1.240 1.352 14.256	B020 0.869 0.929 25.777	D003 1.142 1.220 17.072	C012 0.967 1.039 21.137	E123 1.310 1.453 0.197	E116 1.067 1.348 0.160	D007 0.559 1.002 13.471	
13	D207 1.220 1.299 19.835	E216 1.326 1.491 0.200	D231 1.119 1.220 19.586	B014 0.808 0.912 24.293	E115 1.067 1.348 0.160	C013 0.434 0.805 26.371		
14	E101 1.302 1.509 0.196	B008 0.848 0.917 24.197	E109 1.196 1.419 0.180	E003 1.020 1.346 0.153	D012 0.559 1.003 13.466			
15	D201 0.717 1.017 19.734	E016 0.891 1.229 0.134	D027 0.596 1.036 14.244	Fuel ID Assembly power Peak pin power Assembly burnup				

Figure 4-25: Assembly power distribution at BOC for Cycle03

	H	G	F	E	D	C	B	A
08	C103 0.710 0.747 35.983	D203 0.997 1.130 27.568	E219 1.384 1.536 10.685	C007 0.958 0.991 36.641	D026 1.205 1.304 23.849	D205 1.181 1.247 29.267	E105 1.287 1.450 10.324	D223 0.696 0.974 25.301
09	D225 0.997 1.130 27.568	B207 0.803 0.869 30.421	D214 1.157 1.262 26.461	E221 1.366 1.510 10.553	B007 0.889 0.962 32.685	E210 1.370 1.510 10.744	B002 0.842 0.919 30.818	E015 0.843 1.173 6.926
10	E224 1.384 1.536 10.685	D209 1.157 1.262 26.457	D222 1.104 1.175 27.979	C118 0.920 1.000 31.582	D015 1.110 1.197 25.918	D220 1.073 1.171 28.218	E108 1.160 1.370 9.402	D010 0.582 0.990 18.861
11	C010 0.958 0.991 36.641	E220 1.366 1.510 10.553	C110 0.920 1.000 31.584	E206 1.336 1.466 10.384	C016 0.963 1.041 28.707	B005 0.796 0.868 30.598	E005 0.952 1.246 7.874	
12	D017 1.205 1.304 23.849	B020 0.890 0.962 32.679	D003 1.110 1.197 25.921	C012 0.963 1.041 28.705	E123 1.324 1.465 10.495	E116 1.084 1.324 8.580	D007 0.559 0.970 17.858	
13	D207 1.181 1.247 29.267	E216 1.370 1.510 10.745	D231 1.073 1.171 28.218	B014 0.797 0.868 30.598	E115 1.084 1.324 8.580	C013 0.463 0.839 29.885		
14	E101 1.287 1.450 10.324	B008 0.842 0.919 30.819	E109 1.160 1.370 9.404	E003 0.952 1.246 7.875	D012 0.559 0.970 17.853			
15	D201 0.696 0.974 25.301	E016 0.844 1.174 6.930	D027 0.582 0.991 18.863	Fuel ID Assembly power Peak pin power Assembly burnup				

Figure 4-26: Assembly power distribution at MOC for Cycle03

	H	G	F	E	D	C	B	A
08	C103 0.750 0.784 41.723	D203 0.994 1.093 35.414	E219 1.311 1.423 21.391	C007 0.938 0.964 44.126	D026 1.151 1.239 33.127	D205 1.123 1.176 38.383	E105 1.251 1.377 20.386	D223 0.724 0.981 30.906
09	D225 0.994 1.093 35.414	B207 0.820 0.881 36.804	D214 1.106 1.182 35.405	E221 1.304 1.414 21.183	B007 0.890 0.952 39.704	E210 1.313 1.419 21.417	B002 0.860 0.927 37.532	E015 0.870 1.175 13.660
10	E224 1.311 1.423 21.391	D209 1.106 1.182 35.400	D222 1.067 1.122 36.558	C118 0.919 0.987 38.871	D015 1.093 1.172 34.611	D220 1.062 1.137 36.680	E108 1.169 1.350 18.661	D010 0.626 1.022 23.612
11	C010 0.938 0.964 44.126	E220 1.304 1.414 21.182	C110 0.919 0.987 38.873	E206 1.306 1.413 20.942	C016 0.974 1.039 36.380	B005 0.839 0.901 37.069	E005 0.983 1.250 15.510	
12	D017 1.151 1.239 33.127	B020 0.890 0.952 39.699	D003 1.093 1.172 34.614	C012 0.974 1.039 36.379	E123 1.315 1.430 21.057	E116 1.139 1.341 17.490	D007 0.620 1.027 22.523	
13	D207 1.123 1.176 38.383	E216 1.313 1.419 21.418	D231 1.062 1.137 36.681	B014 0.839 0.901 37.068	E115 1.139 1.341 17.490	C013 0.524 0.900 33.813		
14	E101 1.251 1.377 20.386	B008 0.860 0.927 37.535	E109 1.169 1.350 18.663	E003 0.983 1.250 15.511	D012 0.620 1.027 22.519			
15	D201 0.724 0.981 30.906	E016 0.871 1.176 13.666	D027 0.626 1.022 23.614	Fuel ID Assembly power Peak pin power Assembly burnup				

Figure 4-27: Assembly power distribution at EOC for Cycle03

	H	G	F	E	D	C	B	A
08	D229 0.707 0.745 36.787	E223 0.895 1.003 21.525	F220 1.083 1.220 0.163	D203 0.827 0.870 35.538	D226 0.886 0.971 36.813	F107 1.316 1.446 0.198	D228 0.940 1.088 31.047	F001 0.909 1.188 0.136
09	E217 0.895 1.003 21.525	E102 0.917 0.986 20.523	D216 0.826 0.910 35.529	E008 1.143 1.285 15.681	F211 1.279 1.460 0.192	D006 0.991 1.056 34.760	F218 1.208 1.405 0.182	E007 0.742 1.101 13.771
10	F224 1.083 1.220 0.163	D208 0.827 0.911 35.525	F227 1.179 1.343 0.177	E210 1.085 1.210 21.580	E114 1.189 1.269 18.839	E107 1.219 1.319 17.673	F109 1.230 1.483 0.185	E207 0.497 0.916 21.258
11	D225 0.827 0.870 35.538	E004 1.143 1.284 15.682	E216 1.085 1.210 21.581	D218 0.876 0.940 36.689	D016 1.089 1.166 23.775	D025 1.113 1.228 22.689	F010 1.061 1.446 0.159	
12	D220 0.886 0.971 36.813	F207 1.279 1.460 0.192	E110 1.189 1.269 18.841	D019 1.090 1.166 23.777	F217 1.266 1.435 0.190	F118 1.087 1.384 0.163	E206 0.497 0.933 21.017	
13	F106 1.316 1.446 0.198	D009 0.991 1.056 34.762	E103 1.220 1.320 17.673	D005 1.114 1.229 22.685	F119 1.087 1.385 0.163	D021 0.454 0.852 33.195		
14	D213 0.940 1.088 31.047	F204 1.208 1.405 0.182	F105 1.231 1.484 0.185	F012 1.063 1.448 0.159	E120 0.503 0.981 21.132			
15	F007 0.909 1.188 0.136	E013 0.741 1.101 13.777	E212 0.497 0.916 21.257	Fuel ID Assembly power Peak pin power Assembly burnup				

Figure 4-28: Assembly power distribution at BOC for Cycle04

	H	G	F	E	D	C	B	A
08	D229 0.749 0.783 43.011	E223 0.935 1.044 29.316	F220 1.191 1.316 9.724	D203 0.864 0.908 42.667	D226 0.926 1.006 44.402	F107 1.373 1.502 11.377	D228 0.971 1.111 39.010	F001 0.910 1.206 7.689
09	E217 0.935 1.044 29.316	E102 0.956 1.027 28.475	D216 0.866 0.923 42.679	E008 1.128 1.235 25.197	F211 1.341 1.486 11.117	D006 1.005 1.055 43.059	F218 1.291 1.455 10.538	E007 0.766 1.128 20.031
10	F224 1.191 1.316 9.724	D208 0.866 0.923 42.683	F227 1.247 1.388 10.346	E210 1.044 1.144 30.543	E114 1.110 1.194 28.468	E107 1.134 1.198 27.494	F109 1.213 1.436 10.313	E207 0.521 0.934 25.503
11	D225 0.864 0.908 42.667	E004 1.128 1.234 25.197	E216 1.044 1.144 30.544	D218 0.847 0.906 43.936	D016 1.024 1.096 32.587	D025 1.026 1.114 31.581	F010 0.971 1.298 8.586	
12	D220 0.926 1.006 44.402	F207 1.340 1.485 11.112	E110 1.110 1.194 28.470	D019 1.024 1.095 32.590	F217 1.299 1.442 10.831	F118 1.092 1.356 9.201	E206 0.495 0.879 25.163	
13	F106 1.373 1.502 11.377	D009 1.004 1.055 43.060	E103 1.134 1.198 27.497	D005 1.027 1.114 31.584	F119 1.091 1.356 9.197	D021 0.482 0.875 37.080		
14	D213 0.971 1.111 39.010	F204 1.291 1.454 10.536	F105 1.214 1.436 10.317	F012 0.972 1.298 8.601	E120 0.500 0.914 25.318			
15	F007 0.910 1.206 7.689	E013 0.766 1.127 20.036	E212 0.521 0.934 25.504	Fuel ID Assembly power Peak pin power Assembly burnup				

Figure 4-29: Assembly power distribution at MOC for Cycle04

	H	G	F	E	D	C	B	A
08	D229 0.836 0.868 49.613	E223 1.007 1.100 37.422	F220 1.254 1.362 20.015	D203 0.899 0.949 50.003	D226 0.923 0.982 52.069	F107 1.294 1.390 22.426	D228 0.950 1.065 46.976	F001 0.906 1.178 15.158
09	E217 1.007 1.100 37.422	E102 1.022 1.092 36.716	D216 0.917 0.968 50.118	E008 1.123 1.205 34.507	F211 1.286 1.391 22.036	D006 0.978 1.020 51.238	F218 1.241 1.372 21.087	E007 0.778 1.106 26.396
10	F224 1.254 1.362 20.015	D208 0.918 0.970 50.128	F227 1.265 1.372 20.859	E210 1.043 1.114 39.193	E114 1.081 1.147 37.511	E107 1.092 1.151 36.683	F109 1.173 1.353 20.209	E207 0.551 0.932 29.937
11	D225 0.899 0.949 50.003	E004 1.123 1.205 34.507	E216 1.043 1.114 39.194	D218 0.869 0.919 51.037	D016 1.020 1.080 41.018	D025 1.015 1.082 39.998	F010 0.968 1.246 16.560	
12	D220 0.923 0.982 52.069	F207 1.286 1.391 22.027	E110 1.081 1.146 37.513	D019 1.020 1.079 41.021	F217 1.275 1.386 21.584	F118 1.114 1.334 18.400	E206 0.540 0.904 29.447	
13	F106 1.294 1.390 22.426	D009 0.978 1.020 51.238	E103 1.092 1.151 36.686	D005 1.016 1.082 40.005	F119 1.113 1.334 18.390	D021 0.533 0.910 41.289		
14	D213 0.950 1.065 46.976	F204 1.241 1.372 21.082	F105 1.173 1.353 20.215	F012 0.969 1.246 16.583	E120 0.544 0.930 29.634			
15	F007 0.906 1.178 15.158	E013 0.777 1.105 26.399	E212 0.551 0.932 29.938	Fuel ID Assembly power Peak pin power Assembly burnup				

Figure 4-30 Assembly power distribution at EOC for Cycle04

It can be found that the assemblies with maximum assembly power or maximum pin peaking are fresh fuel assemblies. This is reasonable and also desireable since the fresh fuel is less susceptible to fuel failure compared to once or twice burnt fuel.

Figure 4-31 a to d show the core axial power distribution for Cycle01 to Cycle04. The axial power distribution is gradually flattened with depletion. At BOC, the axial peaking is relatively large. At MOC and EOC, the axial power distribution becomes more flat with maximum peaking around 1.1.

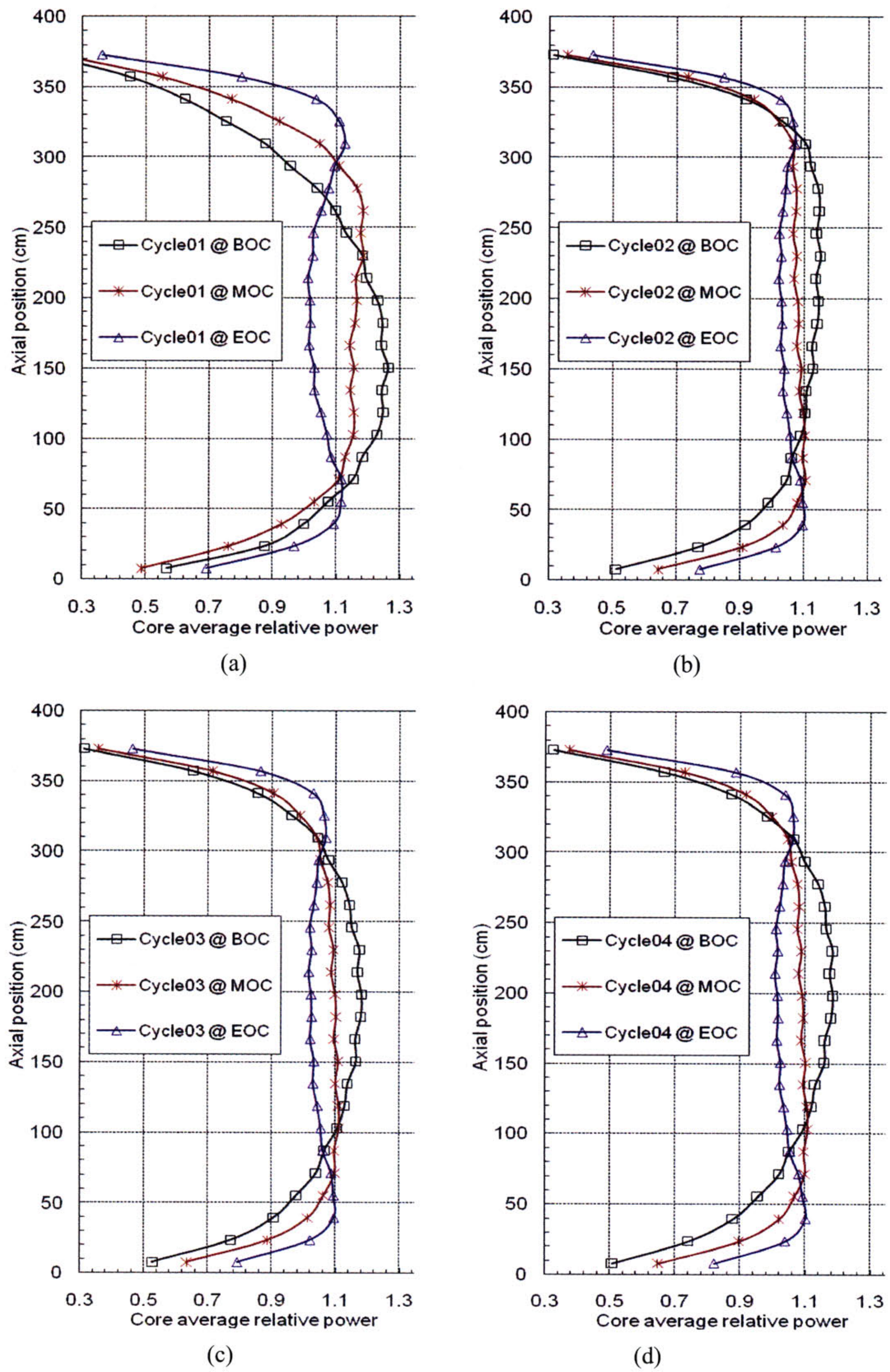

Figure 4-31: Core axial power distribution at BOC, MOC, and EOC for each cycle

Figure 4-32 shows the K-inf of various assemblies calculated by CASMO-4. Burnable poison introduces positive reactivity into the core as burnup increases. Thus, for the assemblies of B1, B2, C1, D2, E1, and E2 with burnable poisons, K-inf decrease slowly or even increases a little (C1) during early burnup. The use of burnable poisons would effectively reduce the power peaking by suppressing reactivity.

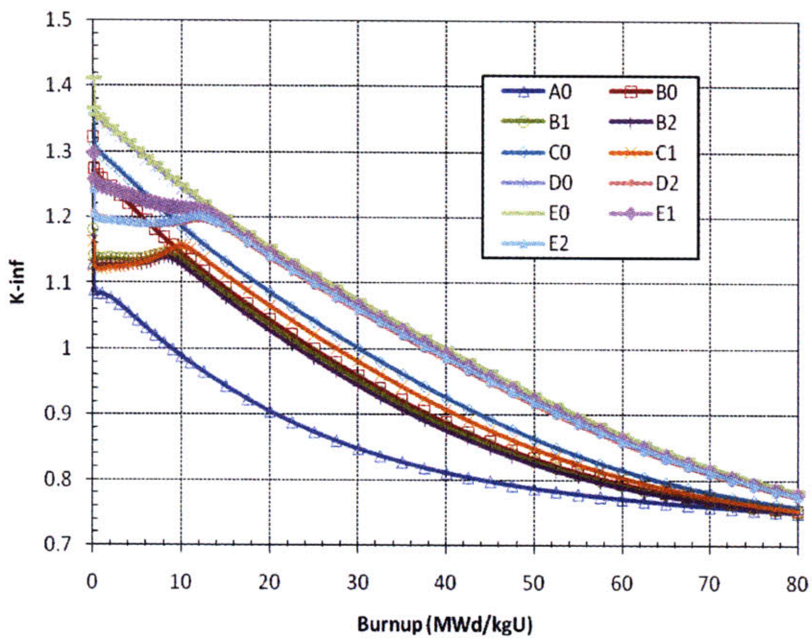

Figure 4-32: K-inf vs burnup for various assemblies

The axial offset which is defined as the percentage difference between the power generated in the upper and the lower halves of the core is shown in Figure 4-33 for different cycles. Cycle01 has relatively large axial offset at BOC, when the lower half of the core generates about 11% more power than the upper half region.

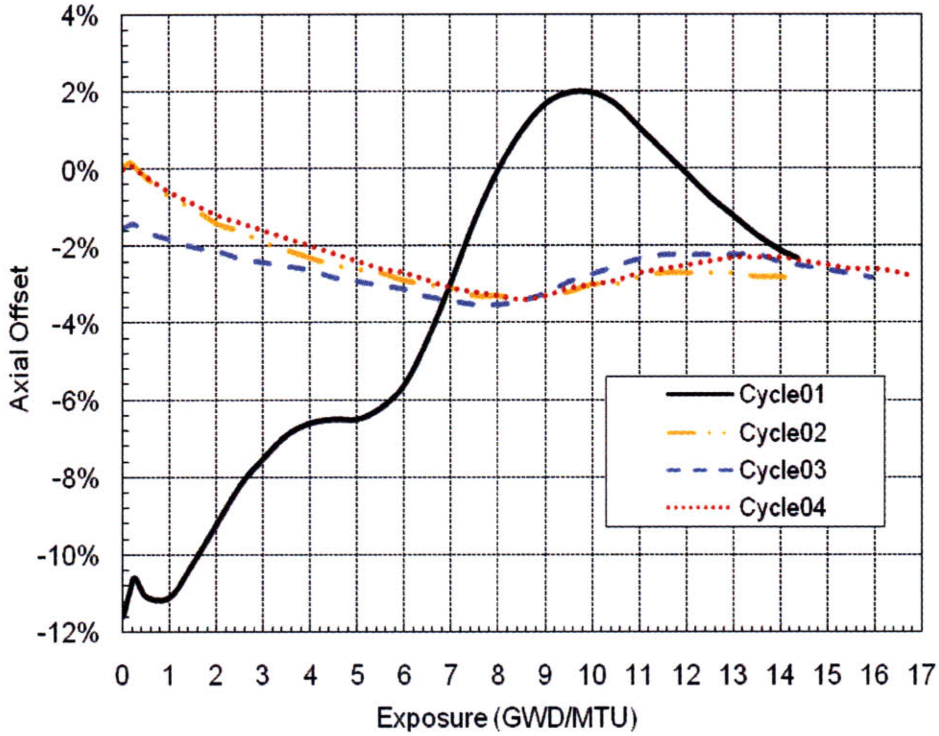

Figure 4-33: Axial offset during burnup for each cycle

The nuclear enthalpy rise hot channel factor and total peaking factor during each cycle are shown in Figures 4-34 and 4-35, respectively. The hot channel factor is under the design target, i.e., the maximum hot channel is around 1.54, well below the constraint of 1.65. The maximum hot spot factor is well within the limitation of 2.5 for all cycles.

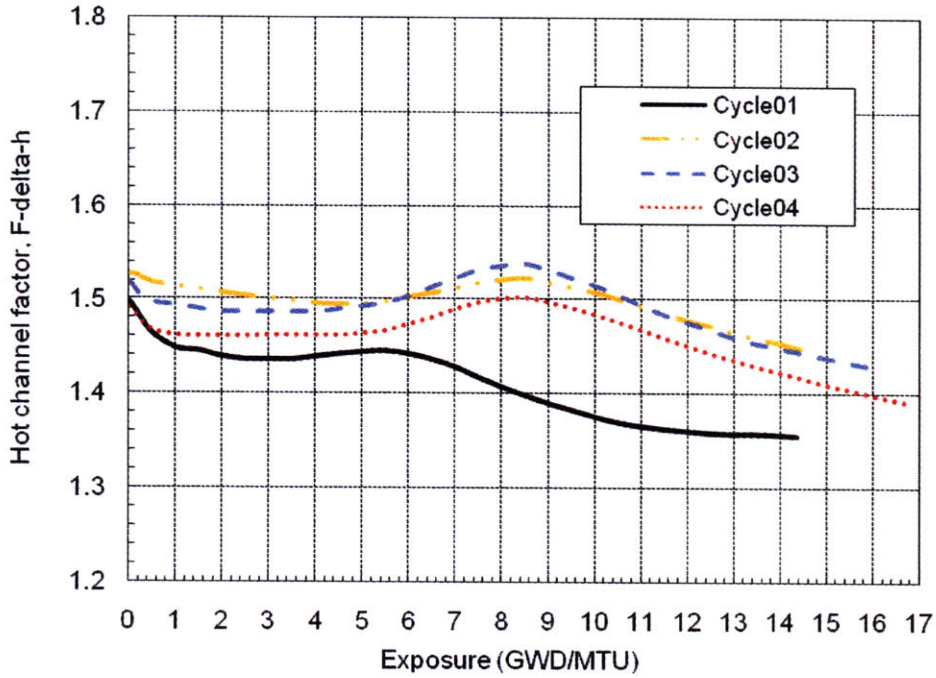

Figure 4-34: The hot channel factor during each cycle

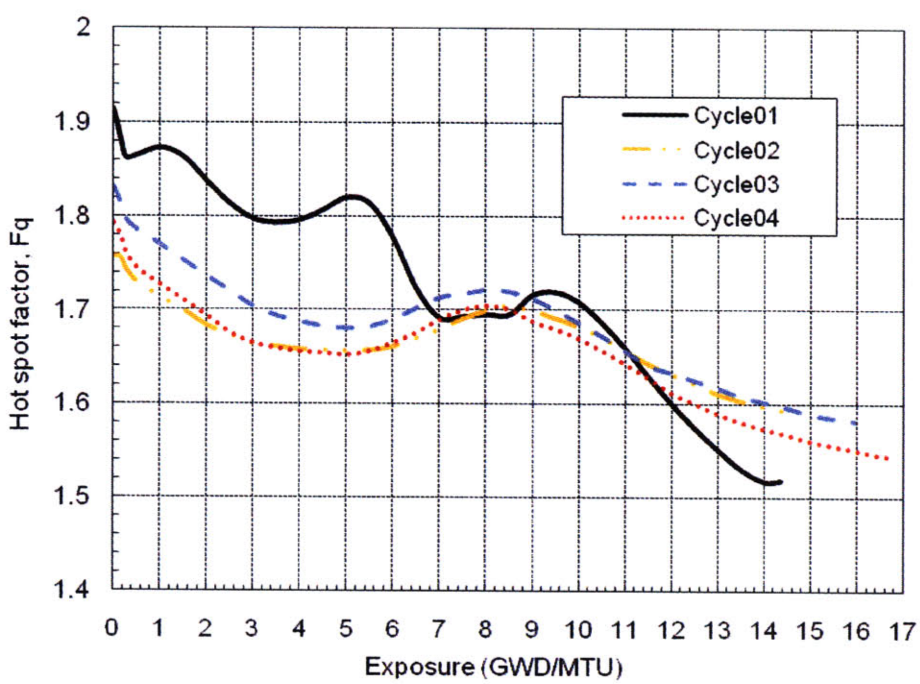

Figure 4-35: The hot spot factor during each cycle

4.5. Equilibrium Annular Fuel Whole Core Design

4.5.1. Annular Fuel Core Description

Since the assembly dimension is kept unchanged for the annular fuel rods, the annular fueled core design should be similar to the reference PWR core with solid fuel. The equilibrium core consists of 193 fuel assemblies using a 3-batch fuel management – 64 fresh fuel assemblies, 64 once-burnt fuel assemblies, and 49 twice-burnt fuel assemblies. The equilibrium concept implies a constant reloading scheme, which means the reload fuel assemblies as well as the shuffling pattern of the burnt fuel assemblies are indentical from cycle to cycle. It represents an ideal situation of refueling strategy with no operational disturbances. Although in practice such equilibrium never exsists, this particular concept is still valuable to providing a point of reference for evaluating the rector core performance. In fact, many actual core reload designs can be viewed as a perturbed equilibrium core by near-term operational targets or sometimes operating requirement changes.

An iterative method is used in SIMULATE-3 to approach the equilibrium core. Specifically, nine successive full power cycles are first operated using the constant loading pattern. Then the finally prepared 10th cycle can be estimated as equilibrium core, which is not depedent on the initialization [Xu et al, 2004].

The optimized annular fuel dimensions are used based on Case 2 in Table 3-7. The annular fuel core is designed to accommodate 20% power uprate, which is about 3378 MWth. The inlet coolant temperature is reduced to 287.7 °C, while fixing the outlet temperature and mass flow rate. For the annular fuel core, B_4C and Gd_2O_3 are chosen as the control rod material and burnable absorber, respectively. The general annular fuel core description is summarized in Table 4-5.

Table 4-5: Summary of equilibrium annular fuel core description

Core performance	
Total thermal power, MW	3378
Heat generated in fuel, %	97.5
Volumetric power density, kW/ltr	115.51
Inlet coolant temperature, °C	287.7
Average coolant temperature, °C	307.85
Fuel rod	
Pellet material	UO_2
Pellet theoretical density, g/cc	10.96
Pellet density, g/cc	10.44
Active length, cm	381
Fuel rod outer diameter, cm	1.580
Fuel rod inner diameter, cm	0.852
Pellet outer diameter, cm	1.442
Pellet inner diameter, cm	0.980
Clad material	ZIRLO
Outer Clad thickness, cm	0.064
Inner Clad thickness, cm	0.057
Control rod	
Poison material	B_4C
Diameter, cm	1.872
Density, g/cc	1.84
Burnable absorber	
Absorber material	Gd_2O_3-UO_2
Theoretical density, Gd_2O_3, g/cc	7.41
Spacer grid	
Material	Zircaloy-4
Number per assembly (active region)	10
Grid spacing, cm	39.93

Different types of assemblies with different enrichments of annular fuel and different weight percent of Gd_2O_3 in burnable absorbers are analyzed within different core loading patterns to satisfy three basic core design targets: 1) 18-month-cycle with a capacity factor of 90% (493.1 days); 2) the peak critical boron concentration is not greater than 1750 ppm; 3) the pin power peaking during the cycle is less than 1.65, and the hot spot factor is less than 2.5. Although there are other constraints such as a negative Moderator Temperature Coefficient

(MTC) at hot full power operations, one should be confident that other requirements are very likely to be satisfied if the above three design targets are met.

One solution is found to satisfy the above conditions with annular fuel. This solution is not unique but it provides valuable reference information for annular fuel refueling strategy in practice. The types of assemblies that were used in the equilibrium core are shown in Figure 4-36. Table 4-6 summarizes the fuel enrichment and burnable poisons in each assembly and Table 4-7 summarizes the number of different assemblies in the equilibrium core. Lower enrichment fuel rods are located around the five guide tubes to reduce the peak pin power factor. The burnable rods consist of uranium oxide with natural U-235 enrichment and various weight percentages of Gd_2O_3, in order to flatten the core power distribution. The cutback regions of 15.24 cm length are at the top and bottom of the burnable poison rods, where there is no Gd but uranium oxide with natural enrichment. This is consistent with the design of burnable poisons in the solid fuel core of OPR-1000.

Table 4-6: Summary of assembly types with annular fuel

Assembly type	Assembly No.	Fuel Enrichment (wt% U-235)	No. of fuel rods per assembly	No. of Gd poison rods per assembly	Gd_2O_3 wt%
0	**001~012**	6.5/7.5	40/80	4	4
1	**101~120**	6.5/7.5	40/76	8	8
2	**201~208**	6.5/7.5	40/72	12	16
2	**209~224**	6.5/7.5	40/72	12	10
3	**301~308**	6.5/7.5	40/68	16	6

Table 4-7: Summary of the number of various assemblies with annular fuel

Assembly No.	Number of Fresh Fuel	Number of Once-burnt Fuel	Number of Twice-burnt Fuel
001~012	12	12	12
101~120	20	20	20
201~208	8	8	1
209~224	16	16	16
301~308	8	8	0

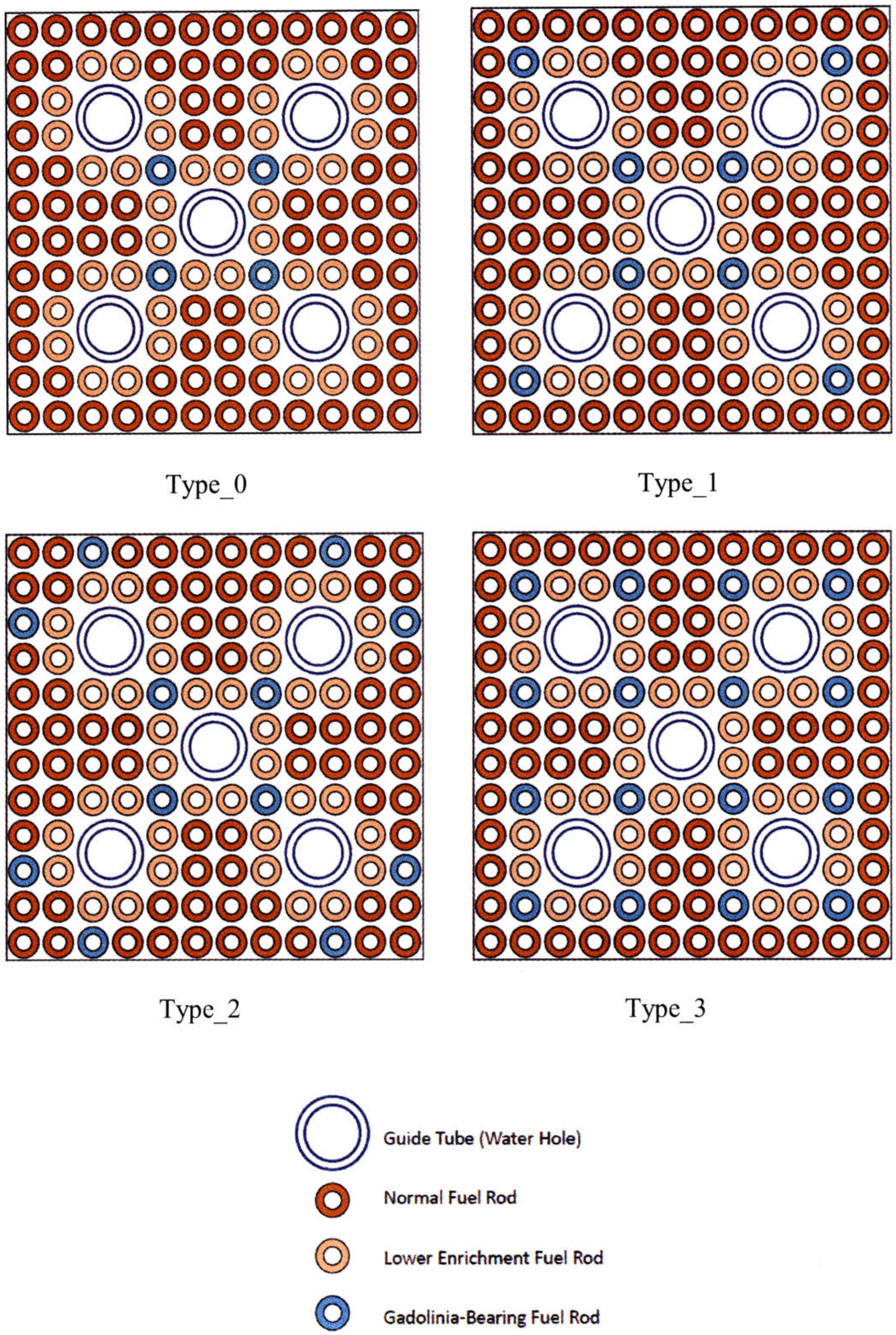

Figure 4-36: Fuel pin and burnable absorber arrangement of various annular fuel assemblies

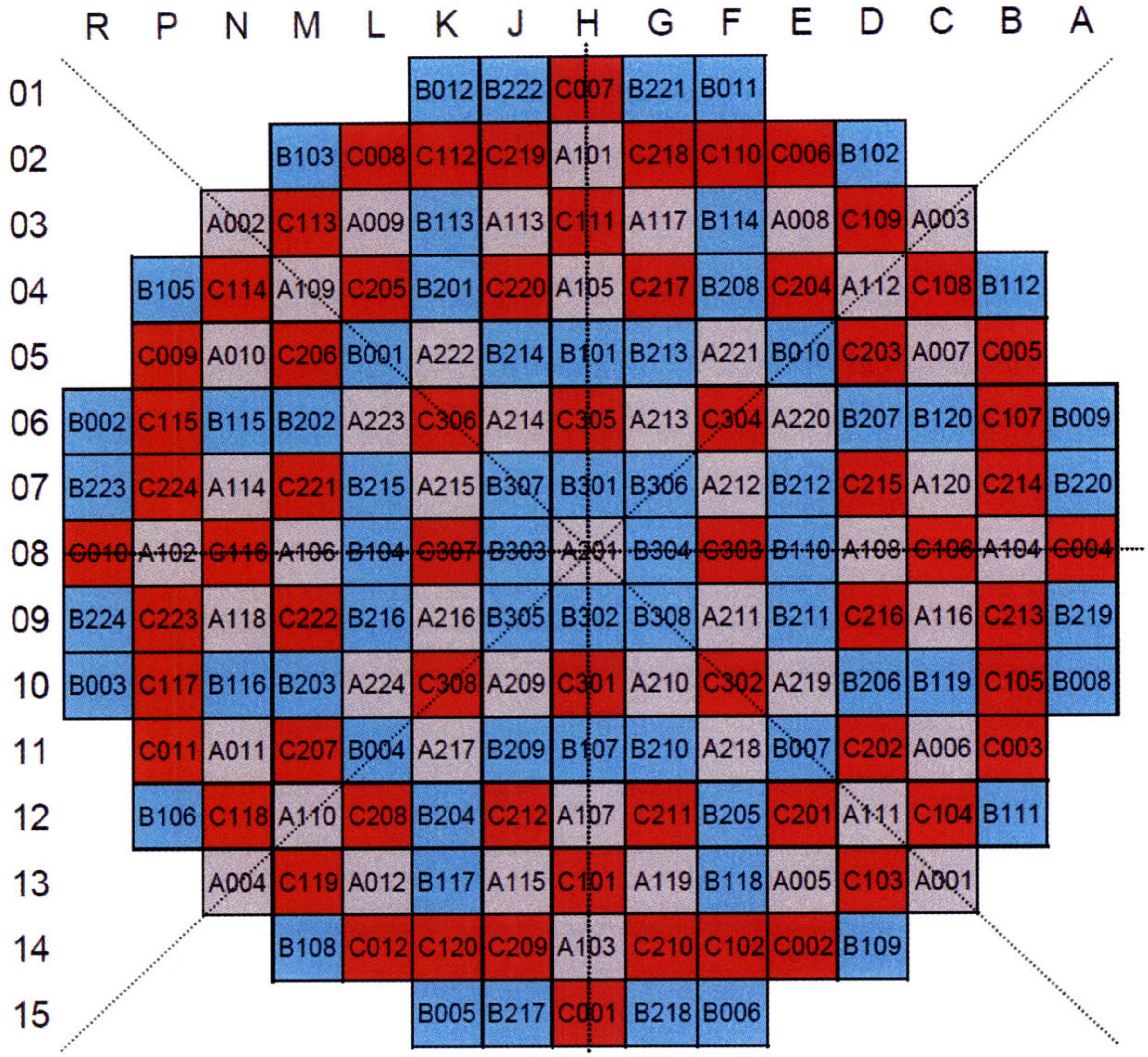

Figure 4-37: Equilibrium core loading pattern for annular fuel design

The equilibrium core loading pattern is shown in Figure 4-37. "Axxx", "Bxxx" and "Cxxx" are twice-burnt, once-burnt, and fresh fuel assemblies, respectively. The first number of "xxx" is the type number of different assemblies shown in Figure 4-36. It can be seen that the whole core is one-eighth symmetric. In particular, the constraint of core symmetry significantly reduces the number of possible core loading patterns for equilibrium core design.

4.5.2. SIMULATE-3 Annular Fuel Core Models

Similar to the solid fuel core model, the annular fuel core is calculated as a quarter core using SIMULATE-3. Each assembly is modeled in three dimensions with 24 axial nodes and 2x2 radial nodes. Various CASMO-4 runs of different assemblies under different operating conditions are prepared for the cross section library needed in SIMULATE-3, as shown in Table 4-8. Compared with the runs for solid fuel, the fuel temperature is reduced because the annular fuel has larger cooling surface and shorter conductance path. The moderator temperature is lower because the inlet coolant temperature is reduced to maintain the same outlet temperature.

Table 4-8: Typical parameters in CASMO-4 runs for annular fuel assemblies at 120% power

Parameters	**Base value**	**Instantaneous branches**
Base case		
Fuel temperature (K)	700	293.2 449.8 549.8 560.9 700 1000
Moderator temperature (K)	581.0	293.2 333.2 449.8 505.4 546.8 560.9 581.0 600.0 616.5
Boron concentration (ppm)	600	0 1200 1800 2400
Control rod position	Fully withdrawn	Fully inserted
Low fuel temperature history		
Fuel temperature (K)	560.9	700
Moderator temperature (K)	581.0	—
Boron concentration (ppm)	600	—
Control rod position	Fully withdrawn	—
High fuel temperature history		
Fuel temperature (K)	1000	700
Moderator temperature (K)	581.0	—
Boron concentration (ppm)	600	—
Control rod position	Fully withdrawn	—
Low moderator temperature history		
Fuel temperature (K)	700	—
Moderator temperature (K)	560.9	581.0
Boron concentration (ppm)	600	—
Control rod position	Fully withdrawn	—
High moderator temperature history		
Fuel temperature (K)	700	—
Moderator temperature (K)	600.0	581.0
Boron concentration (ppm)	600	—

Control rod position	Fully withdrawn	—
Low boron concentration history		
Fuel temperature (K)	700	—
Moderator temperature (K)	581.0	—
Boron concentration (ppm)	0	600
Control rod position	Fully withdrawn	—
High boron concentration history		
Fuel temperature (K)	700	—
Moderator temperature (K)	581.0	—
Boron concentration (ppm)	1200	600
Control rod position	Fully withdrawn	—

4.5.3. Steady-state Annular Fuel Core Performance

This equilibrium design is able to reach at a cycle length of 493.9 days, very close to the 493.1 days requirement. The critical boron contration (CBC) is another one of the most significant core depletion characteristics. The CBC of the equilibrium annular fuel design is shown in Figure 4-38, compared with the results from Cycle04 of the solid fuel core. It can be seen that the peak CBC is 1486 ppm, less than the constraint of 1750 ppm.

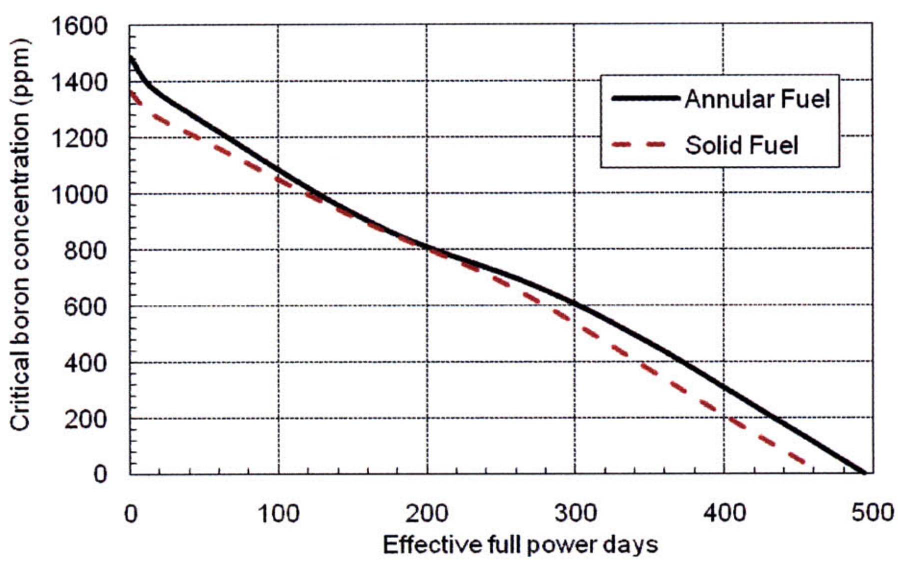

Figure 4-38: Critical boron concentration of annular fuel core and solid fuel core during burnup

Typically, three points in the cycle are of interest: BOC (0.167 GWD/MT, 3.7 days), MOC (11.131 GWD/MT, 248.7 days), and EOC (22.113 GWD/MT, 493.9). The core power and assembly burnup distributions at the BOC, MOC and EOC are shown in Figure 4-39 to 4-41. Only a quarter core is reported because of a 90-degree rotational symmetry of the whole core. The assembly burnup is in units of GWD/MT.

	H	G	F	E	D	C	B	A
08	A201 0.664 0.718 51.723	B304 0.835 0.951 25.172	C303 0.905 1.115 0.150	B110 1.037 1.169 27.610	A108 1.000 1.108 44.480	C106 1.339 1.551 0.224	A104 0.917 1.085 45.035	C004 0.847 1.179 0.142
09	B302 0.835 0.951 25.172	B308 0.825 0.939 25.170	A211 0.701 0.808 51.362	B211 0.999 1.168 28.663	C216 1.292 1.554 0.216	A116 0.985 1.077 49.436	C213 1.183 1.485 0.198	B219 0.653 0.953 27.140
10	C301 0.905 1.115 0.150	A210 0.712 0.834 50.271	C302 0.925 1.193 0.154	A219 0.939 1.137 42.167	B206 1.174 1.343 27.705	B119 1.282 1.461 23.355	C105 1.267 1.596 0.213	B008 0.579 0.999 23.403
11	B107 1.037 1.169 27.610	B210 1.016 1.198 27.200	A218 0.934 1.109 41.912	B007 1.298 1.491 19.951	C202 1.351 1.631 0.226	A006 1.123 1.233 36.746	C003 1.101 1.554 0.185	
12	A107 1.000 1.108 44.480	C211 1.280 1.539 0.214	B205 1.160 1.327 27.535	C201 1.339 1.610 0.224	A111 1.015 1.091 41.482	C104 1.076 1.426 0.180	B111 0.531 1.015 29.756	
13	C101 1.339 1.551 0.224	A119 0.997 1.082 49.087	B118 1.283 1.457 23.717	A005 1.127 1.232 36.906	C103 1.097 1.441 0.184	A001 0.464 0.833 46.134		
14	A103 0.917 1.085 45.035	C210 1.214 1.524 0.203	C102 1.298 1.627 0.217	C002 1.129 1.578 0.189	B109 0.590 1.092 23.240			
15	C001 0.847 1.179 0.142	B218 0.668 0.983 26.667	B006 0.595 1.000 23.280	Fuel ID Assembly power Peak pin power Assembly burnup				

Figure 4-39: Assembly power distribution at BOC for equilibrium annular fuel core

	H	G	F	E	D	C	B	A
08	A201 0.827 0.881 60.072	B304 1.044 1.182 35.537	C303 1.303 1.604 11.851	B110 1.120 1.224 39.477	A108 1.002 1.082 55.462	C106 1.362 1.612 14.787	A104 0.912 1.060 55.022	C004 0.891 1.199 9.654
09	B302 1.044 1.182 35.537	B308 1.032 1.143 35.394	A211 0.881 0.965 60.021	B211 1.060 1.170 40.004	C216 1.296 1.529 14.317	A116 0.951 1.049 60.041	C213 1.179 1.431 12.970	B219 0.667 0.949 34.373
10	C301 1.303 1.604 11.851	A210 0.893 0.991 59.052	C302 1.242 1.528 11.678	A219 0.953 1.047 52.622	B206 1.081 1.192 40.263	B119 1.137 1.243 36.689	C105 1.223 1.519 13.692	B008 0.583 0.981 30.054
11	B107 1.120 1.224 39.477	B210 1.077 1.201 38.736	A218 0.953 1.031 52.342	B007 1.158 1.285 33.576	C202 1.181 1.386 14.207	A006 0.983 1.080 48.404	C003 1.035 1.376 11.965	
12	A107 1.002 1.082 55.462	C211 1.289 1.519 14.216	B205 1.075 1.187 39.989	C201 1.175 1.374 14.113	A111 0.896 0.951 52.039	C104 1.001 1.282 11.560	B111 0.509 0.904 35.517	
13	C101 1.362 1.612 14.787	A119 0.961 1.039 59.805	B118 1.140 1.281 37.066	A005 0.986 1.076 48.600	C103 1.019 1.299 11.776	A001 0.451 0.757 51.213		
14	A103 0.912 1.060 55.022	C210 1.205 1.466 13.269	C102 1.249 1.552 13.993	C002 1.055 1.393 12.236	B109 0.558 0.962 29.597			
15	C001 0.891 1.199 9.654	B218 0.679 0.975 34.038	B006 0.596 0.972 29.816	Fuel ID Assembly power Peak pin power Assembly burnup				

Figure 4-40: Assembly power distribution at MOC for equilibrium annular fuel core

	H	G	F	E	D	C	B	A
08	A201 0.764 0.804 68.638	B304 0.941 1.044 46.230	C303 1.190 1.391 25.547	B110 1.032 1.102 51.271	A108 0.972 1.059 66.384	C106 1.304 1.477 29.674	A104 0.933 1.048 65.297	C004 0.923 1.183 19.735
09	B302 0.941 1.044 46.230	B308 0.939 1.018 46.025	A211 0.829 0.892 69.354	B211 1.001 1.107 51.268	C216 1.283 1.479 28.672	A116 0.951 1.036 70.587	C213 1.241 1.458 26.558	B219 0.716 1.006 42.026
10	C301 1.190 1.391 25.547	A210 0.838 0.913 68.492	C302 1.186 1.388 25.034	A219 0.931 1.042 62.851	B206 1.072 1.152 51.977	B119 1.102 1.188 48.937	C105 1.210 1.430 27.222	B008 0.625 1.025 36.730
11	B107 1.032 1.102 51.271	B210 1.014 1.134 50.166	A218 0.931 1.033 62.564	B007 1.160 1.243 46.071	C202 1.295 1.530 27.515	A006 1.000 1.046 59.173	C003 1.019 1.289 23.183	
12	A107 0.972 1.059 66.384	C211 1.278 1.473 28.499	B205 1.066 1.147 51.635	C201 1.288 1.523 27.347	A111 0.977 1.030 62.159	C104 1.109 1.360 23.149	B111 0.564 0.933 41.333	
13	C101 1.304 1.477 29.674	A119 0.954 1.035 70.421	B118 1.096 1.200 49.289	A005 0.997 1.053 59.363	C103 1.118 1.363 23.509	A001 0.536 0.851 56.584		
14	A103 0.933 1.048 65.297	C210 1.247 1.464 27.035	C102 1.212 1.432 27.649	C002 1.025 1.288 23.576	B109 0.607 0.981 35.911			
15	C001 0.923 1.183 19.735	B218 0.719 1.027 41.774	B006 0.628 0.997 36.572	Fuel ID Assembly power Peak pin power Assembly burnup				

Figure 4-41: Assembly power distribution at EOC for equilibrium annular fuel core

The maximum discharge burnup is 70.421 GWD/MT, which is higher than the values of typical PWR. But the annular fuel is a more robust fuel operating at lower temperatures, so this burnup value could be probably acceptable. Besides, it is still possible to further flatten the power and reduce the maximum EOC assembly burnup by optimizing the core design in practice.

Figure 4-42 shows the core axial power distribution at the BOC, MOC, and EOC. Compared to Figure 4-31 (d) of solid fuel core, the annular fuel core at 120% power has comparable axial power shapes with reasonably low peaking.

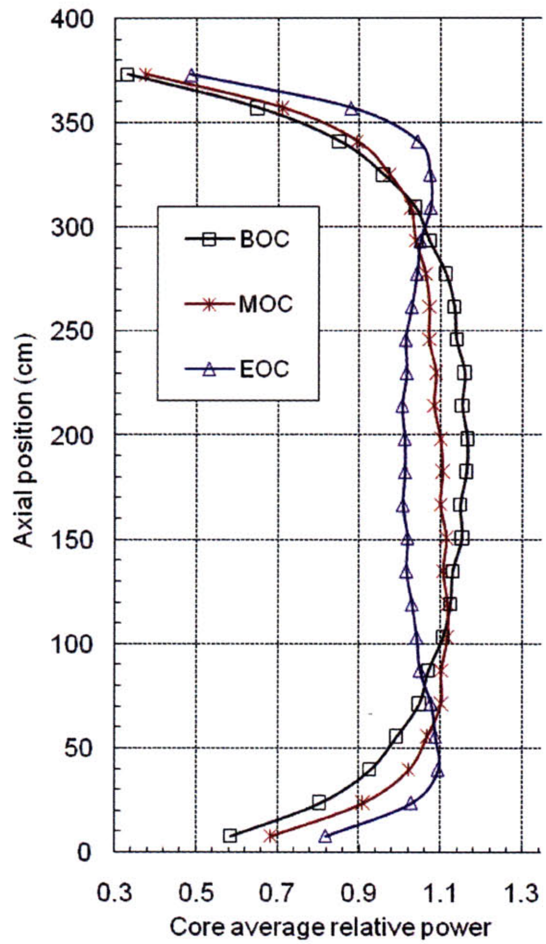

Figure 4-42: Core axial power distribution for equilibrium annular fuel core

The hot channel factor of annular fuel core is compared with that of solid fuel core in Figure 4-43. It shows that the annular fuel rod has a larger hot channel factor than the solid fuel rod. One reason is that the number of annular fuel rods per assembly, 124, is much less than that of solid fuel rods, which is 236. The burnable poison rods in the assembly have less layout options to flatten the power distribution. Nevertheless, the hot channel factor is below the 1.65

limit during the total cycle length with a maximum of 1.634 at BOC. The hot spot factor shown in Figure 4-44, although larger than that of the solid fuel core, is well below the 2.5 limits during the entire cycle life.

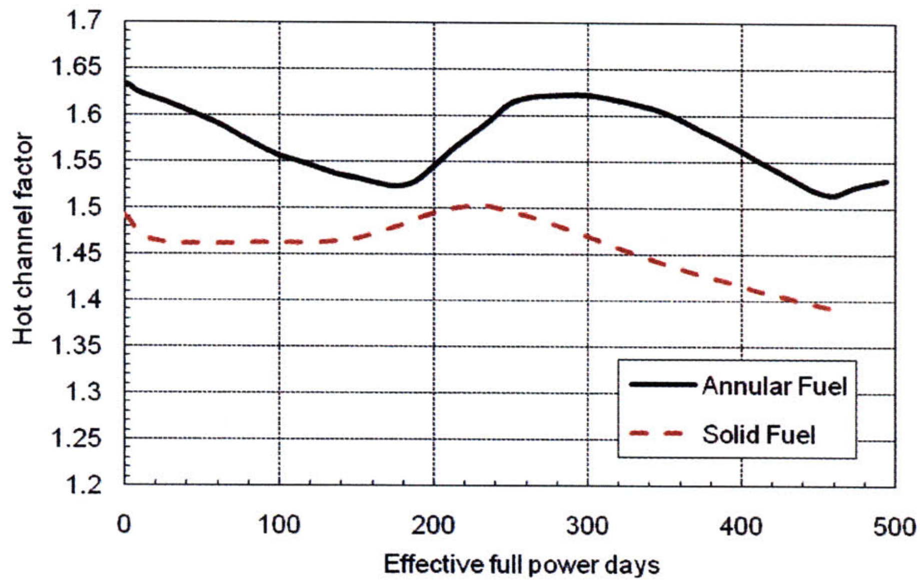

Figure 4-43: Hot channel factor for equilibrium annular fuel core

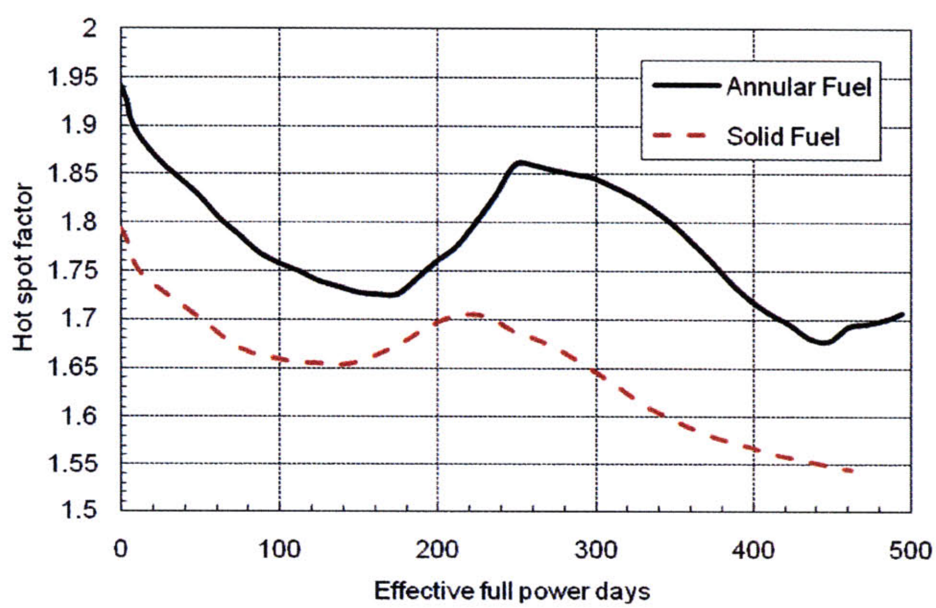

Figure 4-44: Hot spot factor for equilibrium annular fuel core

The axial offset distribution is shown in Figure 4-45. The annular fuel core has more negative axial offset especially around the MOC, and oscillation of axial offset is also larger. Since its absolute value is no greater than 4.5 %, this value should be acceptable.

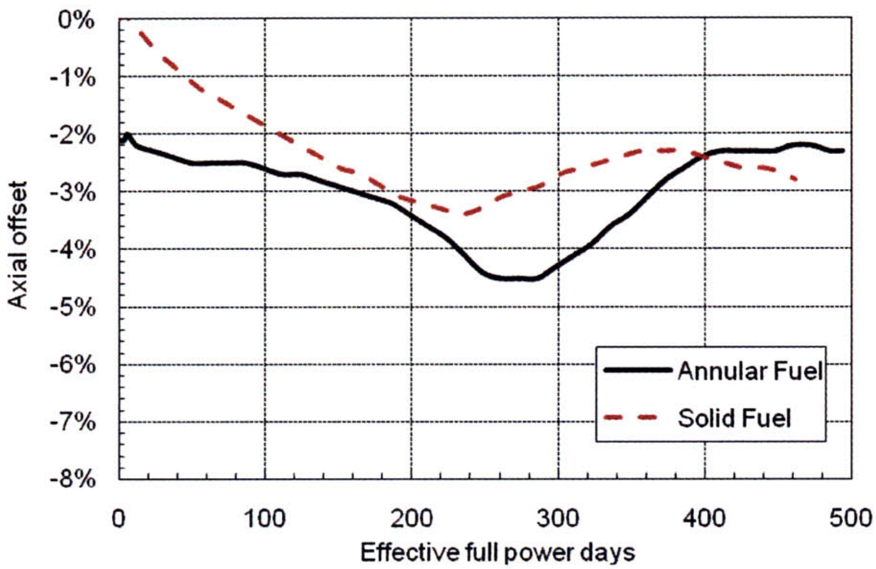

Figure 4-45: Axial offset for equilibrium annular fuel core

4.6. Summary

Computer codes that are used in reactor physics evaluation of OPR-1000 with the annular fuel were briefly described, including CASMO-4, MCNP-4C, and MCODE-2.2. Benchmark of OPR-1000 with conventional solid fuel was examined using CASMO-4 and MCODE-2.2, and good agreement was obtained as expected. In order to take into account the U-238 resonance absorption on the inner surface of the annular fuel and obtain realistic results, CASMO-4 requires an artificial increase of U-238 number densities. Therefore, a search was performed with the conclusion that increasing the U-238 content by 10% in CASMO-4 input yields the closest eigenvalues and the closest amount of plutonium production to the results of MCODE-2.2.

Furthermore, another deterministic code, TRITON, was also benchmarked against MCODE-2.2, and good agreements throughout the irradiation period were achieved.

In addition, a whole core model of Ulchin Nuclear unit 5 with solid fuel has been established using SIMULATE-3. Various CASMO-4 cases with different local conditions were run to prepare the three dimensional data for SIMULATE-3. Steady state core performance has been investigated, including the calculation of cycle length, critical boron concentration, radial and axial power distribution, and peaking factors. This benchmarking has demonstrated that the CASMO-TABLES-SIMULATE progression provides critical boron concentrations and cycle lengths that agree with KAERI's data. The assembly k infinities, assembly peaking, and hot spot peaking appear reasonable. Moreover, one equilibrium annular fuel core is proposed and analyzed. The peak boron concentration and cycle length requirement are well satisfied. The pin peaking factor is larger than that of the solid fuel core, but it is still below 1.65. The peaking factor may be lowered by a better refueling strategy.

5. Conclusions and Recommended Future Work

5.1. Summary of Conclusions

This work examined the feasibility of power uprate for OPR-1000. Whole core models for the originally proposed 12x12 and 14x14 annular fuel designs and reference OPR-1000 with solid fuel were developed for VIPRE-01. The annular fuel designs feature fixed core flow rate, fixed core inlet temperature and reduced core inlet temperature. The whole core results showed that although the 12x12 annular fuel design increases MDNBR margin for the 100% power, it cannot allow power uprate to 120% because of low MDNBR in the inner channel. The MDNBRs for the 14x14 annular fuel design were always inferior to those of the 12x12 annular fuel design because of the insufficient flow in the inner channel. Therefore, major improvement has been focused on the 12x12 array design. An optimization study was then undertaken through fine-tuning of the rod dimensions by slightly increasing the inner channel diameter and outer channel diameter, while keeping the fuel to moderator ratio fixed under two different pairs of inner and outer gap conductances. In either case, the reoptimized dimensions of the OPR1000 annular fuel were found to achieve sufficient MDNBR at 120% power. In addition, the MDNBR sensitivity to manufacturing tolerances was also investigated, showing that the new proposed design can accommodate typical manufacturing tolerances.

Very conservative VIPRE-01 models were established to analyze partial blockage of an inner channel by debris and the impact of corrosion and crud growth. The results show that even if up to 43% of the flow area of the inner channel is blocked in the hottest channel, the MNDBRs will still be above the 1.3 limit. MDNBR results for the corrosion and crud growth show that a maximum thickness of crud and ZrO_2 buildup of about 74μm~94μm can be tolerated under an acceptable MDNBR limitation.

For the reactor physics assessment, the reactivity of the fuel assembly of the reference OPR-1000 with solid fuel was calculated by CASMO-4, MCODE2.2 and TRITON. The results from the three different codes show excellent agreement. Benchmark of OPR-1000 with annular fuel was examined using CASMO-4 and MCODE2.2. In order to match the results of CASMO-4 to MCODE2.2, adjustments were needed in CASMO-4 input to account for the U-238 resonance absorption on the inner surface of the annular fuel rod. It was demonstrated that after fictitiously increasing the amount of U-238 by 10% for the rod, CASMO-4 could match MCODE-2.2 with small deviation. Last but not least, a neutronic whole core analysis of OPR-1000 was performed using the CASMO-4/TABLES-3/SIMULATE-3 package. The first four cycles of UCN Unit 5 were calculated. The critical boron concentration of the first three cycles shows excellent agreement with the data provided by KAERI. The distributions of the radial assembly power, axial core averge power, peaking pin power, and assembly burnup of four cycles were reasonably presented. In addition, an equilibrium annular fuel core was presented and analyzed. Specific fuel assemblies and enrichments of fuel rods were proposed to satisfy the design target, such as peak boron concentration, cycle length, and peaking factors.

5.2. Future Work

Future work should be focused on linkage between the MDNBR and mechanical behavior of the inner and outer gap conductances through burnup. As shown in this work, the MDNBR is very sensitive to the variance of the gap conductance. The range of inner and outer gap conductances needs to be determined carefully, since they are a crucial factor for the optimization of the annular fuel dimensions. A fuel performance code should be applied to investigate the expected conductance for various designs.

Next steps of neutronic analyses should be focused on the calculation of reactivity feedback and control, i.e. temperature coefficient, shutdown margin, etc. However, before these detailed neutronic analyses can be performed it is important to first confirm the thermal hydraulic design of the annular fuel, or possibly reoptimize it to achieve the largest possible MDNBR margins.

Appendices

Sample Inputs: CASMO-4

```
* FUEL SEGMENT: A0
*
* CASE MATRICES:
*     - BASE CASE WITH INSTANTANEOUS BRANCHES
*     - LOW TFU HISTORY WITH BRANCHES TO NOMINAL
*     - LOW TMO HISTORY WITH BRANCHES TO NOMINAL
*     - LOW BOR HISTORY WITH BRANCHES TO NOMINAL
*     - HIGH TFU HISTORY WITH BRANCHES TO NOMINAL
*     - HIGH TMO HISTORY WITH BRANCHES TO NOMINAL
*     - HIGH BOR HISTORY WITH BRANCHES TO NOMINAL
*
TTL * OPR-1000 PWR ASSEMBLY, A0, 16X16 LATTICE

***** STATE POINT PARAMETERS *****
TFU=900.0 TMO=585.4 BOR=600 VOI=0.0
SIM 'A0' 1.42 0.0 0 0  * no burnable poisons

***** OPERATING PARAMETERS *****
PRE 155.1296  * CORE PRESSURE, bars
PDE 96.26 'KWL'  * POWER DENSITY, KW/ltr

***** MATERIAL COMPOSITIONS *****
FUE 1 10.44/1.42
SPA 22.71475  * zircaloy grids

***** GEOMETRY SPECIFICATION *****
PWR 16 1.285 20.78
PIN 1 0.4095 0.418 0.475/'1' 'AIR' 'CAN'
PIN 5 1.145 1.245/'COO' 'BOX' //4  * C-E GUIDE TUBE
PIN 9 1.145 1.245/'COO' 'BOX' //4  * C-E control rods
PIN 9 0.936 0.9475 1.0365 1.145 1.245/'B4C' 'AIR' 'CRS' 'COO' 'BOX'
    //4 'RCC' 'ROD'
LPI 5
    1 1
    1 1 1
    1 1 1 9
    1 1 1 9 9
    1 1 1 1 1 1
    1 1 1 1 1 1 1
    1 1 1 1 1 1 1 1

***** BASE CASE WITH INSTANTANEOUS BRANCHES *****
DEP -80
STA
COE ,,0 0.5 1 2 3 4 5 6 7 8 9 10 15 20 25 30 40 50 60 70 80
TMO 293.2 333.2 449.8 505.4 546.8 569.3 585.4 600.0 616.5
+ TFU 293.2 449.8 549.8 569.3 900 1200
TMO 293.2 333.2 449.8 505.4 546.8 569.3 585.4 600.0 616.5
+ BOR 0 1200 1800 2400
TMO 293.2 333.2 449.8 505.4 546.8 569.3 585.4 600.0 616.5 ROD 'RCC'
```

```
SDC 100 100 100 100 100 1691.5 6574.5 8766.0 26298.0 43830.0/'DT'

***** LOW TFU HISTORY WITH BRANCHES TO NOMINAL *****
TTL * LOW TFU HISTORY
TFU=569.3 TMO=585.4 BOR=600 VOI=0.0
DEP -80
STA
COE ,,0 0.5 1 2 3 4 5 6 7 8 9 10 15 20 25 30 40 50 60 70 80
TFU 900

***** LOW TMO HISTORY WITH BRANCHES TO NOMINAL *****
TTL * LOW TMO HISTORY
TFU=900.0 TMO=569.3 BOR=600 VOI=0.0
DEP -80
STA
COE ,,0 0.5 1 2 3 4 5 6 7 8 9 10 15 20 25 30 40 50 60 70 80
TMO 585.4

***** LOW BOR HISTORY WITH BRANCHES TO NOMINAL *****
TTL * LOW BOR HISTORY
TFU=900.0 TMO=585.4 BOR=0.0 VOI=0.0
DEP -80
STA
COE ,,0 0.5 1 2 3 4 5 6 7 8 9 10 15 20 25 30 40 50 60 70 80
BOR 600

***** HIGH TFU HISTORY WITH BRANCHES TO NOMINAL *****
TTL * HIGH TFU HISTORY
TFU=1200 TMO=585.4 BOR=600 VOI=0.0
DEP -80
STA
COE ,,0 0.5 1 2 3 4 5 6 7 8 9 10 15 20 25 30 40 50 60 70 80
TFU 900

***** HIGH TMO HISTORY WITH BRANCHES TO NOMINAL *****
TTL * HIGH TMO HISTORY
TFU=900.0 TMO=600.0 BOR=600 VOI=0.0
DEP -80
STA
COE ,,0 0.5 1 2 3 4 5 6 7 8 9 10 15 20 25 30 40 50 60 70 80
TMO 585.4

***** HIGH BOR HISTORY WITH BRANCHES TO NOMINAL *****
TTL * HIGH BOR HISTORY
TFU=900.0 TMO=585.4 BOR=1200.0 VOI=0.0
DEP -80
STA
COE ,,0 0.5 1 2 3 4 5 6 7 8 9 10 15 20 25 30 40 50 60 70 80
BOR 600

END
```

Sample Inputs: TABLES-3

```
'COM' 789012345678901234567890123456789012345678901234567890123456789012345678901234567890
'COM'    1         2         3         4         5         6         7         8

'TIT' 'FUE SEG: A0'/
'PWR' 0 155.1296/
'LIB' 'ADD'/
'OPT' 4 1/
'CAS' '../C4/c4.A0.cax'/
'EXP' 29 1  0 0.5 1 2 3 4 5 6 7 8 9 10 11 12.5 15 17.5 20 25 30 35 40 45 50
            55 60 65 70 75 80/
'RES' 21 1  0 0.5 1 2 3 4 5 6 7 8 9 10 15 20 25 30 40 50 60 70 80/
'TFU'  6 5  293.2 449.8 549.8 569.3 900 1200/
'TMO'  9 7  293.2 333.2 449.8 505.4 546.8 569.3 585.4 600.0 616.5/
'BOR'  5 2  0 600 1200 1800 2400/
'HTFU' 3 2  569.3 900 1200/
'HTMO' 3 2  569.3 585.4 600/
'HBOR' 3 2  0 600 1200/
'CRD'  2 1  '   ' 'RCC'/
'SDC' 11 1  0 0.1 0.2 0.3 0.4 0.5 2.1915 8.766 17.532 43.83 87.66/
'BAS.MAC' 3 'EXP' 'TFU' 'TMO'/
'DEL.MAC' 3 'EXP' 'BOR' 'TMO'/
'DEL.MAC' 3 'EXP' 'CRD' 'TMO'/
'DEL.MAC' 2 'EXP' 'HTFU'/
'DEL.MAC' 2 'EXP' 'HTMO'/
'DEL.MAC' 2 'EXP' 'HBOR'/
'DEL.MAC' 2 'EXP' 'SDC'/
'EPS.MAC' 10*0.000/
'BAS.FPD' 3 'EXP' 'TFU' 'TMO'/
'DEL.FPD' 3 'EXP' 'BOR' 'TMO'/
'DEL.FPD' 3 'EXP' 'CRD' 'TMO'/
'DEL.FPD' 2 'EXP' 'HTFU'/
'DEL.FPD' 2 'EXP' 'HTMO'/
'DEL.FPD' 2 'EXP' 'HBOR'/
'DEL.FPD' 2 'EXP' 'SDC'/
'EPS.FPD' 10*0.000/
'BAS.DFS' 3 'EXP' 'TFU' 'TMO'/
'DEL.DFS' 3 'EXP' 'BOR' 'TMO'/
'DEL.DFS' 3 'EXP' 'CRD' 'TMO'/
'DEL.DFS' 2 'EXP' 'HTFU'/
'DEL.DFS' 2 'EXP' 'HTMO'/
'DEL.DFS' 2 'EXP' 'HBOR'/
'DEL.DFS' 2 'EXP' 'SDC'/
'EPS.DFS' 10*0.000/
'ADF' 1 1 0 0 1 1 0 0/
'PIN.PIN'/
'EPS.PIN' 10*0.000/
'STA'/

'TIT' 'FUE SEG: B0'/
'LIB' 'ADD'/
'CAS' '../C4/c4.B0.cax'/
'STA'/

'TIT' 'FUE SEG: B1'/
'LIB' 'ADD'/
```

```
'CAS' '../C4/c4.B1.cax'/
'STA'/

'TIT' 'FUE SEG: B1c'/
'LIB' 'ADD'/
'CAS' '../C4/c4.B1c.cax'/
'STA'/

'TIT' 'FUE SEG: B2'/
'LIB' 'ADD'/
'CAS' '../C4/c4.B2.cax'/
'STA'/

'TIT' 'FUE SEG: B2c'/
'LIB' 'ADD'/
'CAS' '../C4/c4.B2c.cax'/
'STA'/

'TIT' 'FUE SEG: C0'/
'LIB' 'ADD'/
'CAS' '../C4/c4.C0.cax'/
'STA'/

'TIT' 'FUE SEG: C1'/
'LIB' 'ADD'/
'CAS' '../C4/c4.C1.cax'/
'STA'/

'TIT' 'FUE SEG: C1c'/
'LIB' 'ADD'/
'CAS' '../C4/c4.C1c.cax'/
'STA'/

'TIT' 'FUE SEG: D0'/
'LIB' 'ADD'/
'CAS' '../C4/c4.D0.cax'/
'STA'/

'TIT' 'FUE SEG: D2'/
'LIB' 'ADD'/
'CAS' '../C4/c4.D2.cax'/
'STA'/

'TIT' 'FUE SEG: D2c'/
'LIB' 'ADD'/
'CAS' '../C4/c4.D2c.cax'/
'STA'/

'TIT' 'FUE SEG: E0'/
'LIB' 'ADD'/
'CAS' '../C4/c4.E0.cax'/
'STA'/

'TIT' 'FUE SEG: E1'/
'LIB' 'ADD'/
'CAS' '../C4/c4.E1.cax'/
'STA'/
```

```
'TIT' 'FUE SEG: E1c'/
'LIB' 'ADD'/
'CAS' '../C4/c4.E1c.cax'/
'STA'/

'TIT' 'FUE SEG: E2'/
'LIB' 'ADD'/
'CAS' '../C4/c4.E2.cax'/
'STA'/

'TIT' 'FUE SEG: E2c'/
'LIB' 'ADD'/
'CAS' '../C4/c4.E2c.cax'/
'STA'/
'END'/
'COM' 7890123456789012345678901234567890123456789012345678901234567890123456789 0
'COM'     1         2         3         4         5         6         7
'TIT' 'OPR RADIAL REFLECTOR'/
'REF' 'RADIAL' 0 155.1296/
'LIB' 'ADD'/
'CAS' '../C4/c4.OPRRAD.cax'/
'BOR'  4 2  0 600 1200 2400/
'HBOR' 4 2  0 600 1200 2400/
'TMO'  4 4  293 353 425 563.1/
'HTMO' 4 4  293 353 425 563.1/
'BAS.MAC' 2 'TMO' 'BOR',,'HTMO' 'HBOR'/
'BAS.DFS' 2 'TMO' 'BOR',,'HTMO' 'HBOR'/
'STA'/

'TIT' 'OPR BOTTOM REFLECTOR'/
'REF' 'AXIAL' 0 155.1296/
'LIB' 'ADD'/
'CAS' '../C4/c4.OPRBOT.cax'/
'STA'/
'END'/

'COM' 7890123456789012345678901234567890123456789012345678901234567890123456789 0
'COM'     1         2         3         4         5         6         7         8

'TIT' 'OPR TOP REFLECTOR'/
'REF' 'AXIAL' 0 155.1296/
'LIB' 'ADD'/
'CAS' '../C4/c4.OPRTOP.cax'/
'TMO'  5 4  293 353 425 563.1 603.1/
'HTMO' 5 4  293 353 425 563.1 603.1/
'BOR'  4 2  0 600 1200 2400/
'HBOR' 4 2  0 600 1200 2400/
'BAS.MAC' 2 'TMO' 'BOR',,'HTMO' 'HBOR'/
'BAS.DFS' 2 'TMO' 'BOR',,'HTMO' 'HBOR'/
'STA'/
'END'/
```

Sample Inputs: SIMULATE-3

```
'COM' 78901234567890123456789012345678901234567890123456789012345678901234567890
'COM'    1         2         3         4         5         6         7         8
'COM'
'COM' OPR-1000 4-LOOP PWR WITH CONVENTIONAL SOLID FUEL
'COM'
'COM' Ulchin Unit 5, cycle 1-4


'DIM.PWR' 15/
'DIM.CAL' 24 2 2/  * 24 AXIAL NODES, QUARTER CORE, 2X2 NODES PER ASSY
'DIM.DEP' 'EXP' 'SAM' 'HTMO' 'HBOR' 'HTFU' 'PIN' 'EBP'/  * DEPLETION ARGUMENTS

'TIT.CAS' 'CYCLE 01'/

'LIB' '../T3/t3.OPR.lib'/

'COR.SYM' 'ROT'/
'COR.DAT' 20.78 381.0 96.26 1245.6 -1/
'COR.STM' 0/  * BACKWARD COMPATIBILITY

'PWR.OPT' 'OFF'/

'REF.LIB' ,01 'OPRRAD'/
          ,02 'OPRBOT'/
          ,03 'OPRTOP'/
'SEG.LIB' ,04 'A0'/
          ,05 'B0'/
          ,06 'B1'/
          ,07 'B1c'/
          ,08 'B2'/
          ,09 'B2c'/
          ,10 'C0'/
          ,11 'C1'/
          ,12 'C1c'/
          ,13 'D0'/
          ,14 'D2'/
          ,15 'D2c'/
          ,16 'E0'/
          ,17 'E1'/
          ,18 'E1c'/
          ,19 'E2'/
          ,20 'E2c'/
'SEG.TFU' 0  0 347.38 -5.3799/ * SEGMENT TEMPERATURE FIT

'FUE.ZON' ,01 1 'RADREF' 02 0.0 01 381.0 03/
  ,02 1 'A0' 02 0.0 04 381.0 03/
  ,03 1 'B0' 02 0.0 05 381.0 03/
  ,04 1 'B1' 02 0.0 07 27.95 06 353.05 07 381.0 03/
  ,05 1 'B2' 02 0.0 09 27.95 08 353.05 09 381.0 03/
  ,06 1 'C0' 02 0.0 10 381.0 03/
  ,07 1 'C1' 02 0.0 12 27.95 11 353.05 12 381.0 03/
  ,08 1 'D0' 02 0.0 13 381.0 03/
  ,09 1 'D2' 02 0.0 15 19.05 14 361.95 15 381.0 03/
  ,10 1 'E0' 02 0.0 16 381.0 03/
```

```
  ,11 1 'E1' 02 0.0 18 19.05 17 361.95 18 381.0 03/
  ,12 1 'E2' 02 0.0 20 19.05 19 361.95 20 381.0 03/
  ,13 1 'F0' 02 0.0 16 381.0 03/
  ,14 1 'F1' 02 0.0 18 15.24 17 365.76 18 381.0 03/
  ,15 1 'F2' 02 0.0 20 15.24 19 365.76 20 381.0 03/
'FUE.GRD' 'ON' 10.82  3.36 'ZRC'
               50.75  3.36 'ZRC'
               90.68  3.36 'ZRC'
               130.61 3.36 'ZRC'
               170.54 3.36 'ZRC'
               210.47 3.36 'ZRC'
               250.4  3.36 'ZRC'
               290.33 3.36 'ZRC'
               330.26 3.36 'ZRC'
               370.19 3.36 'ZRC'/
'FUE.TYP' 1
          2 2 2 2 2 2 2 2 1
          2 2 2 2 2 2 2 2 1
          2 2 2 2 2 2 2 2 1
          2 2 2 2 2 2 2 1 1
          2 2 2 2 2 2 2 1 0
          2 2 2 2 2 2 1 1 0
          2 2 2 2 2 1 1 0 0
          2 2 2 1 1 1 0 0 0
          1 1 1 1 0 0 0 0 0/

'COM' FUE.TYP VALUE ON FUE.NEW CARDS OVERLAYS THE VALUES ON THE PRECEDING MAP
'FUE.NEW' 'TYPE01' 'A001' 61 02/
'FUE.NEW' 'TYPE01' 'B001' 24 03/
'FUE.NEW' 'TYPE01' 'B101' 20 04/
'FUE.NEW' 'TYPE01' 'B201' 16 05/
'FUE.NEW' 'TYPE01' 'C001' 16 06/
'FUE.NEW' 'TYPE01' 'C101' 40 07/

'COM' -R-  -P-  -N-  -M-  -L-  -K-  -J-  -H-  -G-  -F-  -E-  -D-  -C-  -B-  -A-
'FUE.SER' 4/
01 1                          B015 B020 C005 B006 B005
02 1                B001 C001 C108 C128 B117 C140 C122 C008 B009
03 1           C013 C130 A026 B207 A060 A045 A001 B201 A034 C127 C002
04 1      B013 C126 B107 B215 A040 C109 A053 C101 A048 B204 B101 C103 B024
05 1      C006 A056 B202 A033 B113 A016 B110 A007 B105 A036 B212 A019 C003
06 1 B010 C125 B211 A055 B102 A044 C119 A013 C118 A041 B112 A052 B203 C124 B018
07 1 B007 C138 A058 C105 A020 C104 A022 A002 A011 C114 A030 C107 A012 C135 B003
08 1 C004 B118 A057 A009 B109 A059 A025 A008 A023 A015 B114 A032 A051 B115 C007
09 1 B011 C106 A054 C121 A061 C110 A006 A004 A028 C111 A027 C120 A024 C139 B023
10 1 B014 C134 B213 A010 B120 A047 C116 A029 C112 A037 B108 A005 B205 C132 B017
11 1      C009 A018 B208 A038 B116 A017 B111 A035 B106 A014 B210 A046 C016
12 1      B022 C102 B103 B209 A039 C117 A042 C115 A050 B206 B104 C129 B002
13 1           C011 C113 A043 B216 A003 A031 A021 B214 A049 C123 C015
14 1                B021 C014 C131 C137 B119 C133 C136 C012 B008
15 1                          B016 B004 C010 B012 B019
 0 0

'RES' 'NEWFUEL'/

'HYD.ITE'/

'BAT.EDT' 'OFF'/
```

```
'PIN.EDT' 'ON' 'SUMM' '2PIN'/

'ITE.BOR' 1000/
'ITE.SRC' 'SET' 'EOLEXP',,0.001,,,'KEF' 1.000 0.00001 'MINBOR' 9.0/

'DEP.CYC' 'CYCLE01' 0.0 01/
'DEP.STA' 'AVE' 0.0 0.15 0.25 0.5 -0.5 20/
'PRI.STA' '2EXP' '2RPF'/
'SUM' './RES/s3.OPR.c1.sum'/
'WRE' './RES/s3.OPR.c1.res' 20/

'STA'/
'END'/

'COM' 78901234567890123456789012345678901234567890123456789012345678901234567890
'COM'    1         2         3         4         5         6         7         8

'DIM.PWR' 15/
'DIM.CAL' 24 2 2/  * 24 AXIAL NODES, QUARTER CORE, 2X2 NODES PER ASSY
'DIM.DEP' 'EXP' 'SAM' 'HTMO' 'HBOR' 'HTFU' 'PIN' 'EBP'/  * DEPLETION ARGUMENTS

'TIT.CAS' 'CYCLE 02'/

'FUE.NEW' 'TYPE01' 'D001' 28 08/
'FUE.NEW' 'TYPE01' 'D201' 32 09/

'COM' -R-  -P-  -N-  -M-  -L-  -K-  -J-  -H-  -G-  -F-  -E-  -D-  -C-  -B-  -A-
'FUE.SER' 4/
01 1                          C012 D012 D021 D004 C014
02 1                C112 D027 D208 B011 B201 B023 D202 D008 C116
03 1           B207 D002 B113 B018 C130 D225 C127 B010 B105 D013 B203
04 1      C111 D001 D222 B208 D210 C136 C010 C131 D226 B210 D224 D003 C110
05 1      D010 B102 B204 B107 C107 B024 B111 B013 C105 B101 B215 B112 D024
06 1 C016 D216 B016 D232 C117 D223 C133 D212 C137 D201 C115 D229 B019 D209 C009
07 1 D007 B006 C126 C132 B021 C139 C015 B119 C011 C106 B008 C134 C103 B020 D018
08 1 D022 B211 D203 C007 B114 D215 B115 A008 B118 D205 B109 C004 D217 B205 D026
09 1 D023 B012 C102 C124 B001 C135 C002 B117 C013 C138 B009 C125 C129 B004 D025
10 1 C003 D204 B015 D227 C109 D213 C140 D207 C128 D228 C101 D220 B005 D206 C006
11 1      D020 B120 B206 B103 C120 B002 B110 B022 C121 B104 B209 B108 D016
12 1      C114 D011 D219 B202 D230 C122 C005 C108 D231 B212 D218 D006 C104
13 1           B213 D015 B116 B017 C113 D221 C123 B014 B106 D009 B214
14 1                C118 D028 D214 B007 B216 B003 D211 D019 C119
15 1                          C008 D014 D017 D005 C001
 0 0

'RES' './RES/s3.OPR.c1.res' 20000/

'ITE.BOR' 1500/
'ITE.SRC' 'SET' 'EOLEXP',,0.001,,,'KEF' 1.000 0.00001 'MINBOR' 10.0/

'DEP.CYC' 'CYCLE02' 0.0 02/
'DEP.STA' 'AVE' 0.0 0.15 0.25 0.5 -0.5 24/
'PRI.STA' '2EXP' '2RPF'/
'SUM' './RES/s3.OPR.c2.sum'/
'WRE' './RES/s3.OPR.c2.res' 24/

'STA'/
'END'/
```

```
'COM' 7890123456789012345678901234567890123456789012345678901234567890123456789
'COM'    1         2         3         4         5         6         7         8

'DIM.PWR' 15/
'DIM.CAL' 24 2 2/  * 24 AXIAL NODES, QUARTER CORE, 2X2 NODES PER ASSY
'DIM.DEP' 'EXP' 'SAM' 'HTMO' 'HBOR' 'HTFU' 'PIN' 'EBP'/  * DEPLETION ARGUMENTS

'TIT.CAS' 'CYCLE 03'/

'FUE.NEW' 'TYPE01' 'E001' 16 10/
'FUE.NEW' 'TYPE01' 'E101' 24 11/
'FUE.NEW' 'TYPE01' 'E201' 24 12/

'COM' -R-  -P-  -N-  -M-  -L-  -K-  -J-  -H-  -G-  -F-  -E-  -D-  -C-  -B-  -A-
'FUE.SER' 4/
01 1                          D019 E013 D213 E014 D028
02 1                D005 E001 E112 B001 E118 B009 E119 E011 D014
03 1           C015 E117 B018 D210 E211 D212 E202 D226 B010 E122 C011
04 1      D025 E121 E120 C001 D011 B012 D021 B004 D006 C008 E124 E103 D023
05 1      E006 B016 C006 E204 C114 E212 C005 E218 C104 E201 C003 B019 E004
06 1 D016 E106 D232 D013 C116 D218 D204 E217 D206 D219 C112 D002 D229 E110 D020
07 1 E007 B013 E213 B023 E207 D202 B214 D221 B213 D208 E214 B011 E205 B024 E010
08 1 D228 E102 D215 D022 C004 E223 D217 C103 D203 E219 C007 D026 D205 E105 D223
09 1 E012 B022 E209 B003 E222 D211 B203 D225 B207 D214 E221 B007 E210 B002 E015
10 1 D024 E113 D227 D009 C119 D224 D216 E224 D209 D222 C118 D015 D220 E108 D010
11 1      E002 B015 C009 E203 C111 E215 C010 E220 C110 E206 C016 B005 E005
12 1      D018 E111 E104 C014 D001 B006 D017 B020 D003 C012 E123 E116 D007
13 1           C002 E107 B017 D230 E208 D207 E216 D231 B014 E115 C013
14 1                D004 E008 E114 B021 E101 B008 E109 E003 D012
15 1                          D008 E009 D201 E016 D027
 0 0

'RES' './RES/s3.OPR.c2.res' 20000/

'ITE.BOR' 1500/
'ITE.SRC' 'SET' 'EOLEXP',,0.001,,,'KEF' 1.000 0.00001 'MINBOR' 10.0/

'DEP.CYC' 'CYCLE03' 0.0 03/
'DEP.STA' 'AVE' 0.0 0.15 0.25 0.5 -0.5 24/
'PRI.STA' '2EXP' '2RPF'/
'SUM' './RES/s3.OPR.c3.sum'/
'WRE' './RES/s3.OPR.c3.res' 24/

'STA'/
'END'/

'COM' 7890123456789012345678901234567890123456789012345678901234567890123456789
'COM'    1         2         3         4         5         6         7         8

'DIM.PWR' 15/
'DIM.CAL' 24 2 2/  * 24 AXIAL NODES, QUARTER CORE, 2X2 NODES PER ASSY
'DIM.DEP' 'EXP' 'SAM' 'HTMO' 'HBOR' 'HTFU' 'PIN' 'EBP'/  * DEPLETION ARGUMENTS

'TIT.CAS' 'CYCLE 04'/

'FUE.NEW' 'TYPE01' 'F001' 12 13/
'FUE.NEW' 'TYPE01' 'F101' 20 14/
```

```
'FUE.NEW' 'TYPE01' 'F201' 28 15/

'COM' -R-  -P-  -N-  -M-  -L-  -K-  -J-  -H-  -G-  -F-  -E-  -D-  -C-  -B-  -A-
'FUE.SER' 4/
01 1                        E220 E016 F003 E009 E215
02 1
E123 F005 F102 F222 D201 F216 F114 F004 E201
03 1
D017 F110 D012 E111 D002 F104 D013 E116 D004 F111 D022
04 1
E204 F117 F208 D027 E113 F205 D232 F213 E108 D008 F210 F116 E104
05 1
F009 D007 D010 D222 E211 E002 D221 E005 E202 D224 D024 D018 F006
06 1  E221 F115 E122 E119 E213 F223 D211 F228 D214 F214 E205 E112 E117 F101 E222
07 1  E015 F206 D001 F215 E011 D206 E105 E224 E101 D204 E001 F201 D003 F221 E012
08 1  F011 D223 F103 D230 D217 F226 E219 D229 E223 F220 D203 D226 F107 D228 F001
09 1  E010 F219 D011 F203 E003 D209 E118 E217 E102 D216 E008 F211 D006 F218 E007
10 1  E214 F120 E115 E109 E209 F212 D202 F224 D208 F227 E210 E114 E107 F109 E207
11 1       F002 D023 D020 D219 E208 E006 D225 E004 E216 D218 D016 D025 F010
12 1       E124 F112 F225 D028 E106 F209 D220 F207 E110 D019 F217 F118 E206
13 1
D026 F113 D014 E121 D015 F106 D009 E103 D005 F119 D021
14 1
E203 F008 F108 F202 D213 F204 F105 F012 E120
15 1
E218 E014 F007 E013 E212
 0 0

'RES' './RES/s3.OPR.c3.res' 20000/

'ITE.BOR' 1500/
'ITE.SRC' 'SET' 'EOLEXP',,0.001,,,'KEF' 1.000 0.00001 'MINBOR' 12.0/

'DEP.CYC' 'CYCLE04' 0.0 04/
'DEP.STA' 'AVE' 0.0 0.15 0.25 0.5 -0.5 24/
'PRI.STA' '2EXP' '2RPF'/
'SUM' './RES/s3.OPR.c4.sum'/
'WRE' './RES/s3.OPR.c4.res' 24/

'STA'/
'END'/
```

Sample Inputs: MCODE-2.2

```
1/8th Full Assembly model of OPR1000 annular fuel
c
c    12x12 Lattice with 4.5w/o UO2 Fuel
c
c    cell specification
c
c     mt   density                          geometry
   4   4   6.98055e-02  -1                    u=1 imp:n=1      $ internal coolant
300K
   6   3   4.34384e-02   1 -2                 u=1 imp:n=1      $ internal clad
   8   2   3.76497e-05   2 -3                 u=1 imp:n=1      $ internal gap
  10   1   6.97094e-02   3 -4                 u=1 imp:n=1      $ fuel pellet 600K
  12   2   3.76497e-05   4 -5                 u=1 imp:n=1      $ external gap
  13   3   4.34384e-02   5 -6                 u=1 imp:n=1      $ external clad
  14   4   6.98055e-02   6                    u=1 imp:n=1      $ extenal coolant
300K
  21   4   6.98055e-02  -21        64   62  u=2 imp:n=1      $ coolant in guide
tube 585.1K
  22   3   4.34384e-02   21 -22    64   62  u=2 imp:n=1      $ inner guide tube
585.1K
  23   4   6.98055e-02   22 -23    64   62  u=2 imp:n=1      $ coolant between
two tubes 585.1K
  24   3   4.34384e-02   23 -24    64   62  u=2 imp:n=1      $ outer guide tube
585.1K
  25   4   6.98055e-02   24        64   62  u=2 imp:n=1      $ coolant out of
guide tube 585.1K
  31   4   6.98055e-02  -31       -63   62  u=3 imp:n=1      $ coolant in guide
tube 585.1K
  32   3   4.34384e-02   31 -32   -63   62  u=3 imp:n=1      $ inner guide tube
585.1K
  33   4   6.98055e-02   32 -33   -63   62  u=3 imp:n=1      $ coolant between
two tubes 585.1K
  34   3   4.34384e-02   33 -34   -63   62  u=3 imp:n=1      $ outer guide tube
585.1K
  35   4   6.98055e-02   34       -63   62  u=3 imp:n=1      $ coolant out of
guide tube 585.1K
  41   4   6.98055e-02  -41       -63  -61  u=4 imp:n=1      $ coolant in guide
tube 585.1K
  42   3   4.34384e-02   41 -42   -63  -61  u=4 imp:n=1      $ inner guide tube
585.1K
  43   4   6.98055e-02   42 -43   -63  -61  u=4 imp:n=1      $ coolant between
two tubes 585.1K
  44   3   4.34384e-02   43 -44   -63  -61  u=4 imp:n=1      $ outer guide tube
585.1K
  45   4   6.98055e-02   44       -63  -61  u=4 imp:n=1      $ coolant out of
guide tube 585.1K
  51   4   6.98055e-02  -51        64  -61  u=5 imp:n=1      $ coolant in guide
tube 585.1K
  52   3   4.34384e-02   51 -52    64  -61  u=5 imp:n=1      $ inner guide tube
585.1K
  53   4   6.98055e-02   52 -53    64  -61  u=5 imp:n=1      $ coolant between
two tubes 585.1K
  54   3   4.34384e-02   53 -54    64  -61  u=5 imp:n=1      $ outer guide tube
585.1K
```

```
  55   4   6.98055e-02   54       64 -61  u=5 imp:n=1      $ coolant out of
guide tube 585.1K
  101  0              -61 62 -63 64 imp:n=1 u=6 lat=1 fill=-5:6 -5:6 0:0
         1 1 1 1 1 1 1 1 1 1 1 1
         1 1 1 1 1 1 1 1 1 1 1 1
         1 1 4 3 1 1 1 1 4 3 1 1
         1 1 5 2 1 1 1 1 5 2 1 1
         1 1 1 1 1 1 1 1 1 1 1 1
         1 1 1 1 1 4 3 1 1 1 1 1
         1 1 1 1 1 5 2 1 1 1 1 1
         1 1 1 1 1 1 1 1 1 1 1 1
         1 1 4 3 1 1 1 1 4 3 1 1
         1 1 5 2 1 1 1 1 5 2 1 1
         1 1 1 1 1 1 1 1 1 1 1 1
         1 1 1 1 1 1 1 1 1 1 1 1
  110  0              -65  66  -67   68      u=12       fill=6  imp:n=1 $ core
  111  4 9.25748e-02  65:-66:  67: -68      u=12               imp:n=1
$ interassembly coolant
  120  4 9.25748e-02 -71  72  -73   74      u=16 lat=1 fill=12 imp:n=1
  130  0              81 82 -501 402 -408            fill=16 imp:n=1 $ FA
  1000 0             -81:-82:501:-402: 408                   imp:n=0
$ outside
c    end of cell specification

c
c    surface specification
c
c    trn card  constants for equations
  1   cz   0.44            $ Inner surface of inner clad
  2   cz   0.497           $ Outer surface of inner clad
  3   cz   0.504           $ Inner fuel surface
  4   cz   0.726           $ Outer fuel surface
  5   cz   0.733           $ Inner surface of outer clad
  6   cz   0.795           $ Outer surface of outer clad
  21  c/z  -0.8565 -0.8565 1.145
  22  c/z  -0.8565 -0.8565 1.245
  23  c/z  -0.8565 -0.8565 1.575
  24  c/z  -0.8565 -0.8565 1.675
  31  c/z  -0.8565  0.8565 1.145
  32  c/z  -0.8565  0.8565 1.245
  33  c/z  -0.8565  0.8565 1.575
  34  c/z  -0.8565  0.8565 1.675
  41  c/z   0.8565  0.8565 1.145
  42  c/z   0.8565  0.8565 1.245
  43  c/z   0.8565  0.8565 1.575
  44  c/z   0.8565  0.8565 1.675
  51  c/z   0.8565 -0.8565 1.145
  52  c/z   0.8565 -0.8565 1.245
  53  c/z   0.8565 -0.8565 1.575
  54  c/z   0.8565 -0.8565 1.675
  61  px    0.8565
  62  px   -0.8565
  63  py    0.8565          $ pin pitch
  64  py   -0.8565          $ pin pitch
  65  px   11.1345          $ FA width
  66  px   -9.4215          $ FA width
  67  py   11.1345          $ FA width
  68  py   -9.4215          $ FA width
```

```
  71   px    11.2465            $ FA pitch
  72   px    -9.5335            $ FA pitch
  73   py    11.2465            $ FA pitch
  74   py    -9.5335            $ FA pitch
  *81   p    1  -1  0  0        $ symmetry  1
  *82  py   0.8564                $ symmetry
  *402 pz   0.0                 $ core-bottom
  *408 pz   10.00               $ core-top
  *501 px   11.24651            $ boundary
c    end of surface specification

c    data specification
phys:n    20   0.0
c
c
c    TMP free-gas thermal temperature card
c    t1n t2n...n=index of time,t1n=temp for cell 1 at time n
#        tmp
    4   2.58510e-08         $300K
    6   2.58510e-08         $300K
    8   2.58510e-08         $300K
   10   2.58510e-08         $300K
   12   2.58510e-08         $300K
   13   2.58510e-08         $300K
   14   2.58510e-08         $300K
   21   2.58510e-08         $300K
   22   2.58510e-08         $300K
   23   2.58510e-08         $300K
   24   2.58510e-08         $300K
   25   2.58510e-08         $300K
   31   2.58510e-08         $300K
   32   2.58510e-08         $300K
   33   2.58510e-08         $300K
   34   2.58510e-08         $300K
   35   2.58510e-08         $300K
   41   2.58510e-08         $300K
   42   2.58510e-08         $300K
   43   2.58510e-08         $300K
   44   2.58510e-08         $300K
   45   2.58510e-08         $300K
   51   2.58510e-08         $300K
   52   2.58510e-08         $300K
   53   2.58510e-08         $300K
   54   2.58510e-08         $300K
   55   2.58510e-08         $300K
  101   2.58510e-08         $300K
  110   2.58510e-08         $300K
  111   2.58510e-08         $300K
  120   2.58510e-08         $300K
  130   2.58510e-08         $300K
 1000   2.58510e-08         $300K
c
c    material specification
c
c     4.5 wt% U-235  (10.4g/cc)
m1         8016.60c  4.64729e-2
          92234.60c  8.46397e-6
          92235.60c  1.05800e-3
```

```
        92238.60c  2.21700e-2
c     AIR (gap)
m2     8016.60c  3.76497E-05
c
c     Zircaloy-4  (6.550g/cc)
m3        8016.60c 3.08257e-4
         24050.60c 7.58604e-5
         26056.60c 1.48326e-4
         40000.60c 4.24242e-2
         50000.35c 4.81797e-4
c
c     H2O (15.5MPa at 300K)  (0.6955g/cc)
m4       8016.60c 2.32685e-2
         1001.60c 4.65370e-2
mt4      lwtr.01t
c
c
c  ksrc    2.8    1.713      2.0
c       2.8    1.713      4.0
c       2.8    1.713      6.0
c        2.8    1.713      8.0
c
c
mode     n
kcode    6000   1.0  30  150
prdmp    150 150 150
print

c   MCODE Input
1    132.966 PWRUE.LIB
mce    /home/zhang/annular/mcnp.exe
mcxs   /usr/local/bin/mcode22/mcnpxs.sum
mcs  2 source
orge   /usr/local/bin/origen22/origen22
orgl   /usr/local/bin/origen22/LIBS DECAY.LIB GXUO2BRM.LIB
tal  1 (10)
pow  52178.329
nor  2 0
cor  1
dep  D   5
        42
        125
        208
        313
        438
        563
        688
        813
        938
        1000
        1063
        1188
        1313
        1438
        1500
sta  0
end
```

Sample Inputs: VIPRE-01

```
***************************************************************
*                   OPR-1000 12x12, 1/8 core, annular         *
***************************************************************
1,0,0                                                                   *vipre.1
OPR-1000 annular                                                        *vipre.2
geom,55,55,20,0,0,0              * 55 channels, 20 axial nodes           *geom.1
150.0,0.0,0.5                                                            *geom.2
**** channel geometry input
1,0.0394190,0.603120,0.390741,2,2,0.093894,0.337205,3,0.024213,0.674409
*geom.4
2,0.109136,1.143928,0.838176,1,4,0.048425,0.674409
3,0.073532,0.983294,0.983294,2,4,0.048425,0.580651,6,0.024213,0.674409
4,0.147065,1.966588,1.966588,2,5,0.048425,0.650197,7,0.048425,0.674409
5,0.109136,1.143928,0.838176,1,8,0.093894,0.505807
6,0.073532,0.983294,0.983294,2,7,0.048425,0.580651,9,0.024213,0.674409
7,0.147065,1.966588,1.966588,2,8,0.048425,0.573248,10,0.048425,0.674409
8,0.078839,1.206239,0.781883,1,12,0.093894,0.573248
9,0.073532,0.983294,0.983294,2,10,0.048425,0.580651,14,0.024213,0.674409
10,0.147065,1.966588,1.966588,2,11,0.048425,0.650197,15,0.048425,0.674409
11,0.073532,0.983294,0.983294,2,12,0.327775,0.337205,16,0.048425,0.650197
12,0.14474,1.304561,0.693058,1,13,0.093894,0.505807
13,0.078839,1.206239,0.781883,2,17,0.093894,0.573248,18,0.048425,0.573248
14,0.073532,0.983294,0.983294,2,15,0.048425,0.580651,19,0.024213,0.718504
15,0.147065,1.966588,1.966588,2,16,0.048425,0.674409,19,0.048425,0.718504
16,0.147065,1.966588,1.966588,2,18,0.048425,0.674409,19,0.048425,0.718504
17,0.109136,1.143928,0.838176,1,20,0.048425,0.650197
18,0.147065,1.966588,1.966588,2,20,0.048425,0.674409,22,0.048425,0.746823
19,0.516351,4.916469,4.916469,2,22,0.136614,2.093332,23,0.121063,2.045276
20,0.147065,1.966588,1.966588,2,21,0.048425,0.562008,22,0.048425,0.746823
21,0.073532,0.983294,0.983294,1,22,0.048425,0.634421
22,0.756518,6.883056,6.883056,1,23,0.213583,2.045276
23,5.043014,60.24375,55.06445,2,24,0.301181,4.090551,25,0.266339,4.77231
24,5.484208,66.14351,60.96421,2,25,0.290551,4.77231,26,0.334646,6.135827
25,10.96842,132.287,121.9284,1,27,0.669291,6.817585
26,10.96842,132.287,121.9284,2,27,0.669291,6.135827,29,0.334646,13.05081
27,21.93683,264.574,243.8569,2,28,0.669291,6.817585,29,0.669291,13.05081
28,10.96842,132.287,121.9284,1,29,0.669291,11.68729
29,153.5578,1852.018,1706.998,1,30,3.011811,18.02602
30,263.242,3174.889,2926.282
31,0.094273,1.088426,1.088426
32,0.047137,0.544213,0.544213
33,0.094273,1.088426,1.088426
34,0.094273,1.088426,1.088426
35,0.094273,1.088426,1.088426
36,0.094273,1.088426,1.088426
37,0.094273,1.088426,1.088426
38,0.094273,1.088426,1.088426
39,0.094273,1.088426,1.088426
40,0.094273,1.088426,1.088426
41,0.047137,0.544213,0.544213
42,0.094273,1.088426,1.088426
43,0.094273,1.088426,1.088426
44,0.094273,1.088426,1.088426
45,0.094273,1.088426,1.088426
46,0.094273,1.088426,1.088426
```

```
47,0.047137,0.544213,0.544213
48,2.922466,33.7412,33.7412
49,2.922466,33.7412,33.7412
50,5.844932,67.4824,67.4824
51,5.844932,67.4824,67.4824
52,11.68986,134.9648,134.9648
53,5.844932,67.4824,67.4824
54,81.82905,944.7536,944.7536
55,140.2784,1619.578,1619.578                                  *geom.4
prop,0,0,2,1                                                   *prop.1
rods,1,27,1,2,4,0,0,0,0,0,0                                    *rods.1
0.0,0.0,0,0,                                                   *rods.2
-1,                                                            *rods.3
1.55    * chopped cosine shape                                 *rods.5
**** rod geometry input
1,1,1.550,1,1,0.198792,2,0.301208,3,0.25,4,0.25
-1,1,1.550,1,31,1
2,1,1.461,1,2,0.125,4,0.25,5,0.125
-2,1,1.461,1,32,0.5
3,1,1.335,1,3,0.25,4,0.25,6,0.25,7,0.25
-3,1,1.335,1,33,1
4,1,1.515,1,4,0.25,5,0.301208,7,0.25,8,0.198792
-4,1,1.515,1,34,1
5,1,1.276,1,6,0.25,7,0.25,9,0.25,10,0.25
-5,1,1.276,1,35,1
6,1,1.480,1,7,0.25,8,0.198792,10,0.25,11,0.125,12,0.176208
-6,1,1.480,1,36,1
7,1,1.226,1,9,0.25,10,0.25,14,0.25,15,0.25
-7,1,1.226,1,37,1
8,1,1.313,1,10,0.25,11,0.25,15,0.25,16,0.25
-8,1,1.313,1,38,1
9,1,1.468,1,11,0.125,12,0.176208,13,0.198792,16,0.25,18,0.25
-9,1,1.468,1,39,1
10,1,1.491,1,13,0.198792,17,0.301208,18,0.25,20,0.25
-10,1,1.491,1,40,1
11,1,1.337,1,17,0.125,20,0.25,21,0.125
-11,1,1.337,1,41,0.5
12,1,1.235,1,14,0.25,15,0.25,19,0.5
-12,1,1.235,1,42,1
13,1,1.261,1,15,0.25,16,0.25,19,0.5
-13,1,1.261,1,43,1
14,1,1.302,1,16,0.25,18,0.25,19,0.25,22,0.25
-14,1,1.302,1,44,1
15,1,1.314,1,18,0.25,20,0.25,22,0.5
-15,1,1.314,1,45,1
16,1,1.302,1,20,0.25,21,0.25,22,0.5
-16,1,1.302,1,46,1
17,1,1.306,1,21,0.125,22,0.375
-17,1,1.306,1,47,0.5
18,1,1.363,1,19,1.25,22,1.875,23,28
-18,1,1.363,1,48,31
19,1,1.363,1,24,31
-19,1,1.363,1,49,31
20,1,1.363,1,25,61.875
-20,1,1.363,1,50,62
21,1,1.318,1,26,62
-21,1,1.318,1,51,62
22,1,1.251,1,27,124
```

```
-22,1,1.251,1,52,124
23,1,1.219,1,28,62
-23,1,1.219,1,53,62
24,1,0.951,1,29,868
-24,1,0.951,1,54,868
25,1,0.952,1,30,1488
-25,1,0.952,1,55,1488
26,2,0.000,1,1,0.051208,2,0.073792
27,2,0.000,1,5,0.073792,8,0.102416,12,0.147584,13,0.102416,17,0.073792
0                                                                              *rods.9
1,tube,0.625984,0.346457,5
*rods.68
2,1,0.022441,0.0,?   * inner cladding
*rods.69
2,2,0.002756,0.0,?   * inner gap
*rods.69
8,3,0.087402,1.0,?   * fuel pellet
*rods.69
2,4,0.002756,0.0     * outer gap
*rods.69
2,1,0.024409,0.0     * outer cladding
*rods.69
2,dumy,1.318898,0.0,0
**** material property data
1,17,409.0,clad
*rods.70
0.0,0.0671,7.3304509,?
25,0.0671,7.3304509
50,0.0671,7.33045093,?
65,0.0671,7.33045093
80.33,0.0671,7.33045093,?
260.33,0.07212,8.11585329
692.33,0.07904,9.80167423,?
1502.33,0.08955,13.2923001
1507.73,0.11988,13.3211893,?
1543.73,0.14089,13.5166505
1579.73,0.14686,13.717249,?
1615.73,0.1717,13.9231981
1651.73,0.1949,14.1347101,?
1687.73,0.18388,14.3519980
1723.73,0.1478,14.5752746,?
1759.73,0.112,14.804753
1786.73,0.085,14.9810589
*2240.33,0.085,18.5665964
2,1,0.025,igap
*rods.70
1,1.240775,0.1415635      *Cp=5195J/kg-K *gap=6000
*rods.71
3,22,650.617,FUO2
*rods.70
86,0.05677357,4.73275874,?
176,0.06078589,4.29917259
266,0.06366347,3.93877428,?
356,0.06581210,3.63454049
446,0.06747631,3.37435643,?
536,0.06880819,3.1493668
626,0.06990545,2.95294976,?
716,0.07083283,2.78005572
```

```
806,0.07163441,2.62676801,?
896,0.07234099,2.49000319
986,0.07297458,2.36730189,?
1076,0.07355124,2.25667975
1166,0.07408294,2.1565193,?
1256,0.07457886,2.06549023
1346,0.07504628,1.98248979,?
1436,0.07549123,1.90659753
1526,0.0759191,1.83704065,?
1616,0.07633503,1.77316713
1706,0.0767443,1.7144247,?
1796,0.07715268,1.66034425
1886,0.07756663,1.61052668,?
1976,0.07799351,1.5646323
*rods.71
4,1,0.025,ogap
*rods.70
1,1.240775,0.283125    *Cp=5195J/kg-K *gap=6000                        *rods.71
oper,1,1,0,1,0,1,0,0,0                                                  *oper.1
-1.0,1.3,0.0,0.005,0                                                    *oper.2
0                                                                       *oper.3
2248.0844,553.46,4089.851,181.6129,0.0
*oper.5
0                  *no forcing functions
*oper.12
corr,2,2,0,                                                             *corr.1
epri,epri,epri,none                                                     *corr.2
0.2                                                                     *corr.3
ditb,thom,thom,w-3l,cond,g5.7     *correlation for boiling curve        *corr.6
w-3s,w-3l            *dnb analysis by w-3l                              *corr.9
0.0                  *w-3s input data
*corr.10
0.042,0.066,0.986    *w-3l input data
*corr.11
drag,1,1,4                                                              *drag.1
0.32,-0.25,0.0,64.0,-1.0,0.0      *axial friction correlation           *drag.2
0.5213675,0.674409                                                      *drag.7
6.472,-.2,0.,6.472,-0.2,0.0       *lateral drag correlation             *drag.8
grid,0,3,                                                               *grid.1
0.6,0.4,1.0,                                                            *grid.2
30,12                                                                   *grid.4
1,2,3,4,5,6,7,8,9,10,11,12,13,14,15,16                                  *grid.5
17,18,19,20,21,22,23,24,25,26,27,28,29,30                               *grid.5
0.0,2,4.1339,1,19.8819,1,35.6299,1,?                                    *grid.6
51.3780,1,67.1260,1,82.8740,1,98.62205,1,
114.3701,1,130.1181,1,145.8661,1,150.0,3                      *grid loc. *grid.6
25,2                                                                    *grid.4
31,32,33,34,35,36,37,38,39,40,41,42,43,44,45,46                         *grid.5
47,48,49,50,51,52,53,54,55                                              *grid.5
0.0,2,150.0,3                                                           *grid.6
0                                 *grid.4 terminated
cont                                                                    *cont.1
0.0,0,150,50,3,1,      *direct solution                                 *cont.2
0.1,0.00001,0.001,0.05,0.01,0.9,1.5,1.0                                 *cont.3
5,0,0,0,0,0,1,1,0,0,0,1,0,0                                             *cont.6
1000.,0.0,0.0,0.0,0.0,0.0                                               *cont.7
Endd                                                          *end of data input
0
```

References

[1] Breismeister J.F., "MCNP^{TM} – A General Monte Carlo N-Particle Transport Code, Version 4C", LA-13709M, Los Alamos National Laboratory, April 2000.

[2] Cronin J.T., K.S. Smith, D.M. VerPlanck, J.A. Umbarger, M. Edenius, "SIMULATE-3 Methodology, Adavanced Three-Dimensional Two-Group Reactor Analysis Code", Studsvik/SOA-95/18, Studsvik of America, Inc., 1995

[3] Edenius M., Ekberg K. Forssen B.H., and Knott D., "CASMO-4, A Fuel Assembly Burnup Program, User's Manual", Studsvik/SOA-95/1, Studsvik of America, Inc., 1995.

[4] EPRI, *VIPRE-01 THERMAL HYDRULIC CODE FOR REACTOR: VOLUME II USRS MANUAL*, EPRI-NP-2511-CCM-A, Revision 3, ,1985.

[5] Feng B. Hejzlar P. and Kazimi M.S., "On the Use of High Performance Annular Fuel in PWRs", Center for Advanced Nuclear Energy Systems, MIT, Topical Report, MIT-NFC-TR-100, June 2008.

[6] Feng D., Hejzlar P. and Kazimi, M.S., "Thermal-Hydraulic Design of High-Power-Density Annular Fuel in PWRs", Sepcial Issue of Nuclear Technology, Vol. 169, pp. 16-33, October 2007

[7] Hejzlar P., Driscoll M.J., and Kazimi M.S., "High Performance Annular Fuel For Pressurized Water Reactors," Transactions of the American Nuclear Society, Vol. 84, Milwaukee, June 17-21, p. 192, 2001.

[8] Hejzlar P. and Kazimi M.S., "Annular Fuel for High Power Density PWRs: Motivation and Overview", Special Issue of Nuclear Technology, Vol. 160, pp. 2-15, October 2007.

[9] Idelchik I.E., *Handbook of Hydraulic Resistance*, 3rd edition, CRC Press, Florida, 1993

[10] KAERI, internal report of UCN Unit 5, 2008

[11] Kazimi M.S., Hejzlar P., ET AL., "High Performance Fuel Design for Next Generation PWRs: 4th Annual Report," MIT-NFC-PR-076, CANES, MIT, October 2005.

[12] Kazimi M.S., Hejzlar P., ET AL., "High Performance Fuel Design for Next Generation PWRs: 1st Quarterly Report," MIT-NFC-PR-001, CANES, MIT, November 2001.

[13] Y. Long, Y. Zhang, and M.S. Kazimi, "Inert Matrix Materials as Hosts of Actinide Nuclear Fuels", MIT-NFC-TR-055, CANES, MIT, March 2003.

[14] ORNL, *SCALE: A Modular Code System for Performing Standardized Computer Analyses for Licensing Evaluations*, ORNL/TM-2005/39, Version 5.1, Vols. I–III, November 2006.

[15] XU Z., HEJZLAR P., DRISCOLL M.J. and KAZIMI M.S., "An Improved MCNP-ORIGEN Depletion Program (MCODE) and Its Verification for High-Burnup Applications," *Proc. of PHYSOR-02*, Seoul, Korea, October 2002.

[16] Xu Z.W., Otsuka Y. Hejzlar P. Driscoll M.J., and Kazimi M.S., "Neutronic Design of PWR Cores with High Performance Annular Fuel", MIT-NFC-TR-063, May 2004.

[17] Xu Z.W. and Hejzlar P., "MCODE, Version 2.2 – An MCNP-ORIGEN Depletion Program", MIT-NFC-TR-104, CANES, MIT, November 2008.

[18] Yang Y.S., Bae K.M., ET AL., "Conceptual Design of OPR-1000 Compatible Annular Fuel Assembly", Proceedings of ICAPP 2007, Paper 7445, Nice, France, May 2007.

[19] Yuan Y., Kazimi M.S., and Hejzlar P., "Thermo-mechanical Performance of High-Power-Density Annular Fuel", Special Issue of Nuclear Technology, Vol. 160, Oct 2007